# Geometric Frequency Reuse for Irregular Cellular Networks


Achonu Oluwole Adejo

Newcastle University

Newcastle upon Tyne, UK

A thesis submitted for the degree of

*Doctor of Philosophy*

July 2018

This project is dedicated to Almighty God.

# Acknowledgements

All praises to the Lord God Almighty; who is the source of all wisdom, purpose, strength, grace, essence and life. I render thanksgiving to God the Father, God the Son and God the Holy Spirit for sustaining me through this research.

My PhD journey was daunting but thankfully, I received tremendous support and encouragement from many people. Deep appreciation goes to Professor Said Boussakta, my first supervisor for his guidance and the wonderful opportunity to learn under him. His contributions were enriching and instrumental to the success and completion of my research. I am also grateful to Mr Jeffrey Neasham, my second supervisor, for his very helpful comments, suggestions and support. I appreciate the National Information Technology Development Agency (NITDA) and Federal University of Technology Minna, both in Nigeria for offering me scholarship and support.

I specially appreciate my loving and dear wife, Martha, for her patience, encouragement and support. To my parents, Arc. & Mrs Adejo, thanks so much for your love, sacrifices, encouragement and inspiration. And to my inspiring and wonderful siblings, Ufedo, Chide and Attah; I appreciate you greatly. I am grateful to Apostle Bright Onoka, Pastor Ufumwen Onoka, Pastor Victor Onwudili, Pastor Kelechi Anyigor, Pastor Kenneth Okaeme, their families and the City of God Christian centre family; thanks for providing homely and spiritual support.

My deep gratitude goes to Dr. Jamal Hussein, Dr. Anvar Tukmanov, Dr. Osianoh Glen, Dr. Salama Ikki, all of whom offered fruitful discussions at various critical points. Many thanks to School of Engineering staff at Newcastle University especially Gill Webber. I wish to thank my close friends and colleagues for their impactful encouragement, including Dr. Adeiza Onumanyi, Dr. Henry Ohize, Dr. Chukwuma Anyigor, Dr.

Enoch Adeniyi, Dr. Akachukwu Okoli, Dr. Uzoma Okoro, Dr. Opeyemi Dele-Ajayi (impact) and Dr. Ayo Lawal. I specially appreciate Pastor Joshua Jeremiah and family, the Great House Assembly Minna family, Prof. E.N Onwuka, Prof. Musa Aibinu, Engr. Tosin Adegoke, Augustine Chukwumah, Chika Umunnawuike, Mr. Simon & Mrs. Mary Akatu, Adaora Onyejeakor, Adim Umeobika, Dr. Beatrice Achan, Denis Ona, Yulong Chen and Sameer Alsudany.

I remember with deep gratitude two of my previous teachers who have had a great impact on my academic career; I owe a lot to Mr. J. G. Lomotey, my Mathematics and Physics teacher at Government Secondary School Karu - Abuja, for teaching me to "think in concepts" and laying the foundation for my academic pursuits. Words cannot express how grateful I am for your selflessness, wisdom and grace. I also thank Dr. Kenneth Li-Minn Ang, for introducing me to research and inspiring me.

To many other friends, family, mentors and well-wishers who I cannot mention due to space constraints, I appreciate and deeply acknowledge all your support.

# Abstract

This thesis uniquely addresses challenges of bandwidth management in cellular networks. The need for enhanced frequency assignment strategies in Long term evolution (LTE) systems arises due to the limiting effects of intercell interference (ICI). In this study, the realistic scenario of irregular network coverage patterns is considered, and in addition, Heterogeneous cellular networks (HetNets). Firstly, extensive analysis using simulations is presented for static frequency reuse (FR) techniques in irregular Homogeneous (single-tier) cellular networks. Investigation was carried out over several network positional and deployment layouts. Second, a model is developed for irregular networks by defining frameworks for their location parameters and relationships, FR bandwidth and power assignment, and the probability of interference in partitioned FR schemes. A novel Geometric FR (GeoFRe) algorithm is then proposed for single-tier networks with random BS placements. Third, an optimization framework based on user fairness is proposed and implemented for single-tier networks based on the concept of virtual UEs in different BS regions. Finally, a framework for HetNets is presented where macro and small BS deployments have imperfect coverage grid patterns. Performance analysis is then carried out for two implementations of the Soft FR (SFR) algorithm. Results from this research provide detailed analysis on impact of BS irregularity on UE performance under FR schemes, a simplified framework for modelling irregular macro BS, an improved FR model, accurate computations for the area of irregular network coverage patterns for intelligent bandwidth assignment, an optimization framework to improve user fairness (and edge UE performance) in single-tier networks and an FR model with performance analysis for irregular HetNets.

# Contents

**List of Figures** **x**

**List of Tables** **xii**

**Nomenclature** **xiii**

**1 Introduction** **1**

1.1 Problem description . . . . . 3

1.2 Research Objectives . . . . . 4

1.3 Scope of Work . . . . . 4

1.4 Publications . . . . . 5

1.5 Thesis Outline . . . . . 6

**2 Theory and Literature Review** **8**

2.1 Introduction . . . . . 8

2.2 Description of network entities . . . . . 8

2.2.1 BS placement models . . . . . 9

2.2.2 Uniform UE distribution models . . . . . 10

2.3 LTE and LTE-Advanced Networks . . . . . 10

2.3.1 OFDMA . . . . . 11

2.4 Interference in OFDMA cellular networks . . . . . 11

2.4.1 Inter-Cell Interference Coordination . . . . . 12

2.4.2 Resource allocation vs Interference mitigation . . . . . 12

2.5 Frequency Reuse algorithms . . . . . 13

2.5.1 Integer frequency reuse . . . . . 13

2.5.2 Fractional frequency reuse . . . . . 14

2.5.3 Soft frequency reuse . . . . . 14

2.5.4 Operational classification of partitioned FR . . . . . 15

2.6 Heterogeneous Cellular Networks . . . 16
2.7 Metrics for Performance measurement . . . 16
2.7.1 Signal-to-Interference-plus-noise ratio . . . 16
2.7.2 Signal outage probability . . . 17
2.7.3 Capacity . . . 17
2.8 Modelling and design approaches . . . 17
2.8.1 Monte Carlo model . . . 17
2.8.2 Stochastic geometry model . . . 18
2.8.3 Single-cell linear model . . . 18
2.8.4 Comparison of models and design approaches . . . 18
2.9 Important system parameters . . . 19
2.9.1 Cell center classification . . . 19
2.9.2 Power ratio . . . 19
2.9.3 Edge bandwidth allocation . . . 19
2.9.4 Other parameters . . . 19
2.10 Related research . . . 20
2.10.1 Performance analysis studies . . . 20
2.10.2 Modified FR algorithms . . . 20
2.10.3 Optimization via iterative algorithms . . . 22
2.10.4 Multiobjective Optimization . . . 24
2.10.5 Stochastic Optimization . . . 24
2.10.6 Summary of Related research . . . 24

**3 Performance Analysis of Frequency Reuse Algorithms 30**

3.1 Introduction . . . 30
3.2 Previous research on FR performance analysis . . . 31
3.3 Overview of frequency reuse algorithms . . . 32
3.4 Simulation Parameters . . . 34
3.4.1 Performance parameters . . . 34
3.4.2 Basic BS parameters . . . 35
3.4.3 Reference BS consideration . . . 36
3.4.4 Grouping of UEs . . . 38
3.5 Irregular BS model . . . 39
3.6 Macro BS network scenarios . . . 40

3.7 Investigating the impact of center radius $r_c$ . . . 41
3.7.1 Case study 1: Single-tier hexagonal BS . . . 41
3.7.2 Case study 2: Single-tier hexagonal BS with dense UE deployment . . . 47
3.7.3 Case study 3: Single-tier irregular BS . . . 49
3.8 Investigating the impact of power ratio, $\mu_{m,s}$ . . . 54
3.8.1 Case study 4 . . . 55
3.9 Investigating the impact of edge bandwidth $f_{e,i}$ . . . 57
3.9.1 Case study 5 . . . 57
3.10 Chapter summary . . . 58

**4 Geometric Frequency Reuse for Irregular Single-tier Networks 59**
4.1 Introduction . . . 59
4.2 Location model . . . 60
4.2.1 Coordinate Locations . . . 60
4.2.2 Relationship between locations . . . 61
4.2.3 Relating UEs to Sectors within BSs . . . 61
4.2.4 Distance between an interfering Macro BS to $U$ . . . 61
4.2.5 BS positional relationships . . . 62
4.3 FR resource allocation model . . . 63
4.3.1 Transmit power for partitioned FR schemes . . . 64
4.3.2 Bandwidth overlap for partitioned FR schemes . . . 65
4.4 Signal-to-interference-plus-noise ratio equations . . . 66
4.4.1 Reuse-1 SINR . . . 66
4.4.2 Reuse-3 SINR . . . 67
4.4.3 FFR SINR . . . 68
4.4.4 SFR SINR . . . 69
4.5 Capacity equations . . . 70
4.5.1 Reuse-1 Capacity . . . 70
4.5.2 Reuse-3 Capacity . . . 70
4.5.3 FFR Capacity . . . 71
4.5.4 SFR Capacity . . . 71
4.6 Spectral Efficiency equation . . . 71
4.7 Analysis of SFR equation with $\beta$ component . . . 72

4.8 Geometric FR algorithm: GeoFRe . . . 73
4.8.1 Computing candidate vertices . . . 73
4.8.2 Testing and selecting vertices . . . 77
4.8.3 Area computation . . . 78
4.8.4 Bandwidth Assignment . . . 79
4.9 Results . . . 80
4.9.1 Network scenarios . . . 80
4.9.2 Testing Area computation . . . 81
4.9.3 Testing Bandwidth from GeoFRe . . . 82
4.10 Chapter summary . . . 84

**5 Optimal configuration for SFR in Irregular Cellular Networks 85**
5.1 Introduction . . . 85
5.2 System Model . . . 86
5.2.1 Location Parameters . . . 86
5.2.2 Power parameters . . . 87
5.2.3 Interference parameters . . . 87
5.2.4 Performance parameters . . . 88
5.3 Optimization problem . . . 89
5.4 Results and Analysis . . . 90
5.5 Chapter Summary . . . 92

**6 Frequency Reuse model for Heterogeneous Cellular Networks 93**
6.1 Introduction . . . 93
6.2 Definition of entities . . . 93
6.3 HetNet Location model . . . 95
6.4 FR model . . . 96
6.4.1 Single tier case . . . 96
6.4.2 HetNet FR model: Variant-1 . . . 98
6.4.3 HetNet FR model: Variant-2 . . . 98
6.5 Signal-to-interference-plus-noise ratio equations . . . 99
6.5.1 SFR HetNet Variant-1 . . . 99
6.5.2 SFR HetNet Variant-2 . . . 101
6.6 Capacity equations . . . 102

6.7 Results and Analysis . . . . . 102
6.7.1 Simulation Parameters . . . . . 102
6.7.2 Effect of power ratio on SINR and Capacity . . . . . 103
6.7.3 Effect of edge Frequency on Capacity . . . . . 106
6.7.4 Chapter summary . . . . . 109

**7 Conclusion and Further research** **110**
7.1 Conclusion . . . . . 110
7.2 Further research . . . . . 112

**References** **114**

# List of Figures


1.1 Heterogeneous cellular network . . . . . 2

2.1 BS layout scenarios . . . . . 10
2.2 Integer frequency reuse schemes . . . . . 14
2.3 Partitioned frequency reuse schemes . . . . . 15

3.1 Coverage Layout for FR schemes . . . . . 33
3.2 Power/Bandwidth allocation for FR schemes . . . . . 34
3.3 Network showing reference BS and interfering BS . . . . . 36
3.4 Comparing average SINR for all BS and reference BS . . . . . 38
3.5 Distance relationship between BS . . . . . 39
3.6 Coverage area plots for macro BS case studies . . . . . 41
3.7 Performance for Single-tier regular BS, full UE: varying $r_c$ . . . . . 42
3.8 Group 1 and Group 2 UEs Locations . . . . . 44
3.9 Number of UEs per Group and Region . . . . . 44
3.10 SFR analysis for Case 1 . . . . . 45
3.11 Performance for Single-tier regular BS, dense UE: varying $r_c$ . . . . . 48
3.12 Performance for Single-tier irregular BS 1 (scenario 2), full UE: varying $r_c$ . . . . . 50
3.13 Performance for Single-tier irregular BS 2 (scenario 3), full UE: varying $r_c$ . . . . . 52
3.14 Performance for Single-tier irregular BS 3 (scenario 4), full UE: varying $r_c$ . . . . . 53
3.15 Performance for SFR in all scenarios, full UE: varying $\mu_{m,s}$ . . . . . 55
3.16 Single-tier regular BS, full UE: varying $f_{e,i}$ . . . . . 57

4.1 Positional layout of Network entities . . . . . 60
4.2 Distance relationship between macro BS . . . . . 62

4.3 Power/Bandwidth allocation for FR schemes . . . . . 63
4.4 SFR Analysis over $\mu_{m,s}$ for center UE (Hexagonal BS) . . . . . 72
4.5 SFR Analysis over $f_{e,i}$ for center UE (Hexagonal BS) . . . . . 72
4.6 Vertices of sector $S_1$ of ref. BS $M$ . . . . . 75
4.7 Network layout scenarios showing reference BS $M$ and interfering BSs $I$ 81
4.8 Testing Area of edge region using Algorithm 5 . . . . . 82
4.9 Results for GeoFRe algorithm . . . . . 83

5.1 Layout of Irregular Macro BS networks . . . . . 86
5.2 SFR Power and Bandwidth allocation for 3 Macro BSs . . . . . 87
5.3 Comparison of capacity (in bps) differences for $CoG$ UE . . . . . 90
5.4 Capacity (in bps) differences with optimal $\mu_{m,i}$ . . . . . 91

6.1 Positional layout of HetNet entities . . . . . 94
6.2 SFR: Power vs Bandwidth allocation for three sectors of $M$ . . . . . 97
6.3 SFR HetNet Variant-1: Pico BS use full bandwidth . . . . . 98
6.4 SFR HetNet Variant-2: Pico BS use macro center bandwidth . . . . . 99
6.5 SINR and Capacity when $\mu_{m,s}$ is varied . . . . . 104
6.6 SINR for Macro UEs when $\mu_{m,s}$ is varied . . . . . 105
6.7 Capacity (in bps) for Macro UEs when $\mu_{m,s}$ is varied . . . . . 105
6.8 SINR for Pico UEs when $\mu_{m,s}$ is varied . . . . . 106
6.9 Capacity (in bps) for Pico UEs when $\mu_{m,s}$ is varied . . . . . 106
6.10 SINR and Capacity when edge frequency is varied . . . . . 107
6.11 Capacity (in bps) macro UEs when $\psi_i$ is varied . . . . . 108
6.12 Capacity (in bps) for pico UEs when $\psi_i$ is varied . . . . . 108

# List of Tables


2.1 Review Summary . . . . . 25

3.1 General parameters for Simulation . . . . . 36
3.2 Average SINR comparison . . . . . 37
3.3 Location parameters for simulation case studies . . . . . 40
3.4 Case study 1 parameters . . . . . 42
3.5 Case study 2 parameters . . . . . 48
3.6 Case study 3 parameters . . . . . 50
3.7 Case study 4 parameters . . . . . 54
3.8 Case study 5 parameters . . . . . 58

4.1 Bandwidth and Power allocation to a UE, $U$ under FR schemes . . . 64
4.2 $\beta$, Probability of interference in fractional-based FR . . . . . 66
4.3 Parameters for Network case studies . . . . . 80
4.4 Parameters and Results . . . . . 82

6.1 Parameters for SFR HetNet Analysis . . . . . 103

# Nomenclature

### Symbols

| | |
|---|---|
| $\alpha$ | Pathloss exponent |
| $\beta$ | Probability of interference in fractional-based FR |
| $\beta_{c,c}$ | Probability of interference from the center transmission of an interfering BS to the center region of a reference base station |
| $\beta_{c,c}$ | Probability of interference from the edge transmission of an interfering BS to the center region of a reference base station |
| $\gamma r$ | Distance between interfering base station and reference macro base station |
| $\lambda r$ | Distance between reference macro base station and a user equipment connected to it |
| $\mathcal{F}$ | Total system bandwidth |
| $\mathcal{F}_{e,i}$ | Total allocated bandwidth to edge region of sector $S_i$ |
| $\mathcal{F}_{e,max}$ | Maximum bandwidth in edge region |
| $\mathcal{F}_{prb}$ | Bandwidth allocation per PRB |
| $\mathcal{F}_{prb}$ | Bandwidth per physical resource block |
| $\mathcal{F}_{u,max}$ | Maximum allowable bandwidth per user equipment |
| $\mathcal{I}$ | Set of interfering macro base stations |
| $\mathcal{M}$ | Set of Macro base stations |
| $\mathcal{Q}$ | Set of small BS in a HetNet scenario |

| | |
|---|---|
| $\mu_{m,s}$ | Power ratio in sector $S_i$ |
| $\omega$ | Angle formed from interfering base station and reference line $L$ |
| $\sigma^2$ | Noise power |
| $\theta$ | Angle formed from a user equipment connected to the reference macro base station and reference line $L$ |
| $C_{m,i}$ | Total number of connected center user equipment in sector $S_i$ |
| $d_a$ | Distance between reference macro base station and interfering macro base station with index $a$ |
| $d_{a,b}$ | Distance between any two interfering macro base stations with indexes $a$ and $b$, which interfere user equipment in reference macro base station |
| $D^c_{g,j}$ | Distance between the $jth$ interfering BS and the Virtual (Center of gravity) user at the center region of the reference base station |
| $D^e_{g,j}$ | Distance between the $jth$ interfering BS and the Virtual (Center of gravity) user at the edge region of the reference base station |
| $d_{min}$ | Minimum allowable distance between two macro base stations |
| $D_{u,I}$ | Distance between a user equipment connected to reference base station and an interfering base station |
| $E_{m,i}$ | Total number of connected edge user equipment in sector $S_i$ |
| $f_{m,i}$ | Bandwidth assigned to a user equipment $U$ from sector $S_i$ of reference macro base station |
| $G_{u,x}$ | Pathloss component between base station with index $X$ and user equipment $U$ |
| $h_{u,x}$ | Fading component between base station with index $X$ and user equipment $U$ |
| $I_a$ | Neighbouring base station with index $a$ to reference base station |
| $L$ | Horizontal reference line from reference macro base station |

| | |
|---|---|
| $M$ | Index for reference macro base station |
| $N_{e,prb}$ | Number of physical resource blocks used in the edge region of a sector |
| $N_{m,i}$ | Total number of connected user equipment in sector $S_i$ |
| $N_{prb}$ | Total number of system physical resource blocks |
| $P_{e,i}$ | Total power budget of edge region of sector $S_i$ |
| $p_{m,i}$ | Signal power transmitted to a user equipment $U$ from sector $S_i$ of reference macro base station |
| $p^c_{m,i}$ | Signal power transmitted to a center user equipment $U$ from sector $S_i$ of reference macro base station |
| $p^e_{m,i}$ | Signal power transmitted to an edge user equipment $U$ from sector $S_i$ of reference macro base station |
| $P_{m,s}$ | Total power budget of sector $S_i$ |
| $P_{u,max}$ | Maximum signal transmit power allowed from a macro base station to a user equipment |
| $r$ | Macro base station coverage radius obtained from hexagonal base station placement |
| $S_i(S_1, S_2, S_3)$ | Index for sectors of reference macro base station |
| $S_j$ | Sector of a neighbouring macro base station with index $j$ |
| $U$ | User equipment connected to reference macro base station |
| $U_g$ | Virtual user located at the center of gravity of a base station region |
| $U_{c,g}$ | Virtual center user located at the center of gravity of the center region of a base station |
| $U_{e,g}$ | Virtual edge user located at the center of gravity of the edge region of a base station |
| $X_A(x_a + jy_b)$ | Cartesian coordinate for any network entity (base station or user equipment |

**Acronyms/Abbreviations**

| | |
|---|---|
| 1G | First Generation |
| 2D | Two dimensional |
| 4G | Fourth Generation |
| 5G | Fifth Generation |
| ACM | Adaptive coding and modulation |
| BS | Base station |
| CoG | Center of gravity |
| CSI | Channel state information |
| DL | Downlink |
| eICIC | enhanced Intercell interference coordination |
| FFR | Fractional Frequency Reuse |
| FR | Frequency Reuse |
| GeoFRe | Geometric Frequency Reuse |
| HetNet | Heterogeneous Cellular Network |
| ICI | Intercell interference |
| ICIC | Intercell interference coordination |
| IFR | Integer Frequency Reuse |
| LTE | Long term evolution |
| LTE-A | Long term evolution-advanced |
| M2M | Machine-to-machine |
| MIMO | Multiple-input and Multiple-output |
| OFDMA | Orthogonal frequency division multiple access |
| PRB | Physical resource block |

| | |
|---|---|
| SFR | Soft Frequency Reuse |
| SINR | Signal-to-interference-plus-noise ratio |
| UE | User equipment |

# Chapter 1

# Introduction

There has been significant evolution in cellular network technology over the last three decades. Initial analogue telecommunication systems, termed first generation (1G) networks offered mainly voice communication in the 1980's. Most of the current networks target achieving fourth generation (4G) specification by providing more sophistication, connectivity and high speed data services in addition to voice communication. Intelligent user equipment (UE) such as smartphones and tablets are not only now ubiquitous but also place tremendous data demand on the networks [1–4].

A snapshot of the current state of cellular networks can be extracted from a recent report from CISCO [5]. It was stated that there were 8 billion mobile devices and connections at the end of 2016, with 429 million added alone that year. Projections are that by 2021, there will be a monthly data traffic of 49 exabytes (billion gigabytes) from 11.6 billion mobile devices (averaging 20.4Mbps per connection speed). This phenomenon has been described using several phrases like "data explosion", "data deluge" and "capacity crunch". Developing techniques to massively enhance network capacity is of importance to service providers and researchers; especially for future fifth generation (5G) networks [6–10].

One of such techniques is Frequency reuse (FR) which exploits the characteristic of electromagnetic signal power to drastically fall with distance. Hence, the same frequency resource can be utilized at different base stations (BSs) spatially separated thereby reducing the effects of spectrum capacity and making more bandwidth available in the network. A straightforward method to improve capacity is by deploying high bandwidth reuse among BSs in cellular networks. While this improves the

overall spectral efficiency, there is increased intercell interference (ICI) to UEs at BS coverage boundaries termed edge UEs. Consequently, the complete frequency reuse (FR) scheme (Reuse-1) has become less attractive than emerging alternative schemes involving partial reuse in different BS coverage regions. These include the popular fractional frequency reuse (FFR) and soft frequency reuse (SFR) techniques which require partitioning BS regions and resources before matching them in resource allocation. FR is increasingly an important factor that determines UE performance in cellular networks. FR consideration also highlights the network design complexity arising from the conflicting performance results of different system goals. On one hand, UE services are driving a need for high spectral efficiency and on the other, edge performance consideration pushes for network fairness through reduced ICI on edge UE [11, 12]. The need for balance motivates a key focus of this research; the extensive analysis and optimization of dynamic partial FR schemes.

In addition to identifying the importance of FR, it is worth noting another key technology gaining widespread attention for capacity enhancement in 4G (and 5G) networks. Extreme BS densification, where large number of BSs are deployed is gradually achieving prominence in modern cellular network architectures. This paradigm is encapsulated in the concept of heterogeneous cellular networks (HetNets) where different classes (tiers) of BSs coexist in the cellular network, shown in Fig. 1.1.

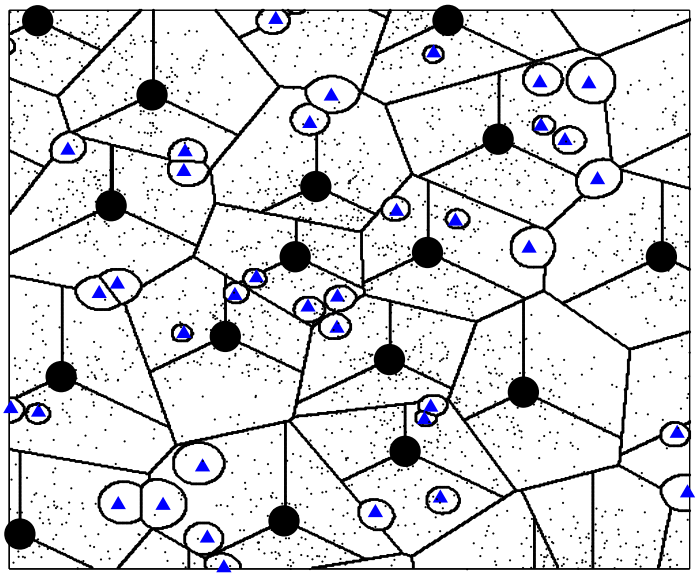

Figure 1.1: Heterogeneous cellular network

The first tier consists of macro BSs (depicted as solid circular shapes), while the second tier consists of small BSs (represented as solid triangles). The traditional macro BSs which are physically massive and have high transmit powers, are overlaid with smaller BS entities having smaller transmit powers such as pico, micro and femto BSs. By allowing these smaller BSs have full BS functionality and complete system bandwidth, HetNets guarantee improvement in network coverage and capacity. However, this comes with the added overhead of increased complexity in network modelling and design [13–17]. The complexity increases when FR implementation is extended into HetNet scenarios, also a consideration of this study.

So far, the impacts on network performance from the number of BS entities (via HetNets) and their bandwidth allocation algorithms (via FR) have been highlighted. Furthermore, in the modelling, analysis and design of cellular networks, consideration of the layout of BSs is unavoidable. Macro BSs have typically been modelled as regularly placed perfect hexagonal grids. However, since this is rarely the case in realistic network deployments, deployment models for irregular networks need to be developed. In this research, a new system model is proposed for irregular cellular networks encompassing both single-tier networks and HetNets.

Generally, there are three main approaches used for analysis of HetNets; stochastic geometry, simulations and the single cell linear model. Linear model was adopted in this research for the benefit it provides for quick analysis of specific system scenarios. The main performance parameters used are signal-to-interference-plus-noise ratio (SINR) and capacity. Specifically, the model is based on the long term evolution (LTE) and LTE-Advanced (LTE-A) network which is the dominant 4G technology that employs orthogonal frequency division multiple access (OFDMA).

## 1.1 Problem description

The high density of intelligent devices on current networks introduce stiff competition for scarce bandwidth. Smartphones, tablets, PCs and machine-to-machine (M2M) gadgets are placing demands on BSs for high data rates. This is required for the data-intensive applications they run such as multimedia streaming, heavy file downloads and online gaming. A natural challenge that arises is the task of optimizing networks by enhancing capacity to meet device requirements. This problem can be considered and tackled via several approaches. In this study, analysis of network

structure and model is considered as it has evolved into more complex formats due to different BS tiers, irregular BS deployments and irregular UE distribution patterns. The specific need to develop more accurate system models for cellular networks is identified and tackled. These include models to capture irregular HetNets employing FR, composed of BSs with random distribution patterns and varying parameter assignments. It is of benefit that the techniques also represent the unique conditions of specific BSs at any particular point in time. Compared with models that represent only network snapshots of several BSs, these models aid the implementation of tailored distributed optimization schemes that are flexible. A second problem is the improvement of current FR algorithms which define basic BS resource parameters of frequency and power. It has been shown that these variables alone do not guarantee optimal performance especially for vulnerable edge UEs. Therefore, a strong motivation for this research was to add location of network entities as a parameter for improving basic FR algorithms.

## 1.2 Research Objectives

The study aims to develop techniques for describing and enhancing irregular cellular networks that implement resource allocation via bandwidth reuse. To achieve this, the objectives are outlined thus:

- Performance analysis using simulations of FR implementation in cellular networks with irregular BS placements.
- Design and analyse network location models defined on the coordinate system for irregular cellular networks.
- Design FR-based bandwidth assignment models and new performance metrics describing FR schemes in irregular single-tier networks and HetNets.
- Develop enhanced partitioned FR algorithms based on the geometry properties of BS coverage patterns in cellular networks.

## 1.3 Scope of Work

Cellular networks are complex systems composed of several entities having numerous parameters. Research in the field typically involves techniques to improve spectral

efficiency such as the multiple-input and multiple-output (MIMO) technology, and for improving network efficiency e.g HetNets. In this research, the focus is on improving network efficiency through consideration of bandwidth allocation at BSs. The resource allocation can be analysed based on the frequency assignments among BSs or the assignments from BSs to their connected UEs. The study is restricted to the first case and the FR algorithms considered are Reuse-1, Reuse-3, FFR and SFR. The underlying focus of this research is to investigate and develop models and techniques that enhance capacity of cellular networks. Two existing technologies are considered. Intelligent FR improves network capacity by performance enhancement through intelligent allocation of the BS resources (frequency and power). On the other hand, HetNets guarantee capacity enhancement through provision of more frequency resources via increase in the number of BS in the network. Whereas in FR, the concern is mainly about interference mitigation, HetNets focuses on resource (frequency) addition. These technologies are considered separately and then jointly to highlight their models, challenges and the system improvements that can be achieved when combined together.

## 1.4 Publications

The research papers published in the course of this study are listed below

- A. Adejo and S. Boussakta, "Performance analysis of frequency reuse techniques under varying cellular network scenarios," in 2016 IEEE Wireless Communications and Networking Conference, April 2016, pp. 1-6. [18].

- A. Adejo, S. Boussakta, and J. Neasham, "Interference modelling for soft frequency reuse in irregular heterogeneous cellular networks," in 2017 Ninth International Conference on Ubiquitous and Future Networks (ICUFN), July 2017, pp. 381-386. [19].

- A. Adejo, J. Hussein, and S. Boussakta, "Optimal transmit power configuration for soft frequency reuse in irregular cellular networks," in 2017 Ninth International Conference on Ubiquitous and Future Networks (ICUFN), July 2017, pp. 711-713. [20].

## 1.5 Thesis Outline

In Chapter two, an overview is presented of relevant literature to the study. Descriptions of the key concepts, terminologies and technologies are first presented. Furthermore, a survey is presented of related research around performance analysis of FR techniques, improved FR algorithms and optimization schemes.

In Chapter three, detailed performance analysis is provided for frequency reuse algorithm implementations in single-tier cellular networks. The main FR techniques (integer and partitioned FR) are described and investigations are made on the resulting network performance. The results show that it is useful to carry out analysis on specific base station regions. The benefits of grouping UEs is also highlighted, as performance is hugely dependent on UE locations. More insightful analysis are obtained by considering UE groups as opposed to average results for UEs within a BS. A model was presented for irregular macro base stations that takes into account the maximum proximity allowed, then network scenarios were developed based on the model. The investigation of frequency reuse involved considering the impact of base station parameters like the center radius threshold, power ratio and bandwidth allocation. Results showed the varying performance among different algorithms and user groups, highlighting the need for optimal algorithms for varying network scenarios.

In Chapter four, analytical derivations are provided for irregular cellular networks. The key network entities including base stations and user equipment are considered and a location model is developed by considering a reference base station. The parameters for other neighbouring base stations and connected users are then defined based on their relationship between the reference base station. Furthermore, interesting relationships can also be defined between neighbouring base stations and users connected to the reference base station. Investigation into the resource parameters in partitioned frequency reuse schemes revealed interference probabilities that arise. Based on this consideration, a new model was developed for partitioned frequency reuse representation that captures the power and bandwidth rules accurately. By combining the location model with the resource allocation model, new equations for performance parameters were derived. A modified frequency reuse algorithm called Geometric frequency reuse was then proposed as a means of improving the static schemes. The algorithm consists of four sub-algorithms that determine the

vertices of irregular base station regions and the area of edge regions. Based on the computed area, intelligent bandwidth allocation is made. The results showed that for the soft frequency reuse scheme, the proposed geometric frequency reuse guaranteed optimal selection of bandwidth for capacity and spectral efficiency.

In Chapter five, optimization of power configuration parameters for single-tier cellular networks deploying SFR was presented. The concept of a virtual UE was adopted where performance of all UEs in a BS region is approximated by performance of the most central UE. In addition, the minimum acceptable performance for edge UEs was defined using a fairness metric. The irregular location and resource allocation models were then used to develop an optimization framework.

In Chapter Six, the irregular base station model and resource allocation model was extended to the case of heterogeneous cellular networks. New equations for user performance were derived for the macro base station users as well as the pico base station users at different locations. This was based on two variants of the soft frequency algorithm with varying limits on the bandwidth overlaps between base station tiers. Network scenarios were generated using the models and performance analysis was carried out on the macro and pico user performance under both variants of soft frequency reuse that were assumed. Results provide useful insights into the performance of heterogeneous cellular networks.

# Chapter 2

# Theory and Literature Review

## 2.1 Introduction

In this chapter, the theoretical background and review of relevant literature for the research are provided. Descriptions are provided for LTE systems, ICI, FR algorithms and HetNets. Network system models are then mentioned; covering areas like deployment and positioning models for system entities, performance assessment metrics, design approach models and key optimization parameters. Finally, an overview of previous studies in the area of analysis and optimization of FR implementation in cellular networks is presented.

## 2.2 Description of network entities

**Base station (BS):** A BS is an equipment in a cellular network which has sustainable power supply and performs critical network tasks. These include assigning bandwidth to UEs under its coverage and providing reliable backhaul connection to the core network [16]. BSs can be classified based on their physical size, transmit powers, energy consumption, coverage areas and type of backhaul. Macro BSs have very big sizes, high transmit powers and energy consumption and massive coverage areas. Smaller BS entities like the pico, micro and femto BSs have smaller sizes, transmit powers and coverage areas. Pico BSs can be deployed in homes and can be configured in open or closed access modes.

**User equipment (UE):** UE are the mobile devices which connect to BSs, re-

ceiving resources (bandwidth and power) to drive its communication applications. UEs transmit at much lower power levels than BS. They include phones, tablets, mobile PCs and M2M gadgets.

### 2.2.1 BS placement models

**Regular Network Models**: Cellular networks have usually been modelled using BSs whose locations are arranged such that their coverage areas form hexagonal patterns. The BSs with either omnidirectional or tri-sector antennas are regularly placed with properly calculated positions. Figs. 2.1(a) and 2.1(b) show regular macro BS placements in single-tier networks and HetNets respectively deploying tri-sector antennas. In this format, each macro BS is surrounded by six equally spaced macro BSs in the closest set of neighbours. The second set of neighbours consists of twelve equally spaced BSs at a larger distance. Each BS (omnidirectional mode) or BS sector (tri-sector mode) shares its complete bandwidth to connected UEs in its coverage region. These frequency allocations to UEs are carried out via BS transmissions on specific power levels. Hence the bandwidth/power pair can be considered as the basic resource in the downlink transmission from the BSs to UEs. The bandwidth/power assignments of a particular BS and those of its neighbours combine to determine UE performance or quality of service experienced by UEs. This is because interference occurs on a UE when a neighbouring BS transmits signals over the same frequencies as those which the UE connects to its parent BS.

**Irregular Network Models**: Real deployments of cellular networks do not always consist of perfect hexagonal grids. Figs. 2.1(c) and 2.1(d) show irregular coverage plots for a homogeneous network and HetNet respectively. The irregular nature of BS placements is a more crucial consideration in the design and analysis of HetNets [21].

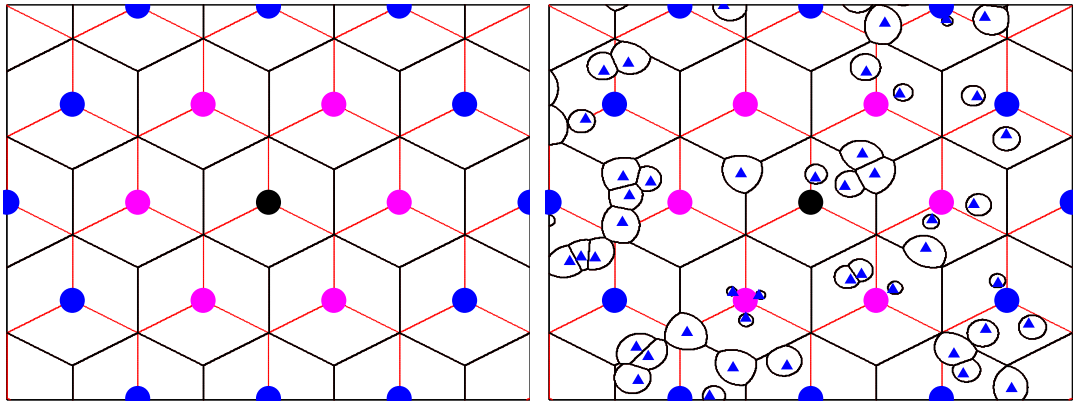

(a) Regular homogeneous network

(b) Regular macro HetNet

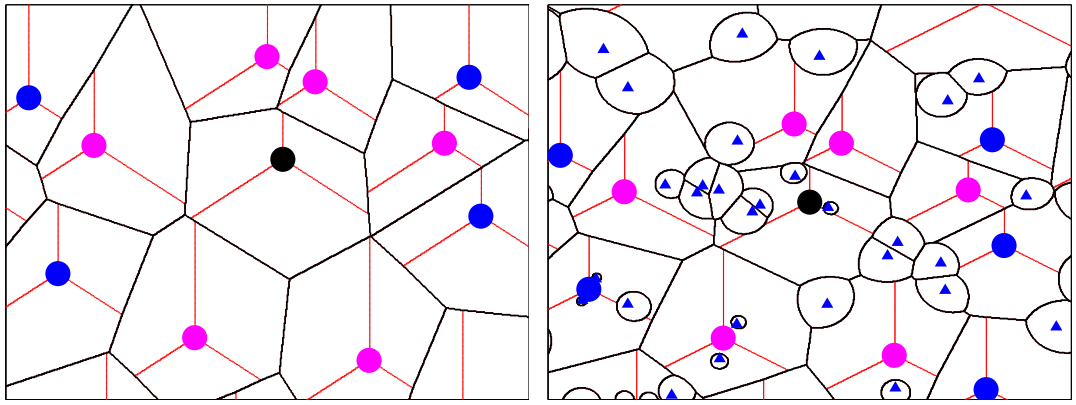

(c) Irregular homogeneous network

(d) Irregular HetNet

Figure 2.1: BS layout scenarios

### 2.2.2 Uniform UE distribution models

The placement of UEs in the coverage area are usually modelled independently and uniformly distributed with a normalized intensity $\lambda_i$ (measured in users per unit area). The probability distribution of the number of UEs, $n_u$ located in a coverage area $A$ follows a poisson distribution thus [22]:

$$Pr\{n_u = M\} = \exp^{-\lambda_i A} \frac{(\lambda_i A)^M}{M!} \tag{2.1}$$

## 2.3 LTE and LTE-Advanced Networks

The LTE and LTE-Advanced networks are the prevalent 4G systems deployed worldwide. OFDMA is employed in the donwlink and high performance specifications are defined for these networks. For example, a target spectral efficiency for LTE-A systems of 30b/s/Hz is required [23]. In LTE, the SINR observed from reference signals

within the OFDMA structure are used for estimating channel quality [24].

### 2.3.1 OFDMA

In OFDMA systems like the LTE, both frequency and time resources are split into units of different sizes. The total bandwidth is divided into channels which are further divided into clustered orthogonal subcarriers. Similarly, either 6 or 7 slots comprising consecutive OFDM symbols make up each time division. Furthermore, consecutive slots form a frame and a number of consecutive frames make a superframe. The smallest resource unit that can be assigned to a UE which lasts the duration of a time slot is called a physical resource block (PRB) [11].

## 2.4 Interference in OFDMA cellular networks

It is widely known that cellular networks are becoming more data-driven and are not exclusively voice oriented. As a result, the system performance is now more dependent on interference than on the radio propagation environment [25]. Considering the BS bandwidth resource allocation to UE, interference occurs when neighbouring BS regions reuse the same PRBs. Interference is directly proportional to the amount of FR permitted, so it is severe in the Reuse-1 scheme. As interference severely limits the system capacity, it is an issue of concern in the design and optimization of cellular networks. In cellular networks, interference can be classified into two [11]:

- **Intra-cell interference**: occurs within a BS region when more than one UE is served on similar bandwidth (frequency channels). Adjacent frequencies in addition to power leakages between channels give rise to this type of interference.

- **Inter-cell interference**: occurs between different BS regions which utilize the same frequency channels thereby creating disruptions to each other.

Intra-cell interference is drastically reduced in OFDMA-based networks and the major challenge is inter-cell interference usually abbreviated as ICI. The impact of ICI is more severe on edge UEs, i.e the UEs located at the BS coverage boundaries [11]. Based on originating source, ICI can be classified into:

- **Downlink interference** which is initiated from BS and occurs on UE.

- **Uplink interference:** Originates from UE and occurs at BS.

Finally, classification of ICI (in HetNets) can be classified based on the tiers of the origin and destination thus [23]:

- **Co-tier interference:** This occurs between network entities that are in the same BS tier, either in the uplink or downlink. For example, a UE connected to a femto BS could cause uplink interference to neighbouring femto BSs.
- **Cross-tier interference:** This occurs between network entities in different tiers e.g between a femto BS and a macro UE.

### 2.4.1 Inter-Cell Interference Coordination

The techniques to alleviate the impact of ICI in OFDMA-based networks are collectively termed Inter-cell interference coordination (ICIC), and also enhanced ICIC (eICIC). In [11], a comprehensive survey is presented on this subject. ICIC can be classified into interference mitigation and interference avoidance schemes. Interference mitigation involves schemes that reduce interference impact during signal transmission or after reception. They include interference randomization, interference cancellation, adaptive beamforming, collaborative frequency scheduling, power control and intelligent spectrum access. This research focuses on interference avoidance which refers to the different frequency reuse planning algorithms employed to reduce interference via allocation of frequency and time resource [11, 23, 26].

### 2.4.2 Resource allocation vs Interference mitigation

It is worth comparing the concept of resource allocation with interference coordination which this research falls under. Resource allocation is a broad term that describes how the available system resources are shared progressively. The first allocation procedure involves sharing of resources between BS or BS geographical reigons. In the second, resources within a BS are allocated to connected UE [27]. This study is restricted to the first stage of resource allocation specifically related to bandwidth planning which are discussed in the proceeding section.

## 2.5 Frequency Reuse algorithms

FR will be discussed in this section for homogeneous (single-tier) cellular networks comprising only macro BS. FR algorithms can be classified broadly into integer FR schemes and fractional-based or partitioned FR schemes. These define the bandwidth allocation procedure for the entire region of either a BS (using omnidirectional antenna) or a BS sector (using sectoral antenna). In integer FR schemes like the Reuse-1 and Reuse-3, whole BS regions use the same reuse factor. For the partitioned FR schemes like fractional frequency reuse (FFR) and soft frequency reuse (SFR), BS regions are divided into geographical parts and different reuse factors are used in each part. The BS regions are usually partitioned into two (center and edge), and UEs are then classified based on the region they are located, to center UEs and edge UEs respectively. Bandwidth and power allocation is also performed differently for the different UE classes. This introduces greater control over ICI and network performance [11].

### 2.5.1 Integer frequency reuse

**Reuse-1**: As Fig. 2.2(a) shows, the entire bandwidth is reused in all BSs and sectors. Neighbouring BSs do not partition their frequency allocations and any UE can be assigned any available sub-band. Reuse-1 results in higher spectral efficiency across the whole network, but there is also high ICI especially on UEs at BS edges [11].

**Reuse-3**: Each BS uses a third of the bandwidth as shown in Fig. 2.2(b). Usually, the regions are divided into three sectors based on antenna, hence the use of 3 as reuse factor. Due to reduced overlaps in transmission, ICI falls significantly but at a cost of spectral efficiency [11].

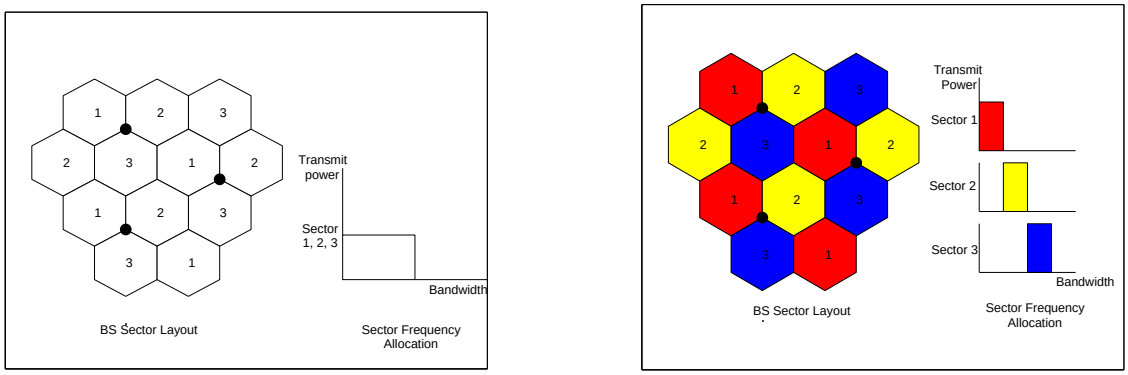


(a) Reuse-1 (b) Reuse-3

Figure 2.2: Integer frequency reuse schemes

In the next sections, the fractional-based FR schemes are explained separately.

### 2.5.2 Fractional frequency reuse

In FFR (also called Strict FR), the BS regions are divided into a minimum of two parts. UEs are also classified based on the number of divisions. Typically, center UEs are UEs located within the interior area of the cell, while edge UEs are those located in the exterior areas closer to the boundaries. Fig. 2.3(a) shows the bandwidth allocation which is thus:

- High reuse factor (low reuse), e.g 3 is used in the edge region such that neighbouring edge UEs from different BS do not interfere with each other. Another key feature is that center UEs do not interfere with edge UEs.
- Low reuse factor (high reuse) is used in the center regions.

This scheme improves the edge UE performance but at the expense of overall network throughput and spectral efficiency [23, 28].

### 2.5.3 Soft frequency reuse

SFR implementation is shown in Fig. 2.3(b). Similar to FFR, in SFR, the BS regions are also divided into a minimum of two regions within which UE are classified and different reuse factors are employed. The unique difference between SFR and FFR

is that in SFR, the center UEs are allowed to utilize the bandwidth of edge UEs connected to neighbouring BSs. This results in better bandwidth efficiency in SFR but at the cost of slightly higher ICI on edge UEs [23, 24, 28–30].

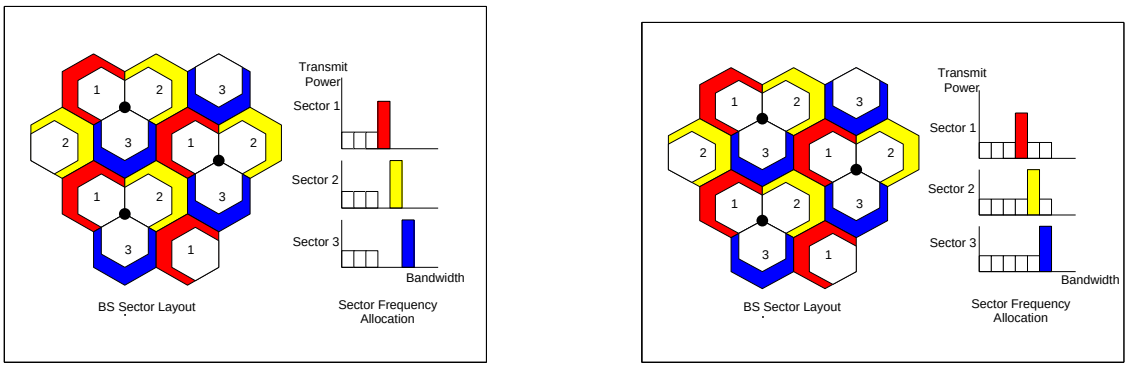


(a) Fractional frequency reuse

(b) Soft frequency reuse

Figure 2.3: Partitioned frequency reuse schemes

### 2.5.4 Operational classification of partitioned FR

The partitioned FR schemes are more complex than integer FR schemes in terms of network implementation. Based on operation, these techniques can be classified into static and dynamic allocation schemes. In static allocation, BS bandwidth and power parameters are fixed and there is no frequent interaction between BSs. Basically, they refer to the standard FFR and SFR when operated over large time-scales. Static techniques are less complex, easy to implement and do not require additional signalling overhead. However, they are not optimal, do not provide the best UE performance and are do not adapt to network changes. Dynamic schemes on the other hand have flexible parameter settings. Bandwidth allocations and power levels can be adjusted and there is coordination among neighbouring BSs. Although dynamic schemes are more complex than the static schemes, they provide better system performance and are more suited for realistic irregular cellular networks [11, 23, 24].

## 2.6 Heterogeneous Cellular Networks

Heterogeneous cellular networks (HetNets), shown in Figs. 2.1(b) and 2.1(d) are a new paradigm in cellular networks motivated by the need for increased capacity. Initial cellular networks consisted entirely of macro BS which are high-power tower-mounted BS. The massive data demand from UE meant that networks had to be expanded by increasing BS density. The addition of macro BS has proven to be not always viable due to high costs and lack of available sites. These challenges are overcome with HetNets, where low-powered BS are used to overlay the macro BS especially in areas with low coverage or heavy traffic. The network then evolves into one composed of a hierarchical deployment of BS in layers [23, 31, 32]. The low-powered BS include micro BS, pico BS, femto BS, relays and distributed antenna systems. Compared to macro BS, they have smaller sizes, transmit powers and coverage areas. However, they offer the same frequency resources as macro BS, providing massive increase in available resources and by extension, spectral efficiency and network capacity [16, 21]. They are integrated into existing cellular networks through wireless backhaul systems (e.g., microwave links) or wired broadband [25]. HetNets introduce more complexities and challenges in the modelling and analysis of cellular networks.

## 2.7 Metrics for Performance measurement

The key metrics for UE performance assessment are discussed in this section.

### 2.7.1 Signal-to-Interference-plus-noise ratio

The SINR refers to the ratio of the received power component on a UE from its connected BS to the received interfering power component from neighbouring BSs. The SINR of any arbitrary UE, $U$ connected to a sector $S_i$ of a reference BS, $M$ (which employs tri-sector antenna) is given by:

$$SINR_u = \frac{p_{u,i} h_{u,i} G_{u,i}}{\sum\limits_{S_j \epsilon \mathcal{J}} p_{u,j} h_{u,j} G_{u,j}}, \tag{2.2}$$

where $p_{u,i}$ is the signal power transmitted to $U$ from $M$, $h_{u,i}$ is the fading component and $G_{u,i}$ is the pathloss based on the distance from $U$ to $M$ with the gain radiation

(based on the angular position of $U$ relative to $M$) added. $\mathcal{I}$ is the set of interfering BSs, while $p_{u,j}, h_{u,j}, G_{u,j}$ are respectively the transmitted power, fading component and pathloss relating $U$ and a sector $S_j$ of any interfering BS $I_j$.

The SINR will differ with each FR scheme, based on the transmit power allocation and the amount of interference permitted. In some previous works, fast fading effects where considered such as in [33], while in other cases the simple exponential pathloss model and small scale fading were considered for simplicity [28].

### 2.7.2 Signal outage probability

Outage probability is also an important metric used to measure UE performance. It is the probability that the instantaneous SINR of a UE is below a threshold, taking into account the serving BS and interfering BSs. [28].

### 2.7.3 Capacity

In practice, UE capacity, also called data rate or throughput can be measured by estimating the channel state information (CSI) using adaptive coding and modulation (ACM). However, to preserve generality and for simplicity, the theoretical Shannon's channel equation has been adopted widely in literature as against throughput mapping through ACM [34]. The capacity which represents the data rate at $U$ is given by:

$$Cap_u = \min[\mathcal{F}_{u,max}, \frac{\mathcal{F}_r}{N_{u,i}}][\log_2(1 + SINR_u)], \tag{2.3}$$

where $\mathcal{F}_{u,max}$ is the maximum allowable bandwidth per UE, set appropriately for each FR scheme. $\mathcal{F}_r$ is dependent on the FR scheme in operation.

## 2.8 Modelling and design approaches

The three different approaches for the modelling and design of cellular networks are discussed in this section.

### 2.8.1 Monte Carlo model

This usually involves the analysis of multiple BS where several network parameters can be considered. These parameters include antenna patterns, ray-traced path loss

models, terrain, cell-specific configuration data and clutter. The method also requires computations of large volumes of data. Iterative techniques and optimization methods like integer programming and genetic programming methods can also be used for system design [25].

### 2.8.2 Stochastic geometry model

This is an approach where statistical analysis is made to characterize network-wide performance through mathematically tractable techniques. It is convenient for modelling non-uniform cellular systems [25], [35], [36].

### 2.8.3 Single-cell linear model

In this approach, a single cell within the network is analysed to capture performance variations within its coverage area. A typical assumption is to consider only the interference from a dominant interfering BS [25].

### 2.8.4 Comparison of models and design approaches

In [25], it is shown that when properly configured, each model can give results that are near accurate to realistic networks. However, the advantage of using any of the models over the others would depend on the key requirement of the analysis. The Monte Carlo model is best suited for analysis specific network challenges by altering network parameters. On the other hand, the strength of the stochastic geometry model is in the area of analysing cell density, transmit powers and path loss, all of which are easily modelled using probability distributions. The linear model is a hybrid of the other two models that considers a single cell and provides a faster analysis than the simulation model. The demerits of the Monte Carlo model include the requirement for large data, high complexity and long time for simulations. The stochastic geometry model has a drawback that it only provides statistical results (usually average network performances) and gives little information about specific BS performance. Finally for the linear model, its ease and simplicity of analysis is limited to the assumption of a single dominant interferer.

## 2.9 Important system parameters

In this section, the system parameters considered in analysis and optimization of FR in cellular networks are discussed, especially for the partitioned R schemes where BS parameters can be adjusted.

### 2.9.1 Cell center classification

This determines the boundary that separates the classification of center UEs from edge UEs. It is a factor that determines the performance of UEs in a network as the FFR and SFR schemes allocate power and bandwidth differently to the different UE groups.

### 2.9.2 Power ratio

The power ratio is the ratio of power allocation of an edge UE to that of a center UE. Due to the exposure of edge UEs to interference from neighbouring BSs, FFR and SFR compensate these vulnerable group of UEs by increasing their power allocations. The power ratio is an important metric that defines the power levels and affects the SINR experienced.

### 2.9.3 Edge bandwidth allocation

The edge bandwidth allocation is the amount of bandwidth allocated to the edge region. It determines how much frequency resources are available to be shared among UEs in different regions of the BS. It is dependent on the FR scheme in operation.

### 2.9.4 Other parameters

Other parameters considered in cellular networks include antenna patterns, access schemes, modulation techniques, receiver noise floors and backhaul connectivity [23]. Scheduling schemes include proportional fair, round-robin and best channel effort. In proportional fair scheduling, each UE has the same chance of accessing any available PRBs in its region. On the other hand, in the best channel effort, UEs are given priority to access PRBS based on their channel quality [34].

## 2.10 Related research

In this section, a review of literature related to interference management in cellular networks with emphasis on FR is implemented. The studies are grouped into research that present performance analysis of FR, techniques that modify parameter allocation of basic FR schemes and optimization algorithms for FR enhancement. Several criteria were also selected in network parameters such as coverage divisions, virtual UE concept, network scenario selections and distributed optimization in some cases.

### 2.10.1 Performance analysis studies

In [28], analysis of Reuse-1 (FR1), FFR (Strict FR) and SFR is presented for homogeneous hexagonal networks. UEs are assumed to be uniformly distributed with the bandwidth allocation to the BS regions dependent on the size of the interior radius. Their results show how the different performance parameters like spectral efficiency and edge UE data rates conflict themselves when optimized. Under several scenarios, SFR is also less flexible than FFR, due to the impact of low power ratios on performance. This occurs if the network goal is to select an interior radius that balances outage probability with other metrics or in the case where edge UE SINR is considered. However, SFR was observed to be more effective than FFR in balancing interference avoidance with resource utilization.

### 2.10.2 Modified FR algorithms

Several research works have shown that even without optimization, UE performance can improve significantly if the BS parameters are smartly selected and controlled in partitioned FR schemes.

A modified SFR algorithm termed Multilevel ML-SFR is proposed in [30]. The authors show how performance of the traditional SFR can improve when BS coverage areas are divided into smaller units and intelligent bandwidth allocation is made after the spectrum is correspondingly divided. In the algorithm, at each BS region the spectrum is divided into groups with each group comprising two frequency bands. Within each group, a separate SFR scheme with a unique power ratio is implemented. Furthermore, an intelligent resource allocation methodology

is used for UE frequency assignment. The allocations in neighbouring BS regions are considered to ensure that edge ICI is reduced and spectral efficiency improved. For example, the band assigned the highest transmit power in a BS region is assigned the lowest transmit power in the two nearest regions. A multi-level SFR-8 scheme was presented with 4 groups and 8 power density levels.

The authors in [23] propose a variation of FFR-3 called optimal static FFR. Simulations were used to find the center zone radius and frequency allocation to the center zone that gives optimal network throughput for a HetNet. The coverage area was divided into several regions and a subband allocation algorithm was performed for the HetNet scenario to reduce interference

Modified FR and optimization algorithm: [37] presents a HetNet where a modified FFR algorithm is implemented. It involves splitting both the macro and the micro BS coverage areas into two (center and edge). The technique involves assigning: 1) The same frequency bands to macro BS center and micro BS edge regions, and 2) The same frequency bands to macro BS edge and micro BS center regions. The concept of range expansion is also incorporated to aid user association to micro BS, by extending micro BS coverage area. After the mobile association scheme is computed, the algorithm jointly optimizes 1) partitioning of frequency subbands into center and edge and 2) the transmit power in the macro center subband. Both spectrum efficiency and fairness are addressed through an equation for the average throughput to achieve proportional fairness. In [38], a modified FFR scheme based on frequency partitioning is proposed. Two frequency partitioning methods are proposed to mitigate the interference between macro BSs and femto BSs. The whole frequency band is partitioned into several non-overlapping parts. The downlink and uplink frequency bands are both divided into four nonoverlapping parts. The macrocell and femtocell coverage areas are divided into three or four regions, with one part of the frequency band allocated to one region. The division of the BSs into four regions is based on the use of three sectorized antennas, so there is an inner region and three outer regions.

[39] proposed a semistatic ICIC scheme called adaptive frequency reuse. It involves two algorithms; 1) Primary subchannel self-configuration which performs ICIC and 2) interference-aware resource allocation that served as intracell resource allocation. The total subchannels are divided into primary and secondary. A robust primary subchannel allocation scheme was first developed that was non dependent

on the UE locations. Given the fixed transmit power, a sum-rate maximization problem is equivalent to minimizing the sum interference to some extent. Their first optimization problem minimizes the sum interference received by all femto access points. Long term channel gain is considered so the algorithm is considered semistatic and runs at large time scales.

### 2.10.3 Optimization via iterative algorithms

In [33], UEs are assigned "chunks" comprising 12 adjacent sub-carriers, so different chunks have different channel quality due to flat fading. The joint optimization problem of chunk (bandwidth) allocation and selection of edge FR factor, subject to minimum capacity data rate requirements is considered. The original formulation is a combinatorial problem which is simplified by allowing UEs to share sub-carriers on time scales. The resulting integer optimization and linear continuous optimization problems are solved iteratively using exhaustive search by considering the throughput for all values of the number of interior chunks.

Cellular automata is used in [27], states are defined specifying the power amplification factor (power ratio) for BS regions (sectors). The concept of a virtual UE is used here, but is termed the center of gravity UE. First of all, UE distribution in each sector is characterized by the sector's center of gravity. Using interior point method, a quadratic subproblem is solved iteratively to obtain the center of gravity. Based on proximity of the center of gravity to the serving BS, the power ratio of the sector is assigned and set as the sector state. In the second stage, Cellular automata theory is used to obtain a global emergent state for all sectors. At initialization, a sector's state is chosen as the least used configuration state of its neighbours. For each run of this algorithm at each sector, the power ratio is determined by considering the sector's current state, ratio of edge to center UE within the sector and the current state of neighbouring sectors. The average SINR is used to monitor the UE performance within a sector and in cases of low performance (below a threshold) Cellular automata is implemented to trigger a new state change.

Mixed Integer programming technique has also been widely used to optimize FR algorithms. The authors in [40] proposed a distributed algorithm that employs mixed integer programming to maximize system throughput through jointly optimizing the subcarrier and power allocation. They use the concept of virtual UEs;

i.e a virtual cell center and virtual cell edge UE as the UE with the worst channel gains in the center and edge respectively. A minimum data rate requirement is determined for each UE in each BS region. The optimization problem is decomposed into subproblems solvable at the BSs which consider the power and subcarrier allocations at adjacent BS. In the first step of the iterative algorithm, the minimum transmit power requirement for virtual UEs are computed using exhaustive search. Then power reallocation is performed to increase cell throughput for cases where the minimum power obtained is less than the maximum allowable power.

Another presentation of mixed integer programming is given in [41] where a HetNet uplink model is considered comprising 1 macro BS and several small BS within its coverage. The first problem solved is that of computing the minimal power that guarantees the rate requirement of macro UEs. A minimal number of subchannels are assigned to macro UEs, with the remaining left for UE connected to small BS. The first problem is an analytically complex mixed integer non linear problem solved iteratively by successive application of the hungarian algorithm. In the next stage, the interference between small BSs is treated via a non cooperative game where the players are the BS transmitters in adjacent BS regions. The contention and competition for bandwidth and power which are the network resources are analysed in the context of ICI.

In [42], energy efficient resource allocation is considered in HetNets comprising macro and femto BSs. Three optimization problems are identified: 1) Maximize total throughput and energy efficiency 2) Minimize total power consumption and maximize energy efficiency 3) Maximize throughput and minimize total power consumption. All three are considered subject to minimum data rate requirements and interference thresholds for UEs. The optimization problem is a mixed integer non linear problem and multiobjective problem solved using NSGA-II.

A novel multi-level SFR scheme is proposed in [43] where users in three different regions of a macro BS adopt distinct frequency segments and different transmission power levels. The optimization of power control parameters and cell association with is a non-convex problem. Therefore an iterative algorithm is proposed where the main optimization problem is divided into two sub problems that can be solved through classical optimization methods.

### 2.10.4 Multiobjective Optimization

The approach of designing schemes with multiple SFR configurations and providing trade-offs between performance parameters is promoted in [24]. The algorithm is based on multiobjective optimization and the SFR implementations enhance both network capacity and cell edge performance while reducing energy consumption. The coverage area is divided into pixels and sectored antennas are used at the BSs. Variables are grouped into local and global (network) variables and then sets of solutions are created.The objective functions consider system spectral efficiency, edge UE capacity and energy consumption. The edge classification threshold controls the trade-off between spectral efficiency and edge UE capacity while energy consumption is controlled by the power ratio.

### 2.10.5 Stochastic Optimization

In [44], a theoretical framework based on stochastic geometry approach was derived to jointly analyse the area spectral efficiency and area energy efficiency in HetNets. FFR with proportional fairness resource allocation was proposed for the maximization of both performance parameters. An optimal power reduction factor and fractional bandwidth partition in FFR were defined for joint parameter consideration under different scenarios and system performance was evaluated under equal bandwidth allocation per UE and equal data rate per UE. Equations were also derived for the macro transmit power which reduces the power of center transmission and also for the area spectral and energy efficiencies.

### 2.10.6 Summary of Related research

The summary of reviewed works are shown in Table. 2.1.

Table 2.1: Review Summary

| Ref | BS parameter | Methodology | Evaluation parameter | Key metrics | Remarks |
|---|---|---|---|---|---|
| **[23]** | Hexagonal, FFR, HetNet | Monte Carlo Simulation, Optimization through exhaustive search | Outage probability, Network sum rate, Spectral efficiency | Reuse factor, Center radius, Power ratio, Bandwidth | 6 sectors for macrocell, modified FFR, Maximize network capacity |
| **[24]** | Irregular, SFR, Homogeneous | Multiobjective optmization (NSGA-II, SPEA-2) | System capacity, Cell edge capacity, Energy efficiency | Cell edge classification, power ratio | Several solutions adapted to network conditions, SINR based on channel conditions, Pixel-based division of irregular BS coverage |
| **[28]** | Hexagonal, FFR/SFR, Homogeneous | Performance analysis | Outage probability, Network sum rate, Edge SINR, Spectral efficiency | | Distance based SINR computation |

| | | | | | |
|---|---|---|---|---|---|
| [27] | Hexagonal, SFR, Homogeneous | Cellular automata, Non-linear optimization | Edge sum rate, SINR | Power ratio | Modified SFR with optimization, UE distribution considered based on Center of gravity UE, distributed algorithm |
| [30] | Hexagonal, SFR, Homogeneous | Multilevel SFR, resource allocation | Spectral efficiency | Power ratio | BS coverage divided into several regions with different power density |
| [33] | FFR, Homogeneous | Optimization, resource allocation | Cell capacity | Bandwidth allocation, Center radius, reuse factor | Uniform UE, Iterative optimization, Uses minimum rate requirement, considers fairness Scheduling techniques |
| [34] | Hexagonal, SFR, Homogeneous | Performance analysis | Average, edge and center capacity | Traffic load, power ratio | (opportunity fairness and best channel effort), non uniform UE placement |
| [40] | Irregular, SFR, Homogeneous | Joint optimizaton, distributed algorithm | System capacity, Cell edge performance | Subcarrier (bandwidth) and power allocation | Minimum data rate requirement, CoG UE with worst channel giain, interference from adjacent cells, fixed center radius |

| | | | | | |
|---|---|---|---|---|---|
| [45] | Hexagonal, SFR, Homogeneous | Optimization | Capacity | Center radius and power ratio | Considered Pathloss models, scheduling techniques, analysis of separate BS regions |
| | | Resource allocation,2-stage iterative | | | Single macro BS analysis,priorty to macro UE over small BS UE, |
| [41] | Irregular, HetNet | algorithm,Mixed integer non linear optimization,Game theory | Network efficiency, Energy efficiency | Subchannel assignment(Bandwidth), | scheduling, uplink, minimum data rate requirement, no macro BS partitioning into center and edge |
| | | Resource allocation,Multiobjective | Energy efficiency,Spectral efficiency,Power consumption | Capacity, power consumption | Single macro BS, 3 optimization problems defined,minimum rate requirement, uplink |
| [42] | HetNet | optimization(NSGA-II), Game theory | | | |
| | | 2-stage optimization | Log-scaled throughput (capacity),Spectral efficiency,UE fairness | Subband partitioning (bandwidth), transmit power | Power control,Range expansion based mobile association,Minimum data rate requirement, uniform UE,fairness |
| [37] | Hexagonal, FFR, HetNet | using (brute-force search and convex optimization) | | | |

| | | | | | |
|---|---|---|---|---|---|
| [44] | FFR, HetNet | Stochastic geometry,Multiobjective Optimization,Resource allocation | Area spectral efficiency,Area energy efficiency,Log-scaled throughput | Power reduction factor,Bandwidth partition | Proportional fairness,UE fairness,range expansion based mobile association,Pico coverage divided into 2 regions |
| [38] | HetNet | Frequency partitioning,Modified FFR/SFR, Semistatic Adaptive FR,2-stage algorithm,Modified SFR,Game theory,Graph coloring | Capacity | Bandwidth allocation | Downlink and uplink considered,Coverage and bandwidth splitting,independent resource allocation per tier,Uniform UE,No inter-tier interference |
| [39] | SFR, HetNet | | Spectral efficiency | Subchannel configuration (Bandwidth) | Distributed scheme,random femto BS deployment |

| | | | | | |
|---|---|---|---|---|---|
| [46] | Hexagonal, FFR/SFR, Homogeneous | Performance analysis | Throughput(capacity) for edge and overall,Fairness index,Spectral efficiency,UE satisfaction | Power ratio,UE distribution,Traffic load | Vienna simulator,Scheduling,Full resource block buffer,uniform and non uniform UE |
| [43] | Hexagonal, SFR, HetNet | Multilevel SFR,Iterative algorithm | Log-scaled throughput (capacity) | Bandwidth and power ratio, | Macro and Micro BS region splitting,Round robin scheduling,Minimum data rate requirement |

# Chapter 3

# Performance Analysis of Frequency Reuse Algorithms

## 3.1 Introduction

The benefit of FR performance analysis is highlighted in [24] and [28], i.e many BS metrics can be studied thoroughly. In this Chapter, extensive analysis of static FR techniques in cellular networks is presented. The investigations from previous studies are extended and deeper insights provided on FR impact in communication system performance. These form the basis for design of more accurate system models and improved FR algorithms proposed in subsequent Chapters. Several scenarios involving the deployments of BSs and the assignment of BS parameters are considered. These include over irregular macro BS deployments, BS coverage area classification metrics and assignments of BS resource parameters to UEs. The results are obtained through simulations in MATLAB software of single-tier macro BS networks.

Essentially, BSs can be arranged and configured in several formats. These affect how their resources are allocated to connected UEs in the network. As discussed in Chapter Two, the key parameters, considerations and assumptions for BSs can be summarized as:

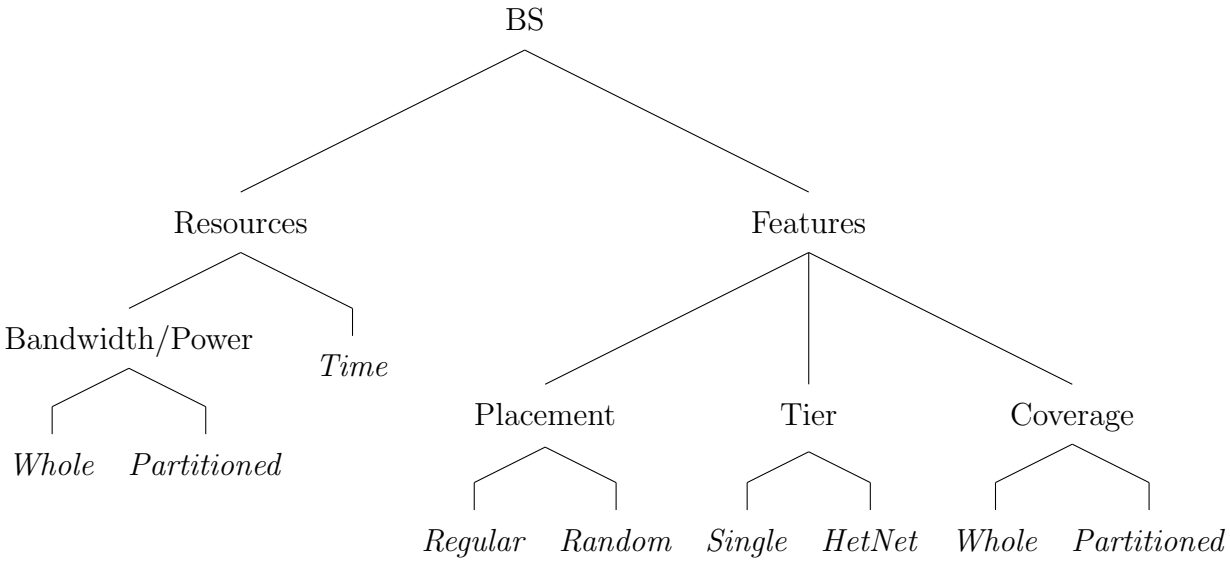


As shown in the tree above, analysis of BSs over different network scenarios can be classified under BS resource management techniques and the features of BS deployments. The key resources available at any given BS and allocated to UE are Bandwidth, Power and time. Bandwidth/Power resources can be distributed by dividing the whole BS portions (Reuse-1, Reuse-3) or by partitioning and dividing smaller segments (FFR, SFR). Time as a resource relates to the duration that a BS allocates the other two resources to connected UE; however this is outside the scope of this research. For BS deployment features, it is relevant to analyse BS placements and the impact on performance. Regular (Hexagonal) and Random (Irregular) BS placements (which more accurately model real networks) are both considered. Based on the number of tiers, there are Homogeneous(single-tier) networks and HetNets (Multi-tier). Homogeneous networks comprising macro BSs are considered in this analysis. Finally, classification based on the structure of the BS coverage areas (formed from their antenna transmissions) are related to the classification of Bandwidth/Power resources. Consideration is given for the whole (Reuse-1, Reuse-3) and partitioned (FFR, SFR) coverage areas.

## 3.2 Previous research on FR performance analysis

The parameters that determine the performance at any given time of a cellular system employing partitioned FR include the center radius, power ratio (between edge and center transmission regions) and traffic load. These affect the degree of

interference, UE bandwidth and determine the resulting SINR and capacity. Several research works exist in literature that present performance analysis of FR techniques. In [47], the authors showed how the system performance of the FR schemes varies over different center radius and power ratios. Specific performance of center and edge UEs were also considered. The authors in [34] presented an evaluation of the capacity of SFR under different traffic loads and power ratio configurations. Analytical derivations and simulations were used in [28] to compare the FR techniques and provide design guidelines. The metrics used were outage probability, network capacity, SINR and spectral efficiency under different center radius and power ratios. In [48], the system capacity was studied under different scheduling techniques. In this thesis, existing analyses of FR performance is extended by consideration of more network parameters and scenarios. Specifically, realistic assumptions for BS deployments and UE placements are considered. Practical cellular networks usually consist of macro BS that are not arranged perfectly to form hexagonal radiation patterns. However, most of the previous research works have assumed hexagonal BS deployments. The analysis presented here shows how the FR schemes perform for uniform UE placements within irregular BS deployments. It extends the system evaluation over varying center radius, BS resources and traffic loads. To aid the analysis, new equations and metrics are proposed to describe the irregularity of BS locations and computation of UE performance. This is crucial for the development of efficient partitioned FR algorithms using dynamic implementation.

## 3.3 Overview of frequency reuse algorithms

Fig. 3.1 shows the coverage layout description for the FR algorithms. $S_1, S_2, S_3$ represent the three sectors of a macro BS within which the FR schemes are deployed. In the cases of FFR and SFR, Fig. 3.1(b) shows the coverage region of $S_1$ of $M$ divided into the center and edge regions. Fig. 3.2 shows the frequency allocation rules for each FR technique under consideration. The diagram shows the assignments for sector $S_1$ of $M$ as described in Fig. 3.1. For each technique, the power allocation per UE at different BS regions are plotted against the respective bandwidth slots. In the Reuse-1 technique, the system bandwidth, $\mathcal{F}$ is fully utilized in each sector, while in Reuse-3, only $\frac{\mathcal{F}}{3}$ is used. Therefore, UEs in Reuse-1 experience high interference while those in Reuse-3 have less bandwidth. In the FFR and SFR schemes, two

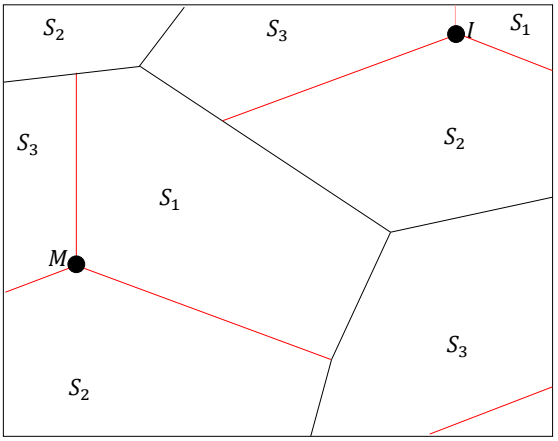


(a) Integer FR schemes (Reuse-1 and Reuse-3)

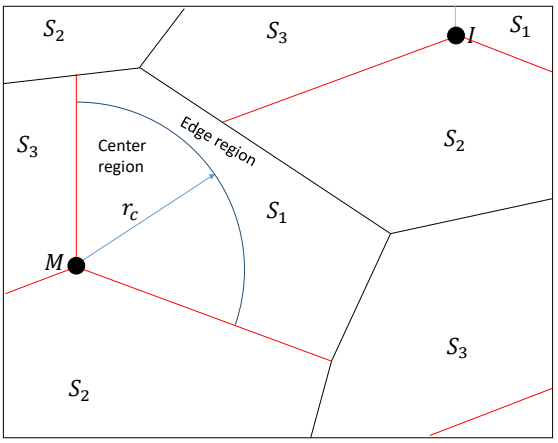


(b) Partitioned FR schemes (FFR and SFR)

Figure 3.1: Coverage Layout for FR schemes

different rules are specified for the two different classes of UEs (center and edge). Consequently, center UEs share the center bandwidth $\mathcal{F}_c$ at the power level $p_u^c$ and edge UEs share the edge bandwidth $\mathcal{F}_e$ at the power level $p_u^e$. In both cases, the edge bandwidth allocations across each sector are separated from each other. This is to prevent interference on a sector from neighbouring sectors (which will usually have a different sector index). The difference between FFR and SFR is that in FFR, $\mathcal{F}_c$ does not overlap with any $\mathcal{F}_e$, meaning that in each sector, part of $\mathcal{F}$ is unused. SFR guarantees full utilization of $\mathcal{F}$, meaning it has a better resource utilization and spectral efficiency than FFR which has better interference management [27].

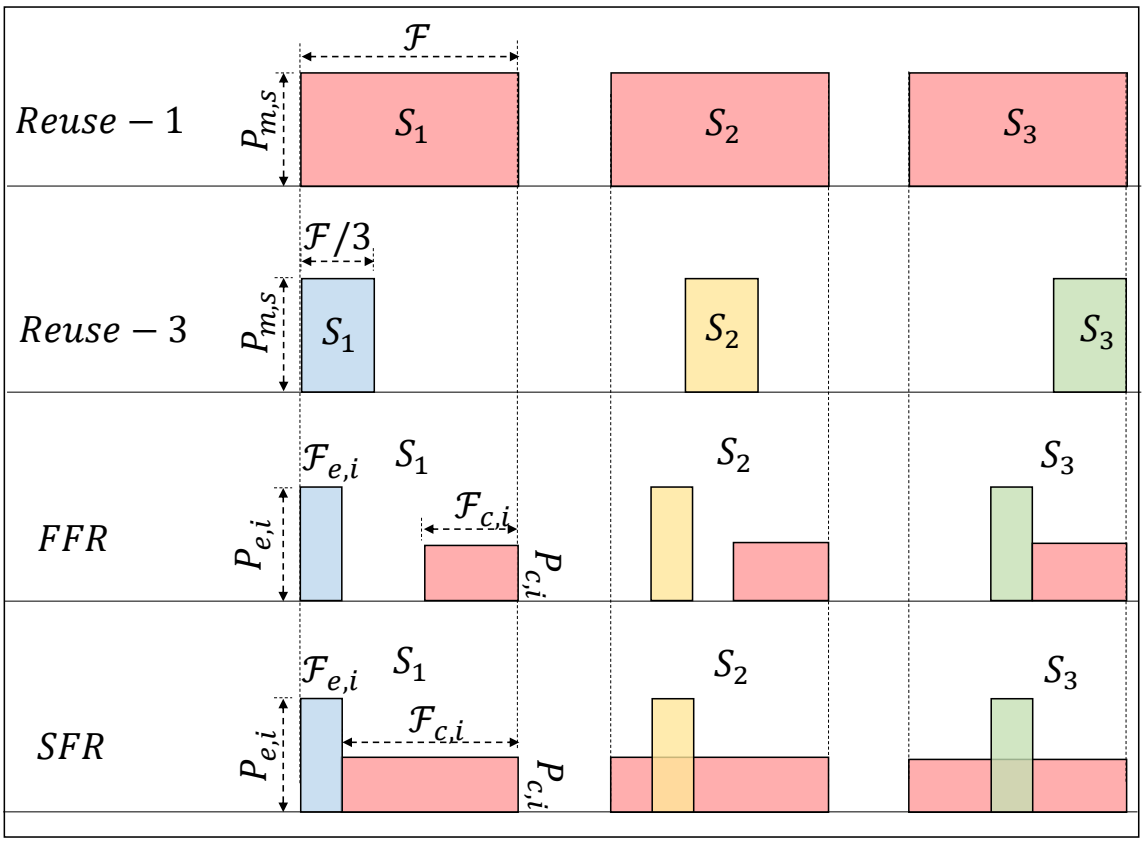


Figure 3.2: Power/Bandwidth allocation for FR schemes

## 3.4 Simulation Parameters

The parameters selected in the simulations that specify UE performance, BS settings and the classification of both BSs and UEs are highlighted in this section.

### 3.4.1 Performance parameters

The performance parameters considered in the analysis are SINR and capacity.

**SINR**: The SINR of any arbitrary UE, $U$ connected to a sector $S_i$ of a reference BS, $M$ is given by:

$$SINR_u = \frac{p_{m,i} h_{m,i} G_{m,i}}{\sum\limits_{S_j \epsilon \mathcal{J}} p_{u,j} h_{u,j} G_{u,j}}, \tag{3.1}$$

where $p_{m,i}$ is the signal power transmitted to $U$ from $M$, $h_{m,i}$ is the exponentially distributed channel fading power and $G_{m,i}$ is the pathloss based on the distance from $U$ to $M$. $\mathcal{J}$ is the set of interfering BSs, while $p_{u,j}, h_{u,j}, G_{u,j}$ are respectively the transmitted power, fading component and pathloss relating $U$ and a sector $S_j$ of any interfering BS $I_j$.

For Reuse-1, $p_{m,i}$ is computed by dividing $P_{m,s}$, the power budget of the BS sector

by $N_{m,i}$, the number of UEs in the sector $S_i$ of $M$, subject to this division being less than a maximum transmit power to any UE, $p_{u,max}$. When $P_{m,s}/N_{m,i} > p_{u,max}$, then $p_{m,i} = p_{u,max}$. For Reuse-3, $p_{m,i} = \min(p_{u,max}, P_{m,s}/3N_{m,i})$. $p_{u,j}$ is computed similarly for each neighbouring BS.

For FFR and SFR, the BS region is divided into two (center and edge). $p_{m,i}$ will be either $p^c_{m,i}$ for a center UE or $p^e_{m,i}$ for an edge UE. $p_{m,i}$ is computed by considering $E_{m,i}$, the number of UEs in the edge region of $S_i$ and $\mu_{m,s}$ the power ratio of the network. $\mu_{m,s}$ specifies the ratio of transmit power towards an edge UE to the transmit power towards a center UE. Similar to the Reuse-1 and Reuse-3 schemes, the threshold for maximum transmit power allowed per UE is considered and if $p_{m,i} > p_{u,max}$, $p_{m,i} = p_{u,max}$.

If $C_{m,i}$ is the number of center UEs, then for FFR, $E_{m,i} + C_{m,i} = N_{m,i}$, $P_{m,s} = 3E_{m,i}p^e_{m,i} + C_{m,i}p^c_{m,i}$, therefore $p^e_{m,i} = \frac{\mu_{m,s}P_{m,s}}{E_{m,i}(3\mu_{m,s}-1)+N_{m,i}}$ if $U$ is an edge UE and $p^c_{m,i} = \frac{P_{m,s}}{E_{m,i}(3\mu_{m,s}-1)+N_{m,i}}$ if $U$ is a center UE.

In the case of SFR, $E_{m,i} + C_{m,i} = N_{m,i}$, $P_{m,s} = E_{m,i}p^e_{m,i} + C_{m,i}p^c_{m,i}$ and $p^e_{m,i} = \frac{\mu_{m,s}P_{m,s}}{E_{m,i}(\mu_{m,s}-1)+N_{m,i}}$ for edge UEs and $p^c_{m,i} = \frac{P_{m,s}}{E_{m,i}(\mu_{m,s}-1)+N_{m,i}}$ for center UEs.

**Capacity**: The capacity which represents the data rate at $U$ is given by the Shannon formula:

$$Cap_u = \min[\mathcal{F}_{u,max}, \frac{\mathcal{F}_r}{N_{m,i}}][\log_2(1 + SINR_u)], \tag{3.2}$$

where $\mathcal{F}_{u,max}$ is the maximum allowable bandwidth per UE, set appropriately for each FR scheme. $\mathcal{F}_r = \mathcal{F}, \mathcal{F}/3$ for Reuse-1 and Reuse-3 respectively. When partitioned FR schemes are considered, $\mathcal{F}_r$ represents the total bandwidth allocation to either the edge region or center region depending on whether $U$ is an edge UE or center UE respectively.

### 3.4.2 Basic BS parameters

The basic parameters used for all analysis are given in Table 3.1.

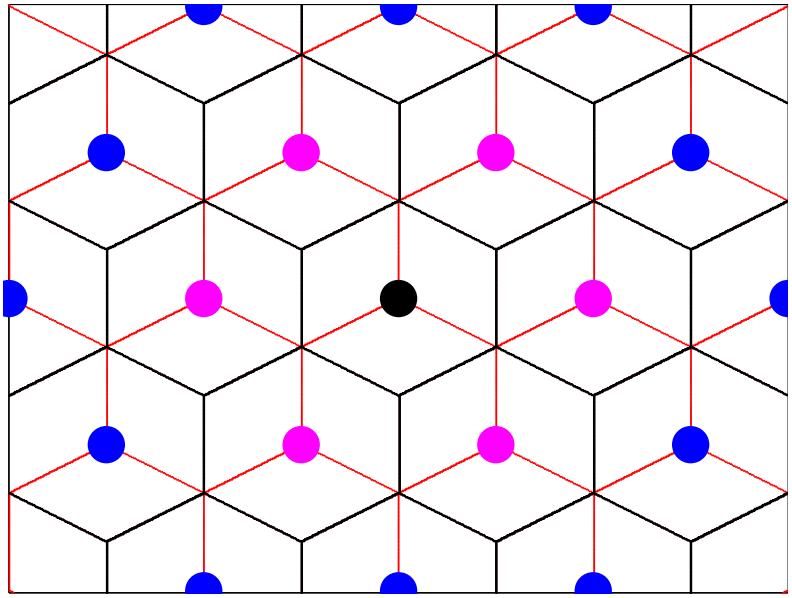

Figure 3.3: Network showing reference BS and interfering BS

Table 3.1: General parameters for Simulation

| Parameter | Value |
|---|---|
| **Number of Sectors per Macro BS** | 3 |
| **Power budget per Sector** | $43dBm$ |
| **Number of PRBs per Sector** | 48 |
| **Bandwidth per sector** | $10MHz$ |
| **Bandwidth per PRB** | $180kHz$ |
| **Macro BS coverage radius** | $0.5km$ |
| **Pathloss Model** | $128.1 + 37.6 \log(distance)$ |
| **Antenna gain** | $0(\theta_u > 60°), 1(\theta_u \leq 60°)$ |
| **UE placement** | Uniform deployment |

### 3.4.3 Reference BS consideration

In this analysis, the single-cell linear model is adopted for investigation of UE performance under different BS scenarios and FR algorithms. The model focuses on single BS regions as opposed to the entire BSs in the network [25]. The advantage is a closer view of UE performance depending on the specific parameters around a group of BS.

To support this choice, an investigation of performance in a reference BS versus network-wide performance is carried out. Consider a network of BSs shown in

Fig. 3.3, with a reference BS (depicted as a solid black circle) at the center of the figure, surrounded by interfering BS at different locations. The average SINR of UEs in the reference BS is compared with the average SINR of UEs for all BSs. This was computed in a Reuse-1 scenario (the highest reuse and worst case interference scenario) for uniform UE deployment in a hexagonal macro BS system. In addition, uniform transmit power from the BS to each UE was assumed, minimum and maximum distance of UEs from their connected BSs were 50m and 0.5km respectively and the number of UEs in the reference BS sector was 48. UE positions were considered and the SINR results are presented for different UE groups based on their proximity to their serving BS. Let $\lambda r (0 < \lambda < 1)$ be the distance between a UE, $U$ and its serving BS, where $r = 0.5$km is the macro base station standard coverage radius in the hexagonal placement. The analysis is presented in Table 3.2.

Table 3.2: Average SINR comparison

| **UE description** | **Ref. BS** | **All BS** | **% difference** |
|---|---|---|---|
| $\lambda r < 0.4r$ | 181.75dB | 442.91dB | 144% |
| $0.4r \leq \lambda r < 0.8r$ | 5.77dB | 12.14dB | 110% |
| $0.8r \leq \lambda r < r$ | 0.77dB | 2.49dB | 223% |
| All UE | 37.42dB | 80.33dB | 115% |

As expected, the average SINR drops drastically with distance away from the serving BS (increasing values of $\lambda$), clearly showing the exposure of UEs at the boundaries (edge UEs) to poor performance. It can also be observed that the average SINR values for the reference BS are significantly lower than that of the entire BSs, with the least percentage increase being 110%. This disparity is further depicted graphically in Fig. 3.4. By considering the network coverage plot in Fig. 3.3, the huge percentage difference in both cases can be explained. The BSs located at the network boundary (depicted in solid blue circles) do not have complete sets of interfering adjacent BSs implying less interference to their UEs in the simulations. Therefore, they contribute a higher SINR when the overall SINR is computed. Fig. 3.4 highlights the importance of considering the performance at each individual BS for analysis and the potential inaccuracies of making assumptions based on overall averages. Based on this observation and similar to [34] and [43], the emphasis of analysis in this thesis will be on the central reference BS which has

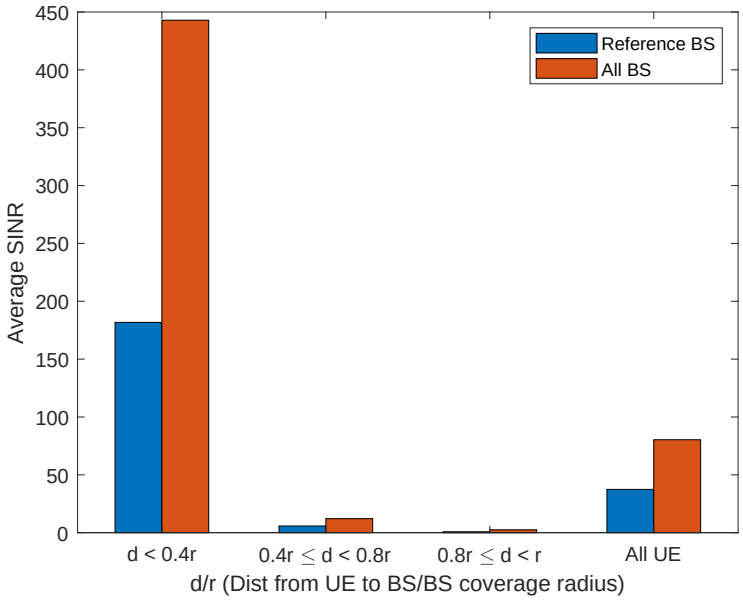


Figure 3.4: Comparing average SINR for all BS and reference BS

a more balanced surrounding interference. Though the graph shows results for the case of Reuse-1, there is no loss of generality, as it basically analyses the property of received power and hence the observations apply to other FR algorithms.

### 3.4.4 Grouping of UEs

Table 3.2 and Fig. 3.4 show the huge variability in UE SINR performance over different UE locations. This implies that computing the average SINR of all UEs in a BS sector may not adequately reveal cases of UEs with severely low SINR. This idea is supported in [34] where it is shown that SFR provides conflicting performances for cell edge and cell center UEs. The authors in [43] address this problem by dividing BS regions into three and analysing UE performance separately in the different regions. This approach of BS coverage area division is also adopted in this Chapter. Therefore the analysis presented is considered for UEs based on their location. However, UEs in the reference BS sector are grouped into two, unlike in [43] where three groups are used. The following rule is adopted:

**Group 1**:

$$0.45r < \lambda r < 0.8r$$

**Group 2**:

$$\lambda r \geq 0.8r, \tag{3.3}$$

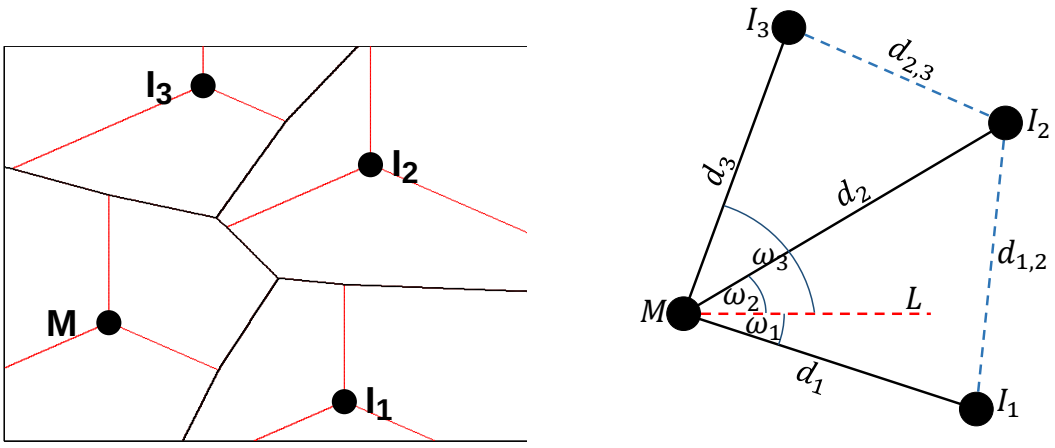


(a) Coverage diagram (b) Distance analysis

Figure 3.5: Distance relationship between BS

where $\lambda r$ is the distance between a UE and the reference BS.

Group 1 UEs represent UEs in the interior region, but not very close to the reference BS, $M$. The UEs very close to $M$ (i.e where $\lambda r \leq 0.45r$) are not considered because their proximity advantage grants them much higher SINR than other UEs. Consequently, group 1 UEs can conveniently provide an assessment of the worst case center UE performance under adverse conditions. Group 2 UEs are located farther away from $M$ and are potentially exposed to high interference from neighbouring sectors.

## 3.5 Irregular BS model

Apart from the network scenario with the regular macro BS placement, scenarios with irregular macro BS deployments are considered. A model to define network scenarios describing random BS placements is presented in this section.

First of all, a distance threshold, $d_{min}$ is defined as the minimum allowable distance between any two macro BS. This eliminates extreme cases where macro BSs are too close together causing a likely underutilization of resources and defeating the purpose of this study.

Consider the group of neighbouring macro BSs shown in Fig. 3.5(a). $M$ is the reference BS and $I_1, I_2, I_3$ are the interfering BSs in close proximity to a sector of $M$. The distance relationships between each adjacent macro BS pair is shown in Fig. 3.5(b). The distances between $M$ and $I_1, I_2$ and $I_3$ are $d_1, d_2$ and $d_3$ respectively, while $d_{1,2}$ and $d_{2,3}$ are the distances from $I_1$ to $I_2$ and $I_2$ to $I_3$ respectively. According

to the minimum distance condition earlier stated, $\{d_1, d_2, d_3, d_{1,2}, d_{2,3}\} \geq d_{min}$. Let $d_i = d_{min} + \delta_i$ where $i = 1, 2, 3$ and $d_{j,k} = d_{min} + \delta_{j,k}$ where $j = \{1, 2\}$ and $k = \{2, 3\}$. In addition to separation distance, the positional relationships between $M$ and each interfering BS is defined with the aid of $L$, a horizontal line from $M$. $\omega_i$ is the anticlockwise angle formed from the displacement of $L$ to the line joining $M$ to $I_i$ where $i = 1, 2, 3$. For the sector of $M$ shown, the following condition holds for $I_1, I_2, I_3$: $-30^\circ \leq \omega_1 < \omega_2 < \omega_3 \leq 90^\circ$. For any two interfering BSs, $(I_i, I_{i+1})$, given their proximity factors to $M$ $(\delta_i, \delta_{i+1})$, proximity factor to themselves $(\delta_{i,i+1})$ and $\omega_i$ (the displacement angle of $I_i$), then $\omega_{i+1}$ can be calculated thus:

$$\omega_{i+1} = \omega_i - \cos^{-1}\left[\frac{(d_{min} + \delta_i)^2 + (d_{min} + \delta_{i+1})^2 - (d_{min} + \delta_{i,i+1})^2}{2(d_{min} + \delta_i)(d_{min} + \delta_{i+1})}\right], \tag{3.4}$$

where $((d_{min} + \delta_i) - (d_{min} + \delta_{i+1}))^2 \leq (d_{min} + \delta_{i,i+1})^2$ by the principles of geometry.

## 3.6 Macro BS network scenarios

Table 3.3 shows the different parameters based on macro BS locations for the different network scenarios that are analysed. Note that $d_{min}$ is set to $\sqrt{3}r$, which is the distance between nearest neighbouring macro BSs in the hexagonal layout ($r = 0.5$km).

Table 3.3: Location parameters for simulation case studies

| | $d_{min}$ | $\delta_1$ | $\delta_2$ | $\delta_3$ | $\delta_{1,2}$ | $\delta_{2,3}$ | $\omega_1$ | **Remark** |
|---|---|---|---|---|---|---|---|---|
| **Case** 1 | $\sqrt{3}r$ | 0 | 0 | 0 | 0 | 0 | $0^\circ$ | Hexagonal Layout |
| **Case** 2 | $\sqrt{3}r$ | 0 | 0 | 0 | 0 | 0 | $-20^\circ$ | Irregular BS Layout-1 |
| **Case** 3 | $\sqrt{3}r$ | 0 | 0 | 0 | $0.27r$ | 0 | $-20^\circ$ | Irregular BS Layout-2 |
| **Case** 4 | $\sqrt{3}r$ | 0 | $0.3r$ | $0.1r$ | $0.2r$ | 0 | $10^\circ$ | Irregular BS Layout-3 |

Other parameters for $I_2$ and $I_3$, i.e $\omega_2$ and $\omega_3$ are computed using (3.4). Coverage plots for the four network scenarios are shown in Fig. 3.6 and the performance analysis is presented in the next sections.

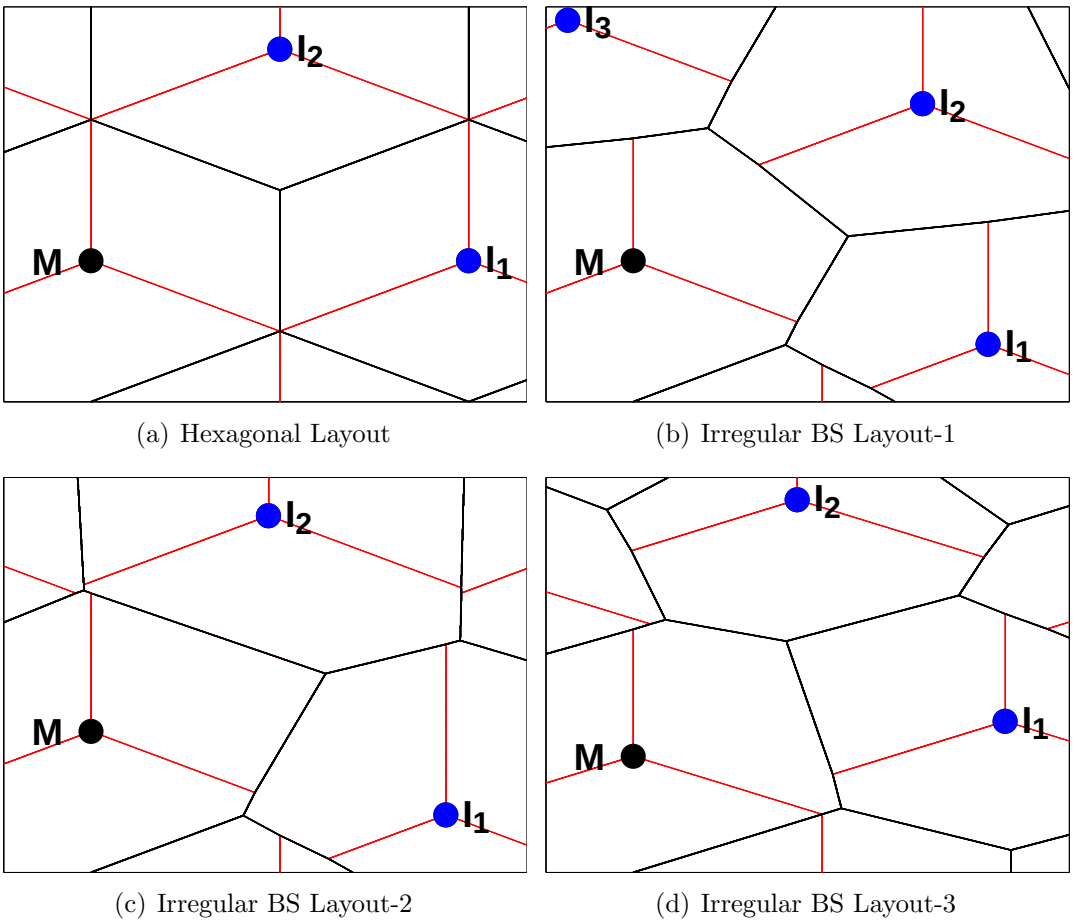


(a) Hexagonal Layout (b) Irregular BS Layout-1

(c) Irregular BS Layout-2 (d) Irregular BS Layout-3

Figure 3.6: Coverage area plots for macro BS case studies

## 3.7 Investigating the impact of center radius $r_c$

Unlike in Reuse-1 and Reuse-3, the partitioned FR algorithms provide macro BSs with parameters that can be varied such as the center coverage radius $r_c$, system power ratio $\mu_{m,s}$ and edge bandwidth $f_{e,i}$. These parameters are studied to determine their impact on the different proximity based UE groups. The first parameter investigated is $r_c$, with its importance highlighted in [24], [28], [34]. $r_c$ is considered in three broad case studies.

### 3.7.1 Case study 1: Single-tier hexagonal BS

The first case study is the homogeneous network with hexagonal macro BS placement depicted in Fig. 3.6(a). Investigation is carried out to study the impact of $r_c$ in this regular BS network. $r_c$ is the coverage boundary that specifies whether a UE is classified as a center UE or an edge UE as depicted in Fig. 3.1(b). As $r_c$ increases, the number of UEs located within the interior region increases, implying more center UEs and less edge UEs. On the other hand, lower settings of $r_c$ result in higher

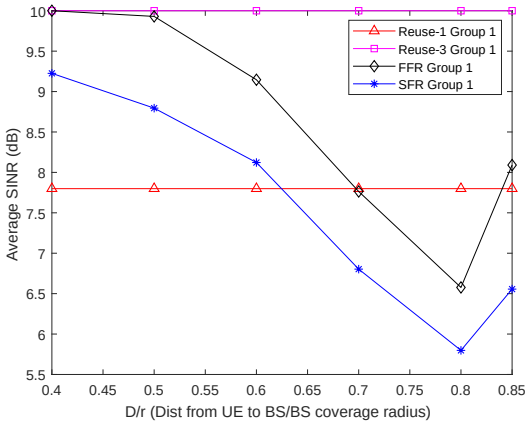


(a) Average SINR for group 1

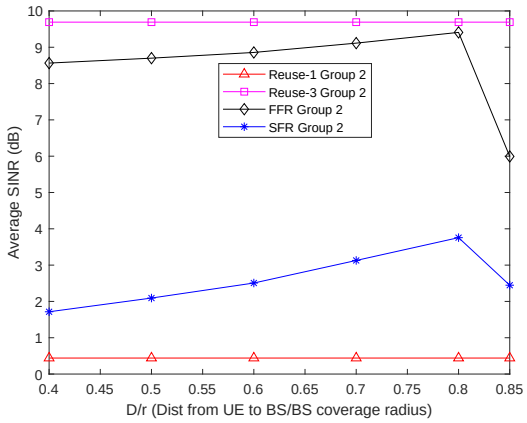


(b) Average SINR for group 2

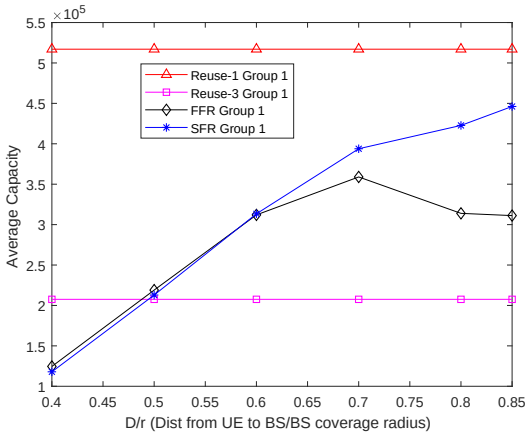


(c) Average capacity (in bps) for group 1

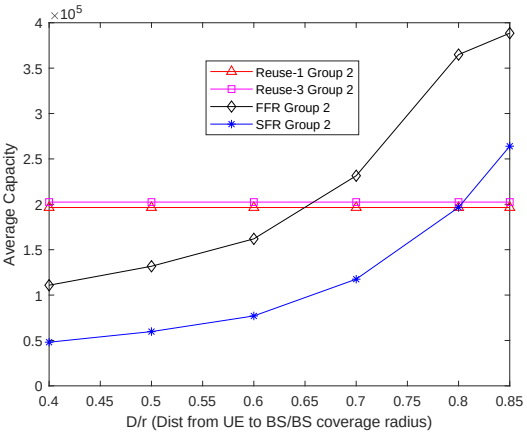


(d) Average capacity (in bps) for group 2

Figure 3.7: Performance for Single-tier regular BS, full UE: varying $r_c$

number of edge UEs resulting in a likely imbalance of bandwidth allocation for partitioned FR schemes as Fig. 3.2 shows. Table 3.4 shows the BS parameters used for simulation.

Table 3.4: Case study 1 parameters

| **Parameter** | **Value** |
|---|---|
| **Center radius** | $0.4r \leq r_c \leq 0.8r$ |
| **Power ratio,** $\mu_{m,s}$ | 2.5 |
| **Edge region bandwidth,** $f_{e,i}$ | $8 \times 180$kHz |
| **Observed number of UEs,** $N_{m,i}$ | 48 |

**SINR for group** 1 **and group** 2 **UEs**: Figs. 3.7(a) and 3.7(b) show the average SINR values for group 1 and group 2 UEs respectively for the different FR schemes. As expected, the results for Reuse-1 and Reuse-3 are always constant since in these

schemes, BS coverage partitions are not defined using $r_c$. For group 1 UEs, high SINR ($> 5.5$dB) is experienced in all the FR algorithms. However for group 2 UEs, there are cases of low SINR ($< 0.5$dB) under Reuse-1. This occurs because compared to group 2 UEs, group 1 UEs are located closer to the serving BS and farther away from interfering BSs. The combined effect of the higher signal power from the serving BS and lower interference then causes the higher SINR experienced in the group 1 case. Reuse-3 gives the best SINR performance in each group, consistent with Fig. 3.2 which shows it guarantees the highest interference minimization.

**SINR for group 1 UEs in partitioned FR:** Considering the partitioned FR schemes (FFR and SFR), in Fig. 3.7(a) the SINR performance for group 1 UEs falls as $r_c$ increases from $0.4r$ to $0.8r$ (where the minimum SINR occurs), then SINR increases again at $r_c = 0.85r$. This observed trend can be explained by considering three factors that affect the average SINR performance in any UE group:

- UE classification,
- Power allocation per UE and
- Interference received per UE.

The UE classification for each group as $r_c$ varies is depicted in Fig. 3.8. The figure describes locations of group 1 and 2 UEs in relation to the location of their serving BS. It also reveals how for different values of $r_c$, each group comprises varying combinations of center and/or edge UEs. When $r_c = 0.4r$, all group 1 UEs (UEs between $0.45r$ and $0.8r$) are edge UEs. Between $r_c = 0.5r$ and $0.7r$, group 1 UEs are made up of both center UEs and edge UEs, with the number of center UEs increasing with $r_c$ and the number of edge UEs decreasing with $r_c$. When $r_c > 0.7r$, all group 1 UEs are center UEs. Therefore, with the assumption that UE locations remain fixed while $r_c$ is increased, it is evident that the classification of group 1 UEs progressively changes from the case of "all edge" to "all center" UEs. The actual number of center and edge UEs for each value of $r_c$ are plotted in Fig. 3.9. As group 1 UEs experience this change in classification, both their received signal power and interference experienced also change (based on rules defined for partitioned FR schemes in Fig. 3.2).

The other two factors affecting the SINR experienced are the power allocation per UE and interference received per UE. Fig. 3.10(a) shows the average transmitted

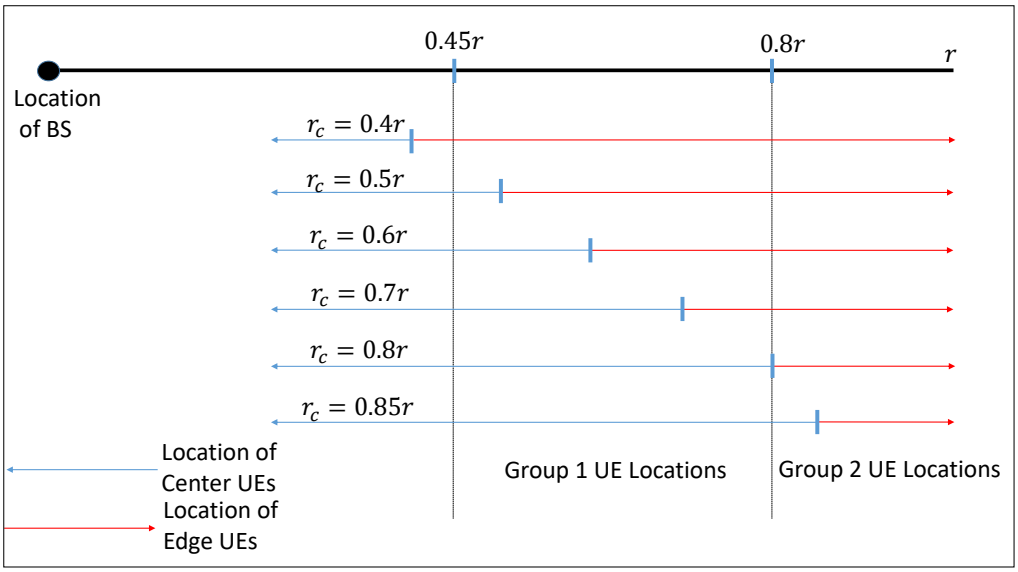


Figure 3.8: Group 1 and Group 2 UEs Locations

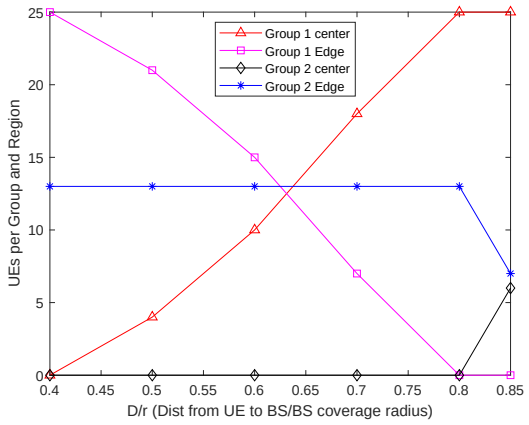


Figure 3.9: Number of UEs per Group and Region

power from the serving BS to the different classes of UEs connected. Both the transmitted power per center UE and the transmitted power per edge UE increase as $r_c$ increases for most of the cases. This is consistent with the discussion presented in Section. 3.4.1 of this Chapter where the transmitted power per UE was shown to be inversely proportional to the number of edge UEs, $E_{m,i}$. However, Fig. 3.10(a) also reveals that when the average transmitted power per group 1 UE is computed, it falls with increasing $r_c$ till $r_c = 0.8r$. This occurs because as $r_c$ increases, there are more center UEs and less edge UEs. Since the power transmitted per center UE is less than per edge UE (based on the partitioned FR algorithm rules and also shown in Fig. 3.10(a)), therefore the average transmitted power per UE in group 1 initially reduces as $r_c$ increases. When the effects of path loss are considered, Fig. 3.10(b) shows the received power for both group 1 center and edge UEs mostly reducing

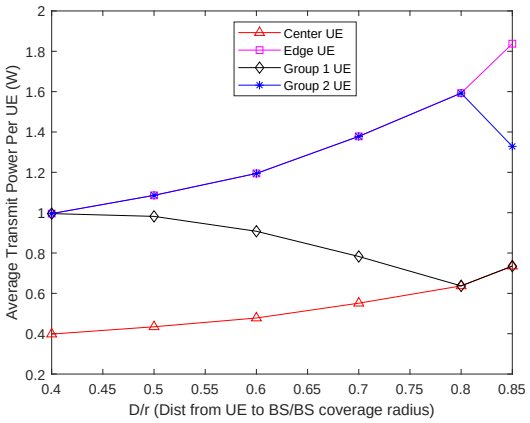


(a) Transmitted Power analysis for SFR

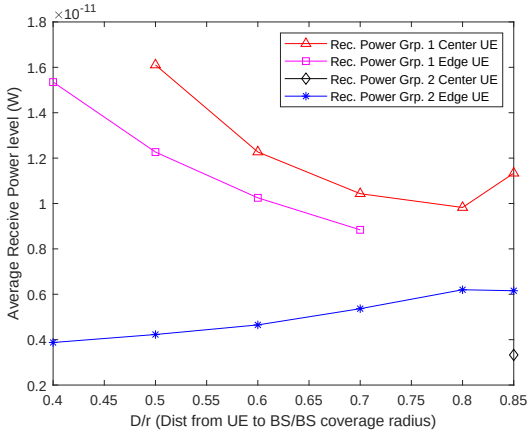


(b) Received Power analysis for SFR

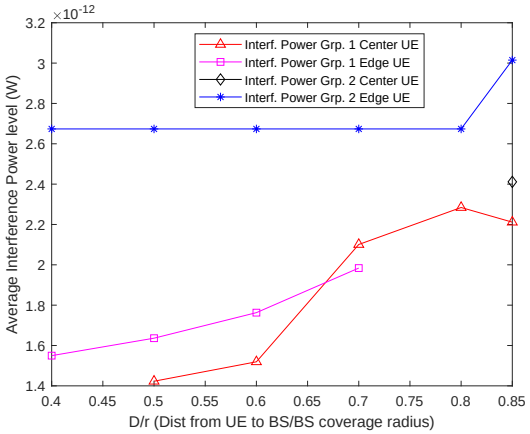


(c) Interference Power analysis for SFR

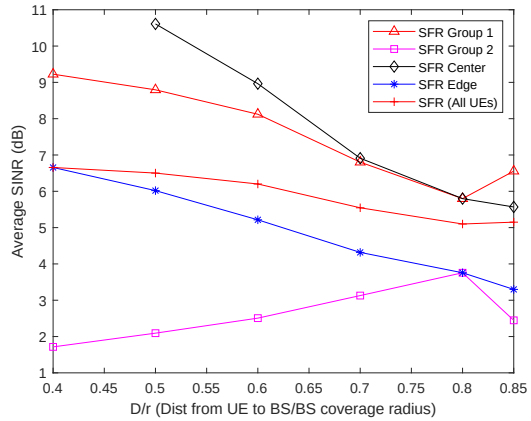


(d) Analysis of SFR SINR

Figure 3.10: SFR analysis for Case 1

with $r_c$ while the interference power increases with $r_c$.

In summary, the behaviour of the SINR for group 1 UEs under FFR and SFR as shown in Fig. 3.7(a) can be explained thus:

- SINR drops as $r_c$ increases to $0.8r$ because the number of center UEs increase, the average transmitted power per group 1 UE drops (Fig. 3.10(a)), the average received power per group 1 UE drops (Fig. 3.10(b)) and the average interference power per group 1 UE rises (Fig. 3.10(c)).

- SINR increases when $r_c > 0.8r$ because the average transmitted power and average received power per group 1 UE increases, while the average interference power reduces.

**SINR for group 2 UEs in partitioned FR:** Fig. 3.7(b) shows that unlike the case of group 1, the SINR for group 2 UEs under FFR and SFR increases for $r_c$ between $0.4r$ and $0.8r$, then falls at $0.85r$. This occurs because: 1) Group 2 UEs are

mostly edge UEs for most cases of $r_c$ (from Fig. 3.9) 2) Both the average transmit power and average received power per group 2 edge UEs increase with $r_c$ for most cases (from Figs. 3.10(a) and 3.10(b)), and 3) The average interference power to group 2 edge UEs remains mostly constant.

**SINR Summary:** The average transmit power per UE had the most significant impact on the SINR for FFR and SFR schemes as the plot patterns in Figs.3.7(a) and 3.7(b) closely follow their corresponding group plots in Fig. 3.10(a). Fig. 3.10(d) shows the combined SINR SFR plots for all UE groups based on UE classification and location. It is clear that neither the overall average performance for all UEs nor the average performance for edge UEs give a good indication of the performance of group 2 UEs. This highlights the importance of using UE locations to group UEs for more thorough analysis. The results obtained are obviously dependent on the classification threshold limits for the groups set in (3.3) (i.e $0.45r$ and $0.8r$) which determine when a particular group is composed of center UEs and/or edge UEs and by how much. The poor performance of the Reuse-1 scheme clearly shows how vulnerable edge UEs are when a high reuse factor is used and the importance of protecting them through partitioned FR schemes like FFR and SFR.

**Capacity Analysis**: Figs. 3.7(c) and 3.7(d) show the capacity results for group 1 and group 2 UEs respectively. Generally for group 1, the capacity performance differs significantly from SINR. Unlike the SINR results, Reuse-1 gives the best capacity performance in all $r_c$ cases in group 1, with Reuse-3 giving the worst performance in most cases. This is due to the much lower bandwidth per UE (a third of Reuse-1) available under Reuse-3 and proves that excellent SINR experienced does not always translate into better capacity. The effects of lower SINR in Reuse-1 for group 1 UEs were not sufficient to limit the capacity performance due to the advantage of proximity (higher received power and lower interference) that group 1 UEs have over group 2. For the partitioned FR schemes, there was also a difference in trend from the SINR result. The capacity rises with the initial values of $r_c$ for FFR and for all cases in SFR because SFR has the advantage over FFR of more bandwidth available for the center region. As $r_c$ increases, more UEs are classified as center UEs in group 1, hence the overall capacity increases for SFR. This also occurs initially for FFR but if the number of center UEs becomes high enough, the bandwidth per center UE might reduce, affecting the capacity performance as observed. Consequently, it is observed that for capacity, SFR outperforms FFR when $r_c > 0.6r$ (even though

FFR always outperforms SFR in SINR). Therefore, apart from SINR, the number of connected UE is an important factor affecting the capacity performance.

Fig. 3.7(d) shows a closer result between Reuse-1 and Reuse-3, but with Reuse-3 outperforming Reuse-1 (unlike in the case of group 1). This implies the effect of low SINR on capacity mostly affects group 2 UEs which are farther away from the serving BS. The capacity for FFR and SFR always rises with $r_c$ because as the number of edge UEs in both groups reduces, the bandwidth available per edge UE also increases. FFR outperforms SFR in all cases of $r_c$ just like in the SINR plots.

**Summary of Results**: In summary, the analysis of SINR and capacity for varying $r_c$ when $\mu_{m,s}, f_{e,i}$ and $N_{m,i}$ are kept constant reveals a number of characteristics of FR algorithms. First of all, segmenting the UEs in a BS based on proximity provides a means for more detailed analysis into UE performance, as opposed to finding an overall average for all UEs. This was obvious in the way group 1 and group 2 UEs performed differently in all FR schemes even for Reuse-1 and Reuse-3 schemes. Secondly, a better SINR performance will not always translate to a better capacity performance, consistent with [49]. Thirdly, in scenarios where the UE deployment is not very dense or the effects of lower SINR are higher (e.g in edge UEs at the cell boundary), FFR will likely always outperform SFR in all SINR cases and in most capacity cases. The benefits of the flexibility of SFR will be likely observed in denser UE deployments where the higher bandwidth available in the SFR edge region could translate to better capacity. Fourthly, the flexibility introduced through partitioned FR schemes alone do not guarantee improved performance. Improved performance, especially for edge UEs is also dependent on the combination of $r_c, \mu_{m,s}$ and $f_{e,i}$. Several criteria also exist for specification of desired network performance, such as overall average SINR or capacity, average SINR or capacity for edge UEs etc. The perception of UE performance in a cellular network is hugely dependent on the assessment metric chosen.

### 3.7.2 Case study 2: Single-tier hexagonal BS with dense UE deployment

The UE density (load) in the network is an important factor that determines system performance [49], [50], [51]. In the second case study, the number of UEs in the reference BS is increased ($N_{m,i} = 134$) for a dense deployment and the impact of $r_c$

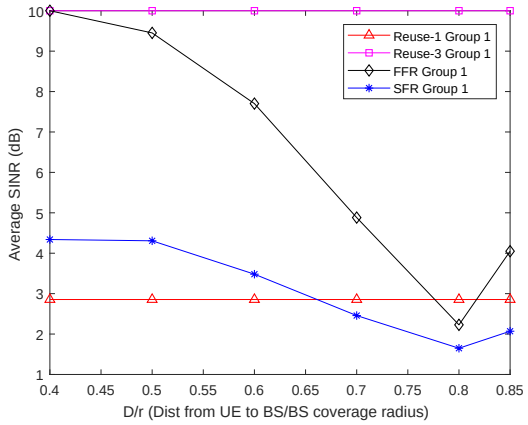


(a) Average SINR for group 1

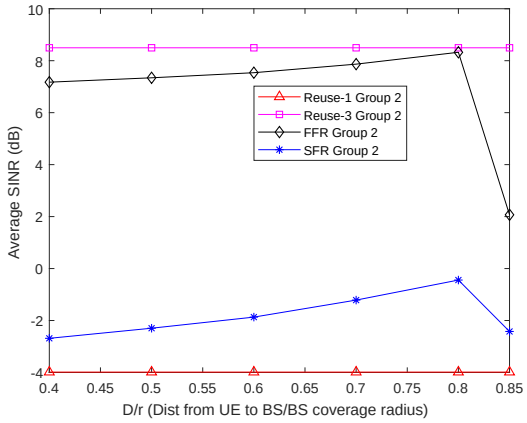


(b) Average SINR for group 2

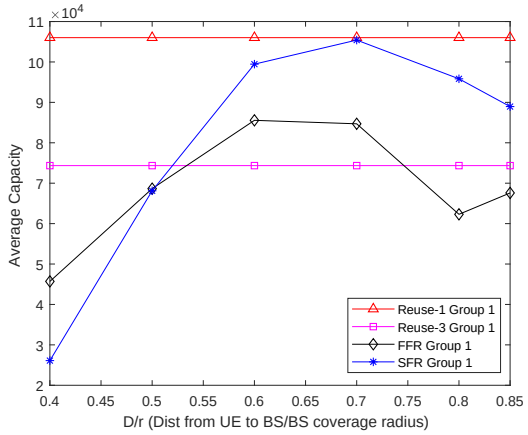


(c) Average capacity (in bps) for group 1

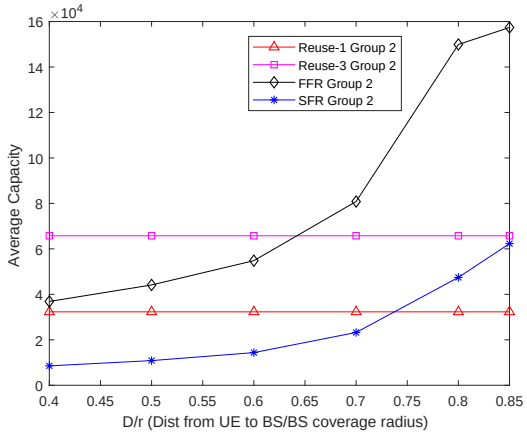


(d) Average capacity (in bps) for group 2

Figure 3.11: Performance for Single-tier regular BS, dense UE: varying $r_c$

is studied while all other parameters remain the same as shown in Table. 3.5.

Table 3.5: Case study 2 parameters

| **Parameter** | **Value** |
|---|---|
| **Center radius** | $0.4r \leq r_c \leq 0.8r$ |
| **Power ratio,** $\mu_{m,s}$ | 2.5 |
| **Edge region bandwidth,** $f_{e,i}$ | $8 \times 180$kHz |
| **Observed number of UEs,** $N_{m,i}$ | 134 |

Compared to the previous result in Fig. 3.7(a), Fig. 3.11(a) shows a drastic drop in the SINR across most cases (except Reuse-3) for both group 1 and group 2 UEs. With the higher number of UEs in dense deployments, the signal transmit power per UE is lower than in Case 1. Considering the assumption that average interference from neighbouring BSs did not change in the new case, (3.1) supports the drop in

SINR observed. The drop in SINR is higher in SFR algorithm than FFR due to the higher effects of interference on SFR described in Fig. 3.2.

Group 1 SFR performance falls lower than Reuse-1 performance at $r_c \geq 0.7r$, FFR performance falls below Reuse-1 at $r_c = 0.8r$ and there is a larger difference between Reuse-1 and Reuse-3 performance. For group 2 SINR shown in Fig. 3.11(b), the maximum SINR for both FFR and SFR occurs at $r_c = 0.8r$ like in the previous case (Fig. 3.7(b)). Reuse-1 and SFR performance are generally poor (mostly under 0dB), with the higher effect of low transmit power at these UEs farther from the serving BS. This suggests these schemes are not suitable for dense UE deployments except their configuration is optimally selected.

The capacity results in Figs. 3.11(c) and 3.11(d) are also lower than the previous cases, due to the lower bandwidth per UE in dense deployment. In group 1 UEs, Reuse-1 maintains the best performance in all cases with SFR approaching it at $r_c = 0.7r$. Whilst SFR rises to a maximum at $r_c = 0.7r$ and drops, FFR fluctuates more. FFR performs worse than Reuse-3 in a number of cases. For group 2, Reuse-3 performs best at low $r_c$ benefiting from its high SINR, then FFR picks up and gives the overall best later. Reuse-1 and SFR give much lower performance than FFR. This is due to the effects of low SINR being more significant in Reuse-1 and SFR. However, SFR is more suited than FFR for overall resource maximization as evidenced in its better group 1 capacity performance.

### 3.7.3 Case study 3: Single-tier irregular BS

The investigation is extended to the case of irregular BS networks with their location parameters listed in Table. 3.3. The specific simulation parameters are similar to those of the hexagonal BS listed in Table. 3.4 except $N_{m,i}$ which changes based on BS locations. They are listed as scenarios $2, 3$ and 4 in Table. 3.6.

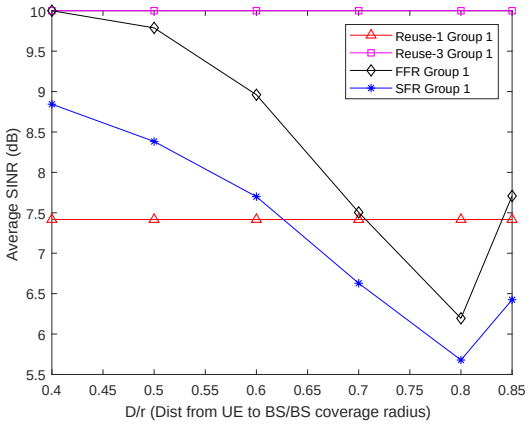


(a) Average SINR for group 1

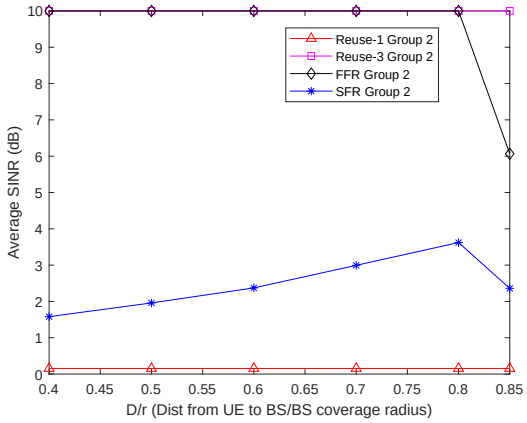


(b) Average SINR for group 2

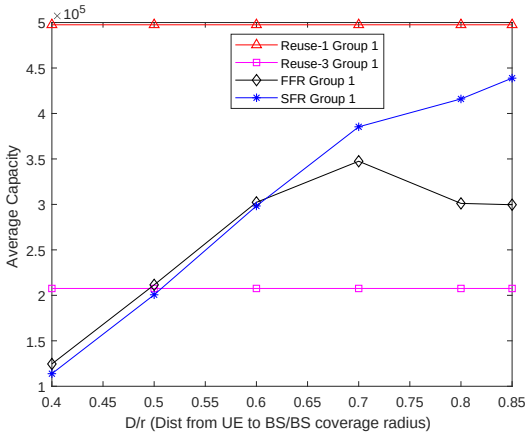


(c) Average capacity (in bps) for group 1

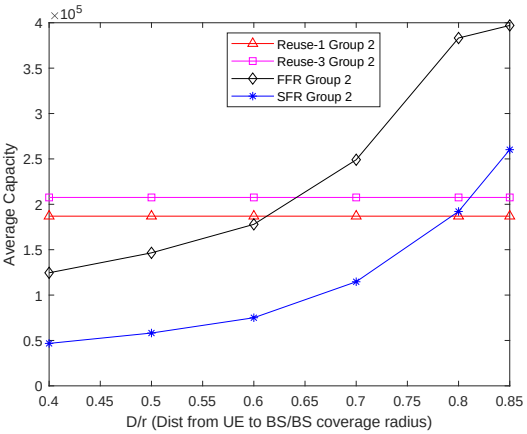


(d) Average capacity (in bps) for group 2

Figure 3.12: Performance for Single-tier irregular BS 1 (scenario 2), full UE: varying $r_c$

Table 3.6: Case study 3 parameters

| **Parameter** | **Sc. 2** | **Sc. 3** | **Sc. 4** |
|---|---|---|---|
| **Center radius** | $0.4r \leq r_c \leq 0.8r$ | | |
| **Power ratio,** $\mu_{m,s}$ | 2.5 | | |
| **Edge region bandwidth,** $f_{e,i}$ | $8 \times 180$kHz | | |
| **Observed number of UEs,** $N_{m,i}$ | 48 | 51 | 62 |
| **Observed number of edge UEs,** $E_{m,i}$ | 13 | 16 | 27 |

**Results for Irregular BS 1 (Scenario 2)**: In the first irregular BS network, Table. 3.6 shows $N_{m,i}$ the total number of UEs in the reference sector is the same as in Case 1 (hexagonal BS scenario) (i.e $N_{m,i} = 48$ given in Table. 3.4). The performance results for this network scenario are shown in Fig. 3.12. The shape of the SINR and capacity curves are similar to the results for the hexagonal BS in

Fig. 3.7. However, for the group 1 UEs, Fig. 3.12(a) shows the SINR for Reuse-1, FFR and SFR are lower than the hexagonal case. Fig. 3.6 reveals that unlike in the hexagonal network that has 2 neighbouring BSs to the reference sector, the first irregular network has 3. This would explain the lower SINR observed. In the case of SINR for group 2 seen in Fig. 3.12(b), there is improvement in SINR for FFR which equals the high SINR in Reuse-3 when $r_c \leq 0.8r$. Group 1 capacity result in Fig. 3.12(c) is similar to the hexagonal case in Fig. 3.7(c) for Reuse-3, FFR and SFR and slightly lower for Reuse-1 due to the effects of lower SINR experienced. The capacity plots in Fig. 3.12(d) show a slightly better performance for FFR than the hexagonal case in Fig. 3.7(d). The similar results for the capacity despite the differences in SINR show that capacity is highly dependent on the bandwidth allocation per UE which is similar in both cases.

**Results for Irregular BS 2 (Scenario** 3**)**: In the second irregular BS network scenario, Table. 3.6 shows $N_{m,i} = 51$, slightly higher than the hexagonal BS case ($N_{m,i} = 48$). The performance results are shown in Fig. 3.13 including SINR and capacity. The plots show differences in the performance for group 2 UEs compared to the hexagonal BS network case. For the SINR, Fig. 3.13(b) shows that SINR is lower for FFR and SFR. The capacity values are also smaller than the previous cases, due to the effects of more UEs. For group 1 UEs, Figs. 3.13(a) and 3.13(c) show that the shape of SINR and capacity curves, and the actual values remain the same for all FR schemes when compared with the previous cases investigated.

So far, some variations from the hexagonal case have been observed with the two irregular BS networks studied. This happens despite the values of $N_{m,i}$ not differing (in the first irregular network) and slightly differing (in the second irregular network). It is important to note that the more significant variations where observed with the group 2 than group 1 UEs. The variations in the two irregular BS networks studied have been observed more significantly with group 2 UE than group 1 under the partitioned FR schemes. This suggests that Reuse-1 and Reuse-3 schemes are less sensitive to BS arrangement than FFR and SFR.

**Results for Irregular BS 3 (Scenario** 4**)**: The last network scenario to be investigated over varying $r_c$ is the third irregular BS network, with the performance results shown in Fig. 3.14. For this network scenario, Table. 3.6 shows $N_{m,i} = 62$

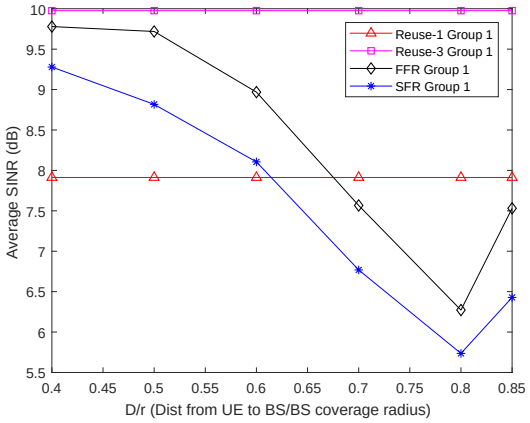


(a) Average SINR for group 1

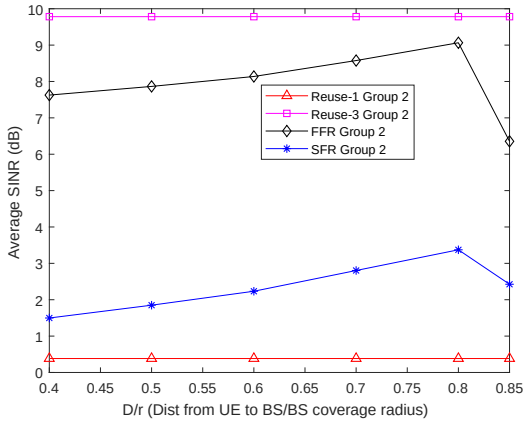


(b) Average SINR for group 2

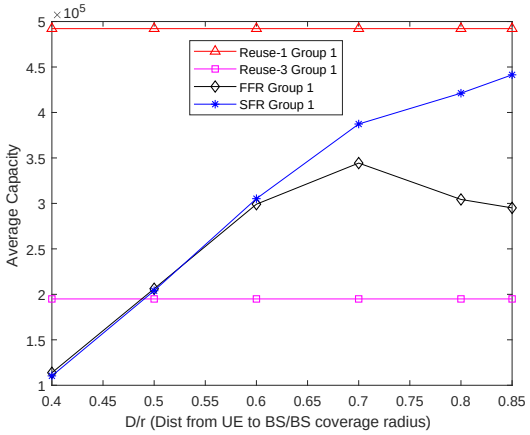


(c) Average capacity (in bps) for group 1

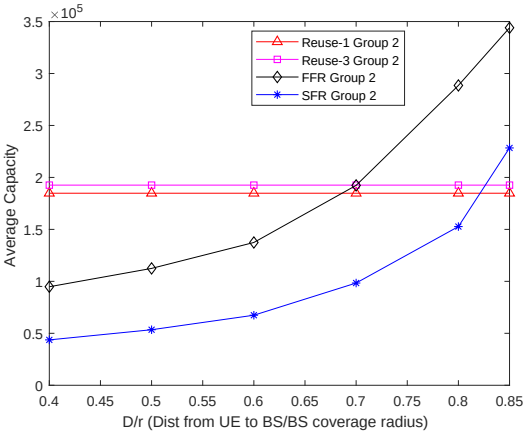


(d) Average capacity (in bps) for group 2

Figure 3.13: Performance for Single-tier irregular BS 2 (scenario 3), full UE: varying $r_c$

which is almost 30% more than the hexagonal BS case. Therefore, it is expected that less signal power and bandwidth resources will be available per UE. For group 1 UEs, Figs. 3.14(a) and 3.14(c) show the variations of SINR and capacity over $r_c$ are similar to all the previous network cases. The values are also slightly lower, for example, than the hexagonal case shown in Figs. 3.7(a) and 3.7(c) respectively, due to lower resources available with higher $N_{m,i}$. For group 2 UEs, there is more significant difference in performance to the hexagonal BS network. The plots in Figs. 3.14(b) and 3.14(d) show significantly smaller values for SINR and Capacity than the hexagonal case (Figs. 3.7(b) and 3.7(d)), especially for the partitioned FR schemes. In relation to Reuse-1 and Reuse-3, the partitioned FR schemes perform poorer for group 2 UEs than in the hexagonal case.

**Summary of results**: The analysis carried out by varying $r_c$ and comparing across

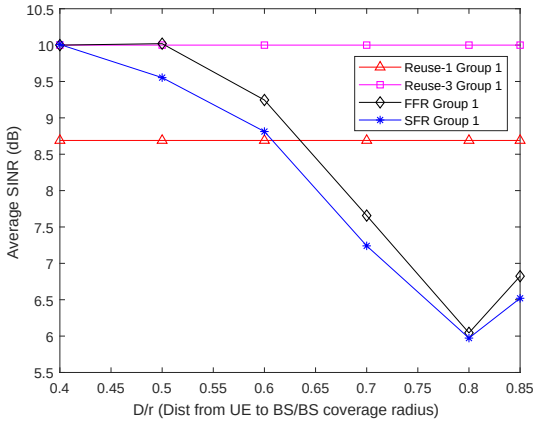


(a) Average SINR for group 1

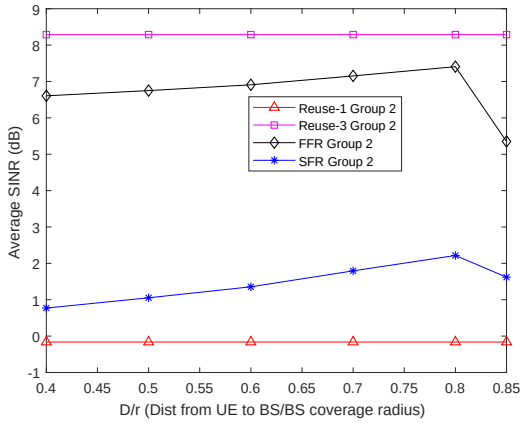


(b) Average SINR for group 2

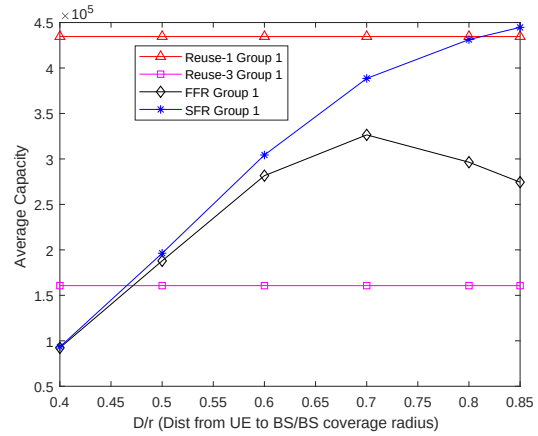


(c) Average capacity (in bps) for group 1

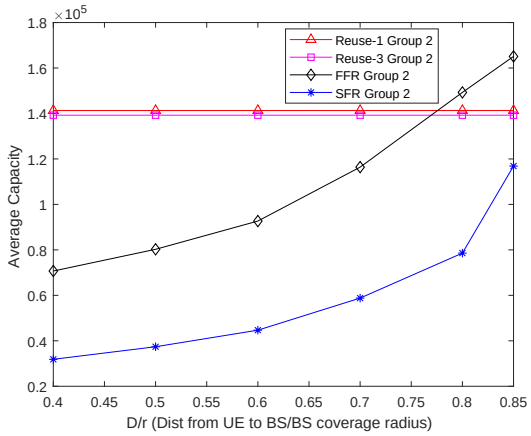


(d) Average capacity (in bps) for group 2

Figure 3.14: Performance for Single-tier irregular BS 3 (scenario 4), full UE: varying $r_c$

the four network scenarios have revealed that structure of the BS network has an effect on the UE performance. The impact of BS regularity is more significant among UEs farther away from the BS (group 2 UEs) and is higher in the partitioned FR schemes (FFR and SFR). This is largely due to the effects of differences in the interference component and in the number of connected UE over different neighbouring BS positioning.

Subsequent analysis will be restricted to the partitioned FR schemes as they are more liable to be altered by BS regularity. Because they involve partitioning the coverage areas, BS parameters can also be altered unlike in the cases of Reuse-1 and Reuse-3.

## 3.8 Investigating the impact of power ratio, $\mu_{m,s}$

SFR is the only FR algorithm where the power ratio, $\mu_{m,s}$ affects SINR and capacity performance. Although FFR employs $\mu_{m,s}$ to control power allocation, because there are no interference components overlapping the center and edge regions, $\mu_{m,s}$ does not directly impact UE performance. Therefore, the results presented in this section are for SFR implementations across the different network case studies.

The parameters used are shown in Table 3.7. Three investigations are conducted. In the first, $r_c$ is fixed at $0.8r$ and the edge bandwidth $f_{e,i}$ is maintained as the previous cases ($8 \times 180$kHz). For the second, $f_{e,i}$ is increased and in the third analysis, $r_c$ is reduced while $f_{e,i}$ is set back to the initial value. The effects of changing $r_c$ in the third case affects the UE classification and by combining different selections for $r_c$ and $f_{e,i}$, $\mu_{m,s}$ is studied in the range 1 to 15.

Table 3.7: Case study 4 parameters

| Analysis | Parameter | Sc. 1 | Sc. 2 | Sc. 3 | Sc. 4 |
|---|---|---|---|---|---|
| 1 | **Center radius,** $r_c$ | | $0.8r$ | | |
| | **Power ratio,** $\mu_{m,s}$ | | $1 \leq \mu_{m,s} \leq 15$ | | |
| | **Edge bandwidth,** $f_{e,i}$ | | $8 \times 180$kHz | | |
| | **Observed number of UEs,** $N_{m,i}$ | 48 | 48 | 51 | 62 |
| | **Observed number of edge UEs,** $E_{m,i}$ | 13 | 13 | 16 | 27 |
| 2 | **Center radius,** $r_c$ | | $0.8r$ | | |
| | **Power ratio,** $\mu_{m,s}$ | | $1 \leq \mu_{m,s} \leq 15$ | | |
| | **Edge bandwidth,** $f_{e,i}$ | | $14 \times 180$kHz | | |
| | **Observed number of UEs,** $N_{m,i}$ | 48 | 48 | 51 | 62 |
| | **Observed number of edge UEs,** $E_{m,i}$ | 13 | 13 | 16 | 27 |
| 3 | **Center radius,** $r_c$ | | $0.7r$ | | |
| | **Power ratio,** $\mu_{m,s}$ | | $1 \leq \mu_{m,s} \leq 15$ | | |
| | **Edge bandwidth,** $f_{e,i}$ | | $8 \times 180$kHz | | |
| | **Observed number of UEs,** $N_{m,i}$ | 48 | 48 | 51 | 62 |
| | **Observed number of edge UEs,** $E_{m,i}$ | 20 | 20 | 23 | 34 |

### 3.8.1 Case study 4

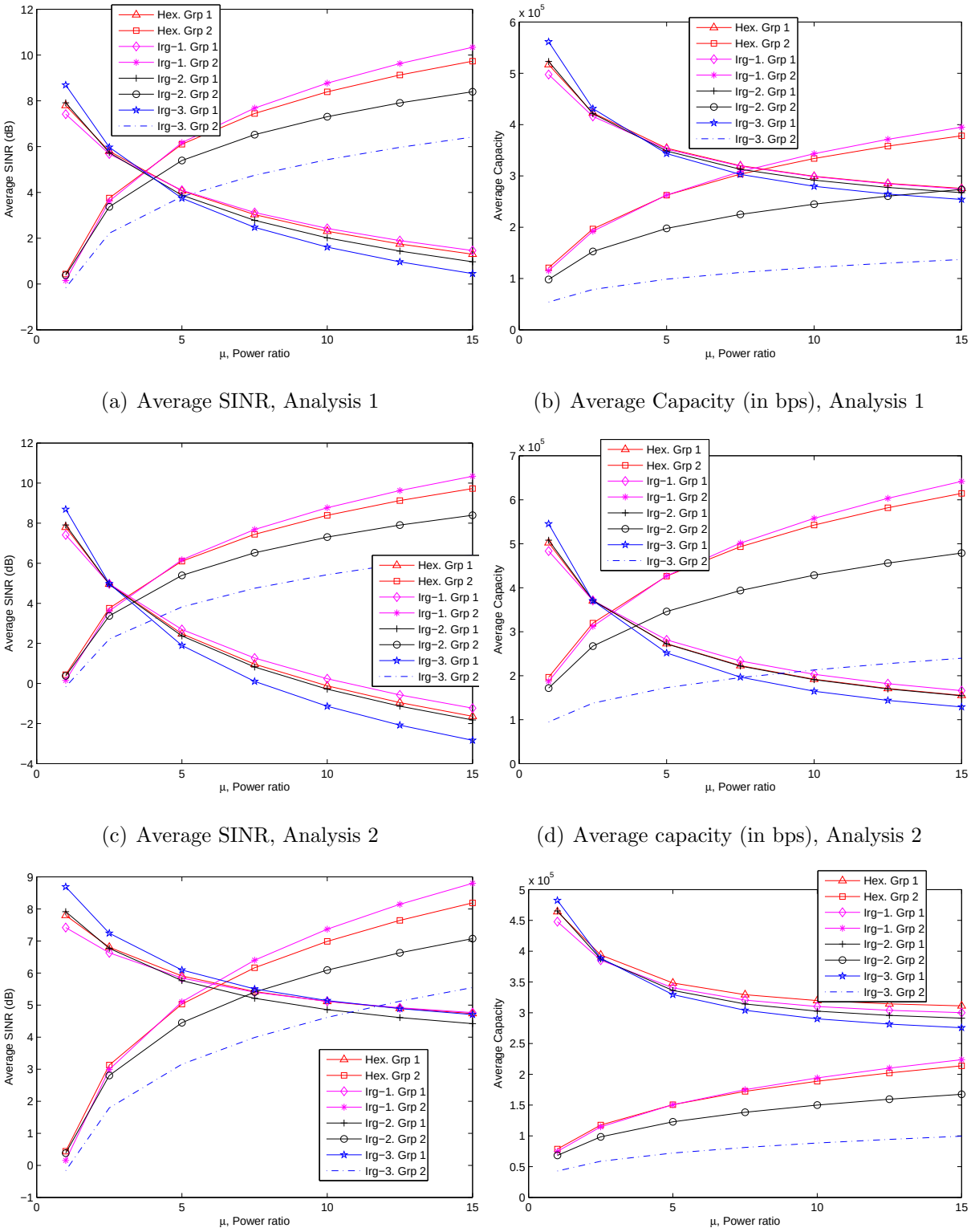


(a) Average SINR, Analysis 1

(b) Average Capacity (in bps), Analysis 1

(c) Average SINR, Analysis 2

(d) Average capacity (in bps), Analysis 2

(e) Average SINR, Analysis 3

(f) Average capacity (in bps), Analysis 3

Figure 3.15: Performance for SFR in all scenarios, full UE: varying $\mu_{m,s}$

Fig. 3.15 shows results for the analysis. As $\mu_{m,s}$ increases, the performance of group 2 UEs improve and that of group 1 UEs suffer. This occurs because group 1 and 2

UEs comprise mostly center and edge UEs respectively, for the values of $r_c$ selected. The observed performance follows that power allocation per edge UE increases with $\mu_{m,s}$ but that of center UEs drops as the explanations after (3.1) show. Most of the plots show that if $\mu_{m,s}$ is sufficiently increased, there is a meeting point between the group 1 and group 2 performance for both SINR and Capacity, above which the group 2 performance exceeds group 1. This reveals the flexibility of SFR technique in guaranteeing edge UE improvement.

At low values of $\mu_{m,s}$, network scenario 4 (Irregular-3) gives the best performance for group 1 UEs, followed by network scenario 3 (Irregular-2), network scenario 1 (Hexagonal) and lastly network scenario 2 (Irregular-1). This occurs in both SINR and capacity for almost all cases observed. However, as $\mu_{m,s}$ increases, the decreasing order of performance is Irregular-1, Hexagonal, Irregular-2 and Irregular-3, which is similar to the case of group 2 UEs. This result shows the effect of reduced performance due to more UEs (Irregular-2 and Irregular-3) is higher in group 2 UEs and in group 1 UEs where $\mu_{m,s}$ is high. For group 1 UEs under low $\mu_{m,s}$, the advantages of proximity to the serving BS nullifies the effect of BS resource allocation.

In the first analysis (Figs. 3.15(a), 3.15(b)), the meeting point for SINR occurs at $3.8 < \mu_{m,s} < 4.5$ and for capacity lies at $7 < \mu_{m,s} < 8$ for most schemes except Group 2 UEs in Irregular-3. Where a meeting point exists, the value of $\mu_{m,s}$ for SINR is usually lower than for capacity. SINR depends on power allocation while capacity depends on both power and bandwidth allocation hence the higher response of SINR to $\mu_{m,s}$. In the second analysis (Figs. 3.15(c), 3.15(d)) where $f_{e,i}$ is increased to $8 \times 180$kHz, the meeting points for SINR and capacity are closer to each other in value except the Irregular-3 network scenario. In the third analysis (Figs. 3.15(e), 3.15(f)) where $r_c$ is reduced, $E_{m,i}$ increases in all cases as Table 3.7 shows and the value of $\mu_{m,s}$ where the meeting point occurs is higher for SINR than in the previous analyses. The higher number of edge UEs ($E_{m,i}$) required higher power allocation to the edge region (higher $\mu_{m,s}$) before appreciable improvement in performance occurred for group 2 UEs. For the third analysis, there is no meeting point for capacity, similar to Irregular-3 in Analysis 1 (in Fig. 3.15(b)). The increase in power ratio was not sufficient to improve the performance of group 2 UEs which are mostly edge UEs since there was no corresponding increase in bandwidth.

## 3.9 Investigating the impact of edge bandwidth $f_{e,i}$

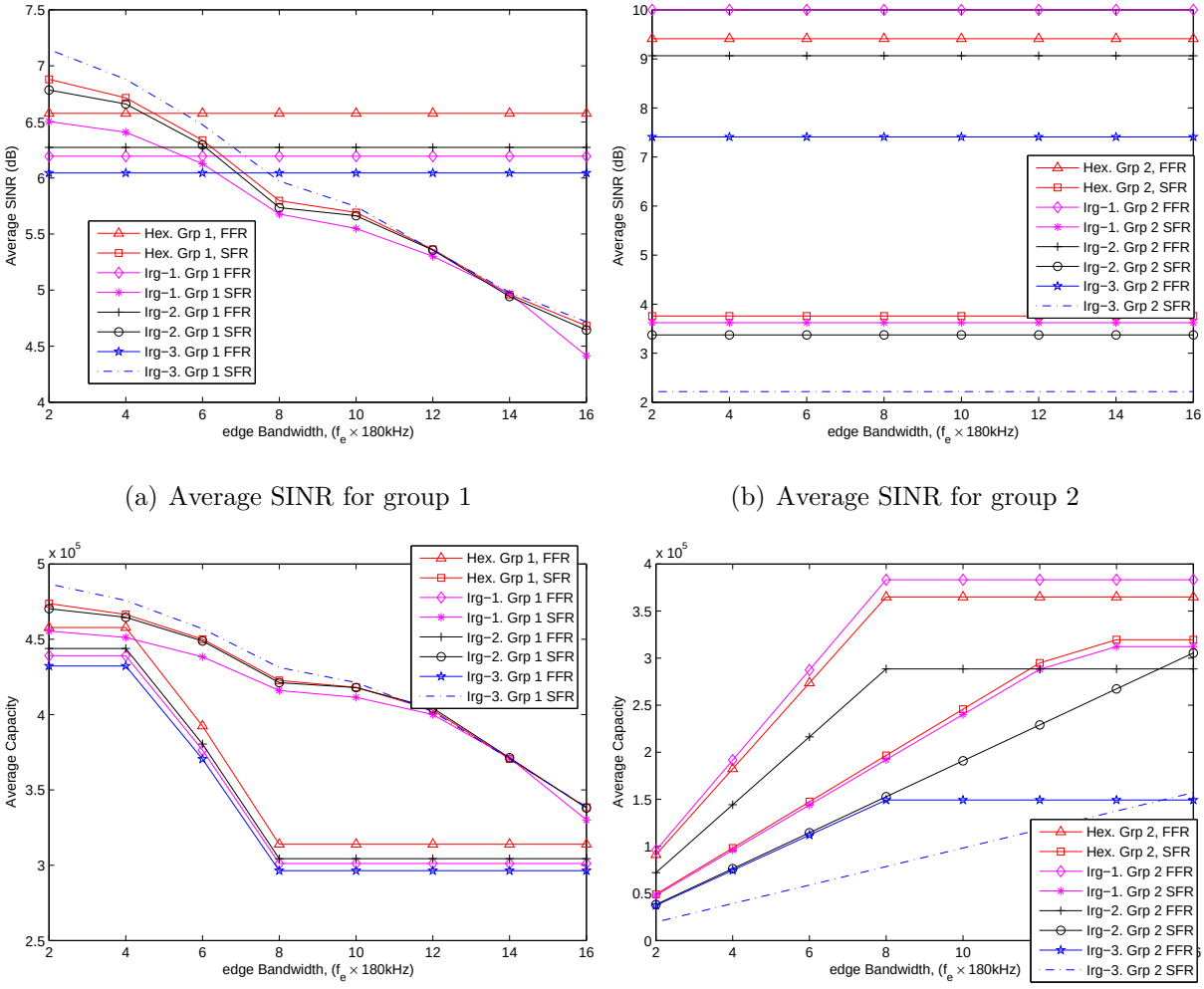


(a) Average SINR for group 1

(b) Average SINR for group 2

(c) Average capacity (in bps) for group 1

(d) Average capacity (in bps) for group 2

Figure 3.16: Single-tier regular BS, full UE: varying $f_{e,i}$

### 3.9.1 Case study 5

The final analysis is based on the edge bandwidth parameter, $f_{e,i}$. The edge (and center) frequency allocation controlled by $f_{e,i}$ is unique to the partitioned FR schemes. Therefore, the analysis presented is exempted for Reuse-1 and Reuse-3. Table. 3.8 shows the simulation parameters (a single value for $r_c$ and $\mu_{m,s}$ are utilized) and Fig. 3.16 shows the SINR and Capacity performance. For group 1 UEs, Fig. 3.16(a) shows a constant SINR performance for FFR, while SFR drops with $f_{e,i}$. Fig. 3.16(b) shows all SINR values constant for group 2 UEs in both schemes, with FFR consistently outperforming SFR. In Fig 3.16(c), the FFR capacity starts of constant,

falls with $f_{e,i}$ then becomes constant again. SFR falls more steeply, showing a faster response over $f_{e,i}$. Finally, in Fig 3.16(d), the capacity increases to a maximum which it maintains. The constant values for capacity occurs because a maximum threshold is set for the bandwidth that can be allocated a UE in the system. Hence, even if the overall bandwidth to a region is increased, the bandwidth per UE may not increase even if the threshold is met. SFR performs better for group 1 UEs while FFR performs better for group 2.

Table 3.8: Case study 5 parameters

| **Parameter** | **Sc. 1** | **Sc. 2** | **Sc. 3** | **Sc. 4** |
|---|---|---|---|---|
| **Center radius,** $r_c$ | $0.8r$ | | | |
| **Power ratio,** $\mu_{m,s}$ | 2.5 | | | |
| **Edge region bandwidth** | $(2 \times 180\text{kHz}) \leq (f_{e,i} \times 180\text{kHz}) \leq (16 \times 180\text{kHz})$ | | | |
| **Observed number of UEs,** $N_{m,i}$ | 48 | 48 | 51 | 62 |
| **Observed number of edge UEs,** $E_{m,i}$ | 13 | 13 | 16 | 27 |

## 3.10 Chapter summary

In this Chapter, the performance of uniform UEs in BS networks of different regularity has been investigated under IFR and partitioned FR algorithms. Initial simulations showed that the network-wide performance did not approximate to the results of a single BS. Therefore, a reference BS was selected for more detailed investigation. UEs were also grouped according to their locations and analysed accordingly. The performance analysis was carried out by considering the center radius classification, $r_c$, power ratio $\mu_{m,s}$ and edge bandwidth $f_{e,i}$. The useful insights obtained give a deeper understanding of FR implementation in cellular networks.

# Chapter 4

# Geometric Frequency Reuse for Irregular Single-tier Networks

## 4.1 Introduction

In this Chapter, an adaptive FR algorithm is proposed for bandwidth allocation in irregular single-tier (macro only) cellular networks. Termed Geometric Frequency Reuse (GeoFRe), this algorithm is based on the geometry characteristics of BS coverage patterns. As observed through simulations in the preceding Chapter, UE performance in cellular networks depends on BS locations and parameters. The proximity of a UE to its connected BS was shown to be a critical factor, therefore necessitating the grouping of UEs for proper analysis. The results revealed the need to develop intelligent FR schemes where BS parameters are smartly selected to guarantee optimal UE performance. Consequently, it is useful to develop mathematical representations for the relationships between the locations of network entities and performance. This is the focus of this Chapter.

A system model for irregular macro BS networks is first described which considers the positional relationships between network entities and resource allocation parameters for each FR scheme. Equations are then presented depicting UE performance in each technique. Finally the different stages for implementation of GeoFRe are presented and evaluation of the algorithm is carried out.

## 4.2 Location model

Consider the downlink (DL) of a single-tier LTE network comprising only macro BSs. Let $\mathcal{M}$ be the set of available macro BSs, where $\mathcal{M}$ comprises a reference BS with index $M$ and a set of neighbouring BSs to $M$. Each BS in $\mathcal{M}$ deploys tri-sector antennas which combine to divide its coverage region into three sectors as shown in Fig. 4.1. The figure shows $S_i$, the sectors of $M$ identified by indexes $S_1, S_2$ and $S_3$. In addition, the positional relationships between $M$ and a connected UE, $U$ or another BS are described with the aid of an imaginary horizontal reference line, $L$ from $M$. Angles measured from $L$ are considered in the anticlockwise direction to a maximum of 180°.

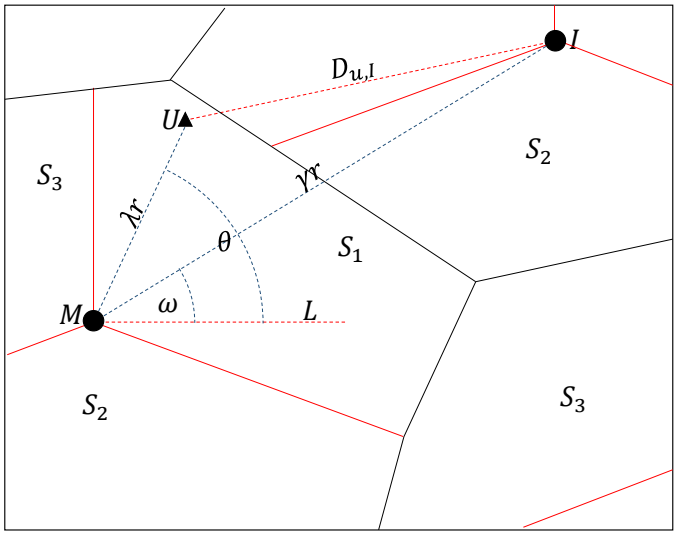


Figure 4.1: Positional layout of Network entities

### 4.2.1 Coordinate Locations

The following notation is used to define the two-dimensional (2D) Cartesian coordinate location for any entity (BS or UE) in the network:

$$X_A = x_a + jy_a, \tag{4.1}$$

where the point location of entity $A$ is referenced by the typical $x(x_a)$ and $y(y_a)$ coordinates.

### 4.2.2 Relationship between locations

An important parameter in this model is the relationship between point locations of a reference entity (e.g $M$) and another entity (e.g a nearby BS or UE). Let $M$ be a reference macro BS with location $X_M$, then if $A$ is a UE within $M$ or a nearby BS, $X_A$ as defined in (4.1) can be expressed in terms of $X_M$ thus:

$$X_A = X_d \angle g = (x_m + dr\cos g) + j(y_m + dr\sin g), \tag{4.2}$$

where $r$ is the standard macro BS coverage radius (defined in the hexagonal placement model), $dr$ is the distance between $A$ and $M$ and $g$ is the angle between line $L$ (defined in Fig. 4.1) and the line joining $A$ to $M$.

Therefore, following (4.1) and (4.2), the Cartesian coordinates of a UE, $U$ shown in Fig. 4.1 at a distance $\lambda r$ from $M$ and angle $\theta$ from $L$ can be written as $X_\lambda \angle \theta$.

### 4.2.3 Relating UEs to Sectors within BSs

Consistent with Fig. 4.1, the sector, $S_i (i = 1, 2 \text{ or } 3)$ of $M$ within which $U$ is located is defined according to the following rule:

$$\begin{cases} S_1 \rightarrow (-30^\circ < \theta \leq 90^\circ) \\ S_2 \rightarrow (90^\circ < \theta \leq 180^\circ) \vee (-180^\circ \leq \theta \leq -150^\circ) \\ S_3 \rightarrow (-150^\circ < \theta \leq -30^\circ) \end{cases} \tag{4.3}$$

### 4.2.4 Distance between an interfering Macro BS to $U$

Fig. 4.1 also shows $I$, which is a neighbouring macro BS to $M$ that provides interference to UEs connected to $M$. Using a similar definition, let the Cartesian coordinate of $I$ be defined as $X_I = (x_m + \gamma r\cos\omega) + j(y_m + \gamma r\sin\omega) = X_\gamma \angle \omega$, where $\gamma r$ is the distance between $M$ and $I$, and $\omega$ is the angle from $M$ to $I$ based on the displacement from $L$. To carry out network analysis and compute UE performance, it is helpful to derive $D_{u,I}$, the distance between $U$ and $I$. In terms of the previously derived location relationships between $M$ and $U$ and between $M$ and $I$, $D_{u,I}$ is given as:

$$D_{u,I} = r\sqrt{\lambda^2 + \gamma^2 - 2\lambda\gamma(\cos(\omega - \theta))}, \tag{4.4}$$

### 4.2.5 BS positional relationships

It is important to specify the allowable proximity in location between any two macro BS in the system. If BSs are too close to each other, their coverage areas would shrink in size to an extent that there might be unused BS resources if UE deployment is low. To prevent such a scenario, the metric used in Chapter 3 (3.4) to define relationships between macro BS positions is also adopted. Consider Fig. 4.2, a case where sector $S_1$ of $M$ is surrounded by three interfering BS, $I_1, I_2$ and $I_3$, located at distances $d_1, d_2$ and $d_3$ respectively from $M$. Different network scenarios depending on the positions of the interfering BS can be studied by defining $d_i (i = 1, 2, 3)$. For any group of three BS including $M$, if $d_i, d_{i+1}, d_{i,i+1}$ and $\omega_i$ are known, then $\omega_{i+1}$ can be calculated thus:

$$\omega_{i+1} = \omega_i - \cos^{-1}[\frac{(d_{min} + \delta_i)^2 + (d_{min} + \delta_{i+1})^2 - (d_{min} + \delta_{i,i+1})^2}{2(d_{min} + \delta_i)(d_{min} + \delta_{i+1})}], \tag{4.5}$$

where $d_{min}$ is the minimum distance between macro BSs in the network and for any interfering BS $I_Z$, $d_z = d_{min} + \delta_z$. For example, if $M, I_1, I_2$ are at the closest possible distances to each other, i.e $\delta_{1,2} = \delta_1 = \delta_2 = 0$, if $\omega_1$ is known, then from (4.5), $\omega_2 = \omega_1 - \cos^{-1}(1/2)$. In addition, $((d_{min} + \delta_i) - (d_{min} + \delta_{i+1}))^2 \leq (d_{min} + \delta_{i,i+1})^2$ by the principles of geometry.

Note that for any interfering BS $I_Z$, $d_z = \gamma_z r$, where $\gamma_z r$ is the distance defined in Fig. 4.1.

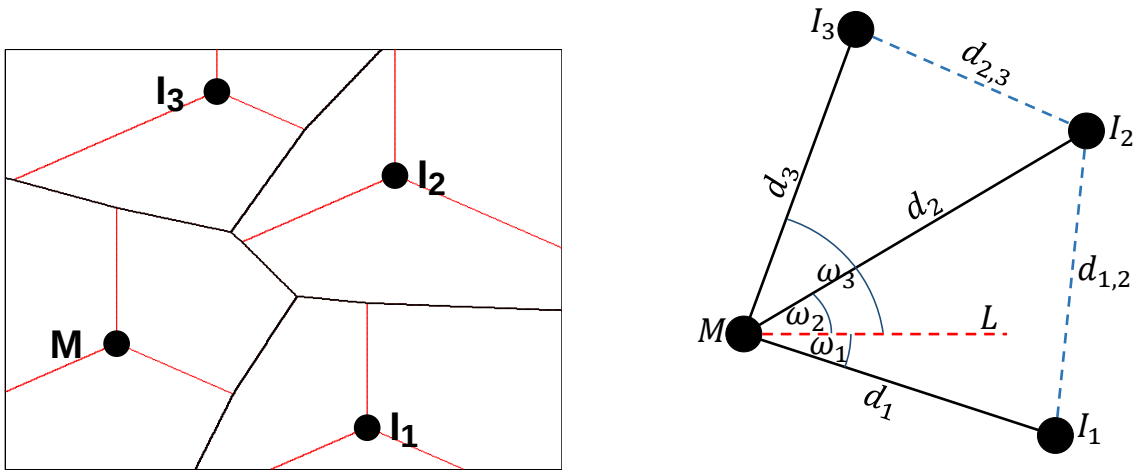


(a) Coverage diagram

(b) Distance analysis

Figure 4.2: Distance relationship between macro BS

## 4.3 FR resource allocation model

Within each sector associated with any BS in the network, portions of the total system bandwidth, $\mathcal{F}$ are allocated to connected UEs based on the FR scheme in operation. This enables the UEs to connect to the network and transmit/receive information. Considering any sector $S_i$ of $M$ which is under investigation, let $f_{m,i}$ be the bandwidth assigned to a UE, $U$, allocated over a specified transmitted power level $p_{m,i}$ from $M$. The size of $f_{m,i}$ is dependent on the FR scheme adopted by $M$ as described in Chapter 3 and reproduced in Fig. 4.3. Recall that in partitioned FR schemes like FFR and SFR, macro BS coverage regions are divided into two: interior (center) and exterior (edge) regions.

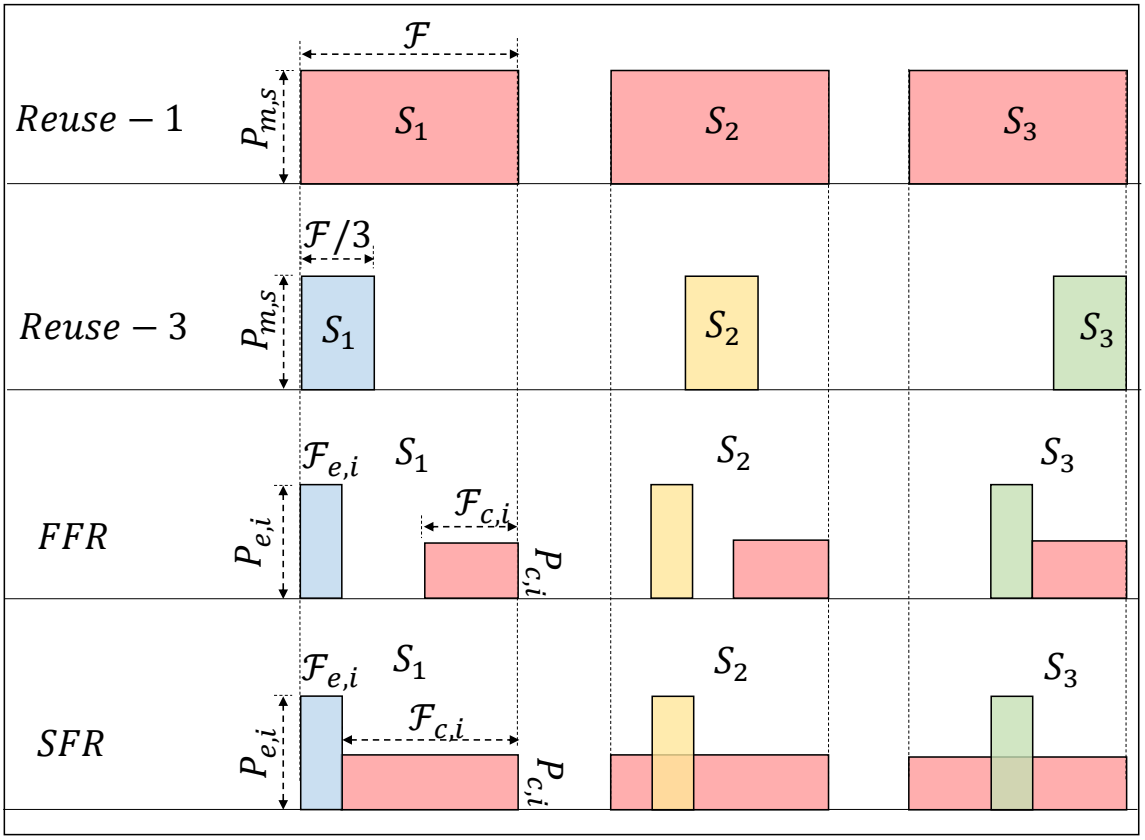


Figure 4.3: Power/Bandwidth allocation for FR schemes

For any sector $S_i$, let $N_{m,i}, E_{m,i}, \mathcal{F}_{e,i}, P_{m,s}$ and $P_{e,i}$ be the total number of connected UE, number of connected edge UE, total allocated edge bandwidth, total power budget and total edge power allocation respectively, Table 4.1 shows $f_{m,i}$ and $p_{m,i}$ for a typical UE, $U$ under the different FR schemes.

Table 4.1: Bandwidth and Power allocation to a UE, $U$ under FR schemes

| **Parameter at** $U$ | **Reuse-1** | **Reuse-3** | **FFR/SFR Center** | **FFR/SFR Edge** |
|---|---|---|---|---|
| **Bandwidth,** $f_{m,i}$ | $\frac{\mathcal{F}}{N_{m,i}}$ | $\frac{\mathcal{F}}{3N_{m,i}}$ | $\frac{\mathcal{F}-\mathcal{F}_{e,i}}{N_{m,i}-E_{m,i}}$ | $\frac{\mathcal{F}_{e,i}}{E_{m,i}}$ |
| **Power allocation,** $p_{m,i}$ | $\frac{P_{m,s}}{N_{m,i}}$ | $\frac{P_{m,s}}{3N_{m,i}}$ | $\frac{P_{m,s}-P_{e,i}}{N_{m,i}-E_{m,i}}$ | $\frac{P_{e,i}}{E_{m,i}}$ |

### 4.3.1 Transmit power for partitioned FR schemes

In any macro BS employing partitioned FR (either FFR or SFR), the total transmit power to a connected center UE differs from that to a connected edge UE. These values are derived and the respective equations for each scheme are presented here.

**FFR power parameter:** In a sector, $S_i$ the total power budget, $P_{m,s}$ can be expressed as:

$$P_{m,s} = 3E_{m,i}p^e_{m,i} + C_{m,i}p^c_{m,i}, \tag{4.6}$$

where $E_{m,i}, C_{m,i}$ are the number of edge and center UEs in $S_i$, respectively, while $p^e_{m,i}, p^c_{m,i}$ are the signal powers transmitted to a single edge and center UE respectively.

The equation for the total number of UEs in $S_i$ based on the different regions is

$$N_{m,i} = E_{m,i} + C_{m,i}. \tag{4.7}$$

Let $\mu_{m,s}$ be defined as the power ratio, the ratio of the transmit power towards an edge UE to the transmit power towards a center UE given as:

$$\mu_{m,s} = \frac{p^e_{m,i}}{p^c_{m,i}}. \tag{4.8}$$

As Fig. 4.3 shows, in both the FFR and SFR algorithms, $p^e_{m,i} > p^c_{m,i}$ to ensure the edge region compensation.

Substituting into (4.6), for $C_{m,i}$ from (4.7) and for $p^c_{m,i}$ from (4.8),

$$p^e_{m,i} = \frac{\mu_{m,s}P_{m,s}}{E_{m,i}(3\mu_{m,s} - 1) + N_{m,i}}. \tag{4.9}$$

Similarly,

$$p^c_{m,i} = \frac{P_{m,s}}{E_{m,i}(3\mu_{m,s} - 1) + N_{m,i}}. \tag{4.10}$$

**SFR power parameter:** For the case of SFR, (4.8) still holds as in the case of FFR, but based on the bandwidth allocation rule, the power budget equation will be:

$$P_{m,s} = E_{m,i}p^e_{m,i} + C_{m,i}p^c_{m,i}, \tag{4.11}$$

consistent with Fig. 4.3. Therefore the transmit power to an edge UE in SFR is:

$$p^e_{m,i} = \frac{\mu_{m,s}P_{m,s}}{E_{m,i}(\mu_{m,s} - 1) + N_{m,i}}. \tag{4.12}$$

For a center UE, the transmit power from the BS in SFR scheme becomes:

$$p^c_{m,i} = \frac{P_{m,s}}{E_{m,i}(\mu_{m,s} - 1) + N_{m,i}}. \tag{4.13}$$

### 4.3.2 Bandwidth overlap for partitioned FR schemes

The bandwidth allocation rules for partitioned FR schemes are presented in Fig. 4.3. It is shown that neighbouring sectors from different BSs allocate different frequency bands to their different regions. For example, separate frequency bands are allocated to the edge regions of sectors from different macro BS in close proximity. This difference in bandwidth allocations is the major element of partitioned FR and is critical to fulfil their goal of reducing interference on edge UE. The amount of interference that a UE in a region (center or edge) within $S_i$ will receive from the transmissions of another region (center or edge) within a sector $S_j$ of an interfering macro BS $I$ can be derived. It is dependent on the amount of overlaps of the frequency bands used by the serving region and the interfering region. Table 4.2 shows the probabilities that interference occurs between regions under the FFR and SFR algorithms.

Table 4.2: $\beta$, Probability of interference in fractional-based FR

| **Sector index** | **Scheme** | **Interference from** | **Interference towards** | |
|---|---|---|---|---|
| | | | Center region | Edge region |
| **Same** ($i = j$) | **FFR/SFR** | Center region | 1 | 0 |
| | | Edge region | 0 | 1 |
| **Different** ($i \neq j$) | **FFR** | Center region | 1 | 0 |
| | | Edge region | 0 | 1 |
| | **SFR** | Center region | $\beta_{c,c} = \frac{\mathcal{F}-2\mathcal{F}_{e,i}}{\mathcal{F}-\mathcal{F}_{e,i}}$ | 1 |
| | | Edge region | $\beta_{e,c} = \frac{\mathcal{F}_{e,i}}{\mathcal{F}-\mathcal{F}_{e,i}}$ | 0 |

The column titled "Sector index" defines whether the index of the sector of the serving region ($i$ from $S_i$) is the same as that of the sector of the interfering region ($j$ from $S_j$). When $i = j$, similar regions provide full interference to each other and zero interference otherwise. This is also true for FFR when $i \neq j$, but in the case of SFR, there are interference probabilities created as Fig. 4.3 shows. Both Table 4.2 and Fig. 4.3 reveal that SFR is more flexible than FFR in resource allocation, consistent with the analysis in Chapter 3. The values obtained for $\beta$ for the different case studies are necessary for accurate computation of the performance parameters (SINR, Capacity) of partitioned FR schemes.

In the next sections, the equations that depict the UE performance are derived for FR schemes in cellular networks. Specifically, the performance parameters considered are the signal-to-interference-plus-noise ratio (SINR) and the Capacity.

## 4.4 Signal-to-interference-plus-noise ratio equations

Note that: 1) The minimum distance pathloss model is used for the received power components of the SINR equations. 2) $\sigma^2$, (the noise power) is considered to be negligible compared to the cumulative interference component, (therefore $\sigma^2 = 0$ in all cases).

### 4.4.1 Reuse-1 SINR

In this scheme, the total interference towards a sector is the combined interference from all sectors of all neighbouring BS. The SINR for a typical UE, $U$ connected to

sector $S_i$ of $M$ is given as:

$$SINR_u^{r1} = \frac{\min(p_{m,i}, p_{u,max}) h_{m,i} G_{m,i}}{\sum_{j \epsilon \mathcal{J}} \sum_{k \epsilon \{1,2,3\}} \min(p_{j,k}, p_{u,max}) h_{j,k} G_{j,k}}, \tag{4.14}$$

where $p_{m,i}$ is the calculated transmit power (based on UE density) from $S_i$ to $U$ as defined in Table 4.1, i.e $p_{m,i} = \frac{P_{m,s}}{N_{m,i}}$, ($P_{m,s}$ is the total transmit power budget per sector which is the same for all sectors and $N_{m,i}$ is the number of active UEs connected to $S_i$). In addition, $p_{u,max}$ is defined as the maximum allowable signal transmit power per UE, so the actual power allocated to $U$ is the minimum between $p_{m,i}$ and $p_{u,max}$. In addition, $h_{m,i}$ and $G_{m,i}$ are the fading component and path loss respectively, associated with $U$'s connection to $S_i$ in $M$. $\mathcal{J}$ is the set of interfering BS to $M$, while $p_{j,k}, h_{j,k}$ and $G_{j,k}$ relate to transmissions towards $U$ from the sector, $S_k$ of an interfering BS $I$ in $\mathcal{J}$ with similar definitions as $p_{m,i}, h_{m,i}$ and $G_{m,i}$ respectively. It is assumed that for each sector $(S_i, \forall S_k)$ under consideration, $(N_{m,i}, N_{j,k})$ is high enough such that $p_{m,i}, p_{j,k} < p_{u,max}$. In addition, with the minimum distance pathloss model used, $h_{m,i} = h_{j,k} = 1$, so (4.14) can be written as:

$$SINR_u^{r1} = \frac{N_{m,i}^{-1}(\lambda r)^{-\alpha}}{\sum_{j \epsilon \mathcal{J}} \sum_{k \epsilon \{1,2,3\}} N_{j,k}^{-1}(D_{i,k})^{-\alpha}} = \frac{N_{m,i}^{-1}\lambda^{-\alpha}}{\sum_{j \epsilon \mathcal{J}} \sum_{k \epsilon \{1,2,3\}} N_{j,k}^{-1}(\lambda^2 + \gamma_k^2 - 2\lambda\gamma_k \cos(\omega_k - \theta))^{-\frac{\alpha}{2}}}, \tag{4.15}$$

where $\alpha$ is the path-loss exponent and $D_{i,k} = r\sqrt{\lambda^2 + \gamma_k^2 - 2\lambda\gamma_k(\cos(\omega_k - \theta))}$ as defined in (4.4). $\lambda, \gamma_k, \theta$ and $\omega_k$ are defined based on the positional descriptions in Fig. 4.1.

### 4.4.2 Reuse-3 SINR

For this scheme, the SINR for $U$ is derived as:

$$SINR_u^{r3} = \frac{\min(\frac{P_{m,s}}{3N_{m,i}}, p_{u,max}) h_{m,i} G_{m,i}}{\sum_{j \epsilon \mathcal{J}} \sum_{k=i} \min(\frac{P_{m,s}}{3N_{j,k}}, p_{u,max}) h_{j,k} G_{j,k}}, \tag{4.16}$$

where all assumptions and parameters are similar to (4.14). However, interference is only received from any neighbouring BS's sector, $(S_k)$ which has the same antenna index as $U$'s serving BS's sector, $S_i$, i.e when $k = i$. This implies that each interfering BS, $I$ contributes interference from only one of its sectors.

Expanding (4.16) like (4.14), but with $p_{m,i} = \frac{P_{m,s}}{3N_{m,i}}$ and $p_{j,k} = \frac{P_{m,s}}{3N_{j,k}}$ based on Table 4.1, then

$$SINR_u^{r3} = \frac{N_{m,i}^{-1}\lambda^{-\alpha}}{\sum_{j\epsilon\mathcal{J}}\sum_{k=i} N_{j,k}^{-1}(\lambda^2+\gamma_k^2-2\lambda\gamma_k\cos(\omega_k-\theta))^{-\frac{\alpha}{2}}}, \tag{4.17}$$

### 4.4.3 FFR SINR

In this scheme, each BS's coverage region is divided into two, with corresponding classes of UEs (center and edge) defined accordingly.

**Center UE**: The SINR for a center UE is:

$$SINR_{u,c}^{ffr} = \frac{\min(p_{m,i}^c, p_{u,max})h_{m,i}G_{m,i}}{\sum_{j\epsilon\mathcal{J}}\sum_{k\epsilon\{1,2,3\}}\min(p_{j,k}^c, p_{u,max})h_{j,k}G_{j,k}}, \tag{4.18}$$

where $p_{m,i}^c = \frac{P_{m,s}-P_{e,i}}{N_{m,i}-E_{m,i}}$ and $p_{j,k}^c = \frac{P_{m,s}-P_{e,k}}{N_{j,k}-E_{j,k}}$ represent the calculated transmissions to $U$ from the center regions of $M$ and $I$ respectively, following Table 4.1. Consistent with Table 4.2 and Fig. 4.3, the center region of $S_i$ receives complete interference from the center regions of all $S_j$ and no interference from any edge region.

The power transmissions to each edge and center UE are dependent on $\mu_{m,s}$, the network power ratio and are derived in (4.9) and (4.10) respectively. Analysing in terms of $\mu_{m,s}$, setting $h = 1$ and assuming $p_{m,i}^c, p_{j,k}^c < p_{u,max}$ as in previous cases, 4.18 becomes

$$SINR_{u,c}^{ffr} = \frac{\frac{P_{m,s}}{E_{m,i}(3\mu_{m,s}-1)+N_{m,i}}(\lambda r)^{-\alpha}}{\sum_{j\epsilon\mathcal{J}}\sum_{k\epsilon\{1,2,3\}}\frac{P_{m,s}}{E_{j,k}(3\mu_{m,s}-1)+N_{j,k}}r^{-\alpha}(\lambda^2+\gamma_k^2-2\lambda\gamma_k\cos(\omega_k-\theta))^{-\frac{\alpha}{2}}} \tag{4.19}$$

$$= \frac{(E_{m,i}(3\mu_{m,s}-1)+N_{m,i})^{-1}\lambda^{-\alpha}}{\sum_{j\epsilon\mathcal{J}}\sum_{k\epsilon\{1,2,3\}}(E_{j,k}(3\mu_{m,s}-1)+N_{j,k})^{-1}(\lambda^2+\gamma_k^2-2\lambda\gamma_k\cos(\omega_k-\theta))^{-\frac{\alpha}{2}}}.$$

**Edge UE**: The SINR for an edge UE is given as:

$$SINR_{u,e}^{ffr} = \frac{\frac{\mu_{m,s}P_{m,s}}{E_{m,i}(3\mu_{m,s}-1)+N_{m,i}}(\lambda r)^{-\alpha}}{\sum_{j\epsilon\mathcal{J}}\sum_{k=i}\frac{\mu_{m,s}P_{m,s}}{E_{j,k}(3\mu_{m,s}-1)+N_{j,k}}r^{-\alpha}(\lambda^2+\gamma_k^2-2\lambda\gamma_k\cos(\omega_k-\theta))^{-\frac{\alpha}{2}}} \tag{4.20}$$

$$= \frac{(E_{m,i}(3\mu_{m,s}-1)+N_{m,i})^{-1}\lambda^{-\alpha}}{\sum_{j\epsilon\mathcal{J}}\sum_{k=i}(E_{j,k}(3\mu_{m,s}-1)+N_{j,k})^{-1}(\lambda^2+\gamma_k^2-2\lambda\gamma_k\cos(\omega_k-\theta))^{-\frac{\alpha}{2}}}.$$

In this case, interference only comes from the edge region of a sector of a neighbouring BS with the same index as the serving sector, similar to the case of Reuse-3.

### 4.4.4 SFR SINR

The equations derived for the second partitioned FR scheme (SFR) are also consistent with Fig. 4.3

**Center UE**: The SINR for a center UE when SFR is deployed is

$SINR^{sfr}_{u,c} =$

$$\frac{\min(p^c_{m,i},p_{u,max})h_{m,i}G_{m,i}}{\sum\limits_{j\epsilon\mathcal{J}}\sum\limits_{k\neq i}[\beta_{c,c}\min(p^c_{j,k},p_{u,max})+\beta_{e,c}\min(p^e_{j,k},p_{u,max})]h_{j,k}G_{j,k}+\sum\limits_{j\epsilon\mathcal{J}}\sum\limits_{l=i}\min(p^c_{j,l},p_{u,max})h_{j,l}G_{j,l}}, \tag{4.21}$$

where $\beta_{c,c}$ and $\beta_{e,c}$ are obtained from Table 4.2. The first term in the denominator refers to interference from the center and edge transmissions of neighbouring sectors whose index differs from that of $S_i$. The second term in the denominator refers to the interference from the center region of neighbouring sectors with the same index as $S_i$. This interference component can be considered negligible as it comes from distant transmissions from $S_i$. $p^c_{m,i}, p^c_{j,k}$ can be obtained from (4.12) and $p^e_{j,k}$ from (4.13), therefore,

$$\begin{aligned} SINR^{sfr}_{u,c} &= \frac{\frac{P_{m,s}}{E_{m,i}(\mu_{m,s}-1)+N_{m,i}}(\lambda r)^{-\alpha}}{\sum\limits_{j\epsilon\mathcal{J}}\sum\limits_{k\neq i}(\frac{\frac{\mathcal{F}-2\mathcal{F}_{e,i}}{\mathcal{F}-\mathcal{F}_{e,i}}P_{m,s}}{E_{j,k}(\mu_{m,s}-1)+N_{j,k}}+\frac{\mu_{m,s}\frac{\mathcal{F}_{e,i}}{\mathcal{F}-\mathcal{F}_{e,i}}P_{m,s}}{E_{j,k}(\mu_{m,s}-1)+N_{j,k}})r^{-\alpha}(\lambda^2+\gamma_k^2-2\lambda\gamma_k\cos(\omega_k-\theta))^{-\frac{\alpha}{2}}} \\ &= \frac{(E_{m,i}(\mu_{m,s}-1)+N_{m,i})^{-1}\lambda^{-\alpha}}{\sum\limits_{j\epsilon\mathcal{J}}\sum\limits_{k\neq i}(\frac{\mathcal{F}-2\mathcal{F}_{e,i}+\mu_{m,s}\mathcal{F}_{e,i}}{(E_{j,k}(\mu_{m,s}-1)+N_{j,k})(\mathcal{F}-\mathcal{F}_{e,i})})(\lambda^2+\gamma_k^2-2\lambda\gamma_k\cos(\omega_k-\theta))^{-\frac{\alpha}{2}}}. \end{aligned} \tag{4.22}$$

**Edge UE**: The SINR for the edge UE when SFR scheme is deployed is:

$$SINR^{sfr}_{u,e} = \frac{\min(p^e_{m,i},p_{u,max})h_{m,i}G_{m,i}}{\sum\limits_{j\epsilon\mathcal{J}}\sum\limits_{k\neq i}\min(p^c_{j,k},p_{u,max})h_{j,k}G_{j,k}+\sum\limits_{j\epsilon\mathcal{J}}\sum\limits_{l=i}\min(p^e_{j,l},p_{u,max})h_{j,l}G_{j,l}}, \tag{4.23}$$

and similarly to 4.21, the second component of the denominator is negligible, so,

$$\begin{aligned} SINR_{u,e}^{sfr} &= \frac{\frac{\mu_{m,s}P_{m,s}}{E_{m,i}(\mu_{m,s}-1)+N_{m,i}}(\lambda r)^{-\alpha}}{\sum_{j\epsilon\mathcal{J}}\sum_{k\neq i}\frac{P_{m,s}}{E_{j,k}(\mu_{m,s}-1)+N_{j,k}}r^{-\alpha}(\lambda^2+\gamma_k^2-2\lambda\gamma_k\cos(\omega_k-\theta))^{-\frac{\alpha}{2}}} \\ &= \frac{\mu_{m,s}(E_{m,i}(\mu_{m,s}-1)+N_{m,i})^{-1}\lambda^{-\alpha}}{\sum_{j\epsilon\mathcal{J}}\sum_{k\neq i}(E_{j,k}(\mu_{m,s}-1)+N_{j,k})^{-1}(\lambda^2+\gamma_k^2-2\lambda\gamma_k\cos(\omega_k-\theta))^{-\frac{\alpha}{2}}}. \end{aligned} \tag{4.24}$$

**Note:** For the partitioned FR schemes (FFR and SFR), while $\mu_{m,s}$ and $\mathcal{F}_{e,i}$ are assumed the same in all sectors, but in FR optimization schemes, these parameters can vary.

## 4.5 Capacity equations

The equations of Capacity for $U$ for the different FR schemes are derived with the aid of the standard Capacity equation and using bandwidth values from Table 4.1

### 4.5.1 Reuse-1 Capacity

When Reuse-1 scheme is deployed, the Capacity is:

$$Cap_u^{r1} = \min[\mathcal{F}_{u,max}, \frac{\mathcal{F}}{N_{m,i}}][\log_2(1+SINR_u^{r1})], \tag{4.25}$$

where $\mathcal{F}_{u,max}$ is the maximum allowable bandwidth allocation per UE, $\mathcal{F}$ is the total system bandwidth and $N_{m,i}$ is the number of UE in sector $S_i$, consistent with the definition in Table 4.2. Therefore the actual bandwidth assigned from $S_i$ to $U$ is the minimum between $\mathcal{F}_{u,max}$ and $\frac{\mathcal{F}}{N_{m,i}}$.

### 4.5.2 Reuse-3 Capacity

For the Reuse-3 scheme:

$$Cap_u^{r3} = \min[\mathcal{F}_{u,max}, \frac{\mathcal{F}}{3N_{m,i}}][\log_2(1+SINR_u^{r3})]. \tag{4.26}$$

### 4.5.3 FFR Capacity

For a center UE when FFR is used:

$$Cap_{u,c}^{ffr} = \min[\mathcal{F}_{u,max}, \frac{\mathcal{F} - \mathcal{F}_{e,i}}{N_{m,i} - E_{m,i}}][\log_2(1 + SINR_{u,c}^{ffr})]. \tag{4.27}$$

Similarly for the edge UE:

$$Cap_{u,e}^{ffr} = \min[\mathcal{F}_{u,max}, \frac{\mathcal{F}_{e,i}}{E_{m,i}}][\log_2(1 + SINR_{u,e}^{ffr})]. \tag{4.28}$$

### 4.5.4 SFR Capacity

The Capacity for a center UE when SFR is used is:

$$Cap_{u,c}^{sfr} = \min[\mathcal{F}_{u,max}, \frac{\mathcal{F} - \mathcal{F}_{e,i}}{N_{m,i} - E_{m,i}}][\log_2(1 + SINR_{u,c}^{sfr})]. \tag{4.29}$$

Finally, the Capacity for the edge UE under the SFR scheme is:

$$Cap_{u,e}^{sfr} = \min[\mathcal{F}_{u,max}, \frac{\mathcal{F}_{e,i}}{E_{m,i}}][\log_2(1 + SINR_{u,e}^{sfr})]. \tag{4.30}$$

**Note**: For the LTE networks, the system bandwidth is allocated via physical resource blocks (PRBs). Therefore if $N_{prb}$ is the total number of PRBs (which is utilized in $S_i$, $N_{e,prb}$ the number of PRBs used in the edge region of $S_i$ and $\mathcal{F}_{prb}$ is the bandwidth per PRB, then $\mathcal{F}_{u,max} = \mathcal{F}_{prb}N_{prb}$ and $\mathcal{F}_{e,i} = \mathcal{F}_{prb}N_{e,prb}$.

## 4.6 Spectral Efficiency equation

For each FR scheme, the spectral efficiency in a reference BS sector, $S_i$ in $M$ is given by:

$$SE_i = \frac{1}{\mathcal{F}} \sum_{j}^{N_{m,i}} Cap_j, \tag{4.31}$$

where $Cap_j$ is the Capacity for a UE in $S_i$.

## 4.7 Analysis of SFR equation with $\beta$ component

The SINR equation for center UEs under SFR algorithm given in (4.21), (4.22) account for the interference probabilities presented in Table. 4.2. The derived equations are used for a hexagonal network and compared with results from simulations, shown in Figs. 4.4 and 4.5. In Fig. 4.4, the SINR is plotted with varying $\mu_{m,s}$ and as expected the SINR drops as $\mu_{m,s}$ increases. $f_{e,i}$ is varied in Fig. 4.5. Both plots show the equations capturing the interference probabilities give closer results to simulations than when they are not considered.

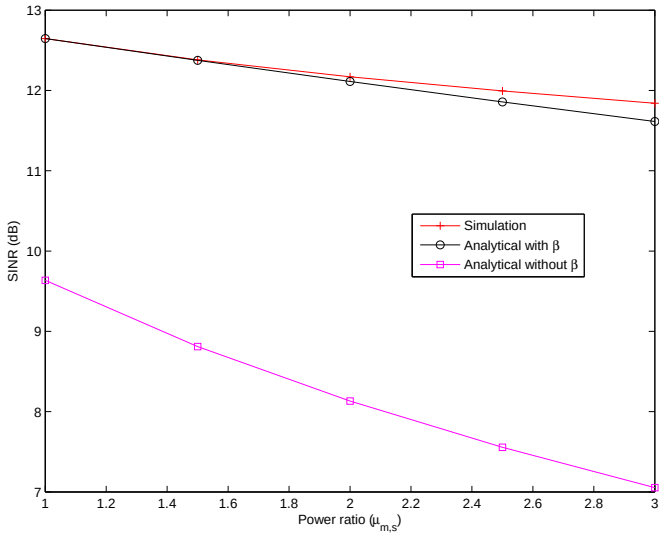


Figure 4.4: SFR Analysis over $\mu_{m,s}$ for center UE (Hexagonal BS)

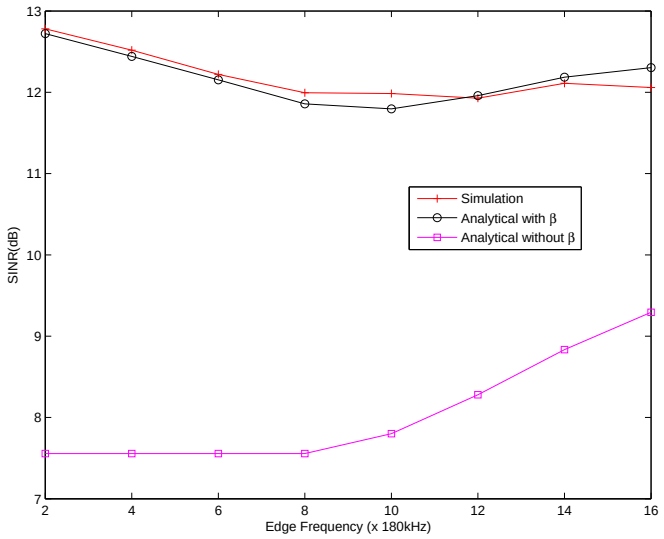


Figure 4.5: SFR Analysis over $f_{e,i}$ for center UE (Hexagonal BS)

## 4.8 Geometric FR algorithm: GeoFRe

A new adaptive algorithm is designed to adjust parameters of the partitioned FR schemes in irregular networks. The algorithm is called Geometric FR (GeoFRe), as it is developed based on the geometric characteristics of macro BS coverage areas. The goal is to compute the geometric area of the irregular coverage patterns of macro BS, then use this area to determine bandwidth assignment. Efficient bandwidth sharing is performed for the center and edge regions for a uniform UE deployment. With intelligent bandwidth allocation that matches the network structure, it is expected that UE performance will improve significantly. The system model and performance parameters earlier developed are used to evaluate the performance of the algorithm over different scenarios. The different stages of the algorithm are:

- Computing candidate coverage vertices,
- Testing and selecting vertices,
- Area computation and
- Bandwidth assignment

### 4.8.1 Computing candidate vertices

In typical networks where the macro BSs are not placed in perfect regular patterns, the coverage vertices do not form regular hexagons. The first task in GeoFRe is to determine for a BS, all the "possible" vertices of its irregular coverage shapes. For example, in Fig. 4.6, the possible vertices of the sector $S_1$ are $\{V_1, V_2, V_3, V_4, V_5\}$; although $V_1$ is not an actual vertex. At a typical BS, $M$, this step of the algorithm is carried out over each of its three sectors $S_i$ by considering the corresponding set $\mathcal{I}_i$, (the set of neighbouring BSs closest to $S_i$). With the assumption that Cartesian coordinates of all neighbouring BSs are known by $M$, the principles of geometry are used to calculate the possible vertices of the coverage of $S_i$. This stage of the algorithm is given in **Algorithm 1**. **Algorithm 1** takes as input $X_m$, the Cartesian coordinate of $M$, $\mathcal{I}$ the set of indexes for all the closest neighbouring macro BSs to $M$, $\mathcal{I}_i$, the set of indexes for neighbouring BSs to each sector $S_i$ of $M$ and $r$ the network radius of coverage for macro BS (the radius for hexagonal arrangements). The elements of the sets $\mathcal{I}$ and each set $\mathcal{I}_i$ are arranged based on the anticlockwise

order of their positions around $M$ and the sectors $S_i$ respectively as shown in Fig. 4.6.

**Algorithm 1** Computing candidate coverage vertices for the sectors of $M$

**Input:** $X_m(x_m + jy_m)$, $\mathfrak{I}$, $\mathfrak{I}_1$, $\mathfrak{I}_2$, $\mathfrak{I}_3, r$
**Output:** $X_R^1, X_R^2, X_R^3, X_{swap,1}, X_{swap,2}$

$X_{swap,1} = \text{Array}[3,1]$, $X_{swap,2} = \text{Array}[3,1]$
**for** $c = 1$ to $3$ **do**
  **if** $c = 3$ **then**
    $I_f = \mathfrak{I}_{c-2}(\text{end})$, $X_{n,1} = X_f$
  **else**
    $I_f = \mathfrak{I}_{c+1}(\text{end})$, $X_{n,1} = X_f$
  **end if**
  $X_R^c = \text{Array}[(\text{SIZE}(\mathfrak{I}_c) + 1), 1]$
  $I_g = \mathfrak{I}_c(1)$, $X_R^c(1,1) = \textbf{JOINPoint}(X_m, X_g, X_{n,1})$
  **for** $d = 1$ to $(\textbf{SIZE}(\mathfrak{I}_c) - 1)$ **do**
    $I_g = \mathfrak{I}_c(d), I_h = \mathfrak{I}_c(d+1)$, $X_R^c(d+1,1) = \textbf{JOINPoint}(X_m, X_g, X_h)$
  **end for**
  **if** $c = 1$ **then**
    $I_f = \mathfrak{I}_{c+2}(1)$, $X_{n,2} = X_f$
  **else**
    $I_f = \mathfrak{I}_{c-1}(1)$, $X_{n,2} = X_f$
  **end if**
  $I_g = \mathfrak{I}_c(\text{end})$, $X_R^c(\text{end},1) = \textbf{JOINPoint}(X_m, X_g, X_{n,2})$
  $X_{b,1} = (x_m + r\frac{\sqrt{3}}{2}) + j(y_m - \frac{r}{2})$, $Z_{b,1} = -\frac{1}{\sqrt{3}}$
  $X_{b,2} = (x_m - r\frac{\sqrt{3}}{2}) + j(y_m - \frac{r}{2})$, $Z_{b,2} = \frac{1}{\sqrt{3}}$
  $X_{b,3} = x_m + j(y_m + r)$, $Z_{b,3} = \infty$
  $I_g = \mathfrak{I}_c(1)$, $X_{m,g} = \frac{x_m + x_g}{2} + j\frac{y_m + y_g}{2}$, $Z_{m,g} = \frac{y_m - y_g}{x_m - x_g}$
  $X_{swap,1}(c,1) = \textbf{INTERSECT}(X_{b,c}, Z_{b,c}, X_{m,g}, -(Z_{m,g})^{-1})$
  $I_g = \mathfrak{I}_c(\text{end})$, $X_{m,g} = \frac{x_m + x_g}{2} + j\frac{y_m + y_g}{2}$, $Z_{m,g} = \frac{y_m - y_g}{x_m - x_g}$
  **if** $c = 1$ **then**
    $k = c + 2$
  **else**
    $k = c - 1$
  **end if**
  $X_{swap,2}(c,1) = \textbf{INTERSECT}(X_{b,k}, Z_{b,k}, X_{m,g}, -(Z_{m,g})^{-1})$
**end for**

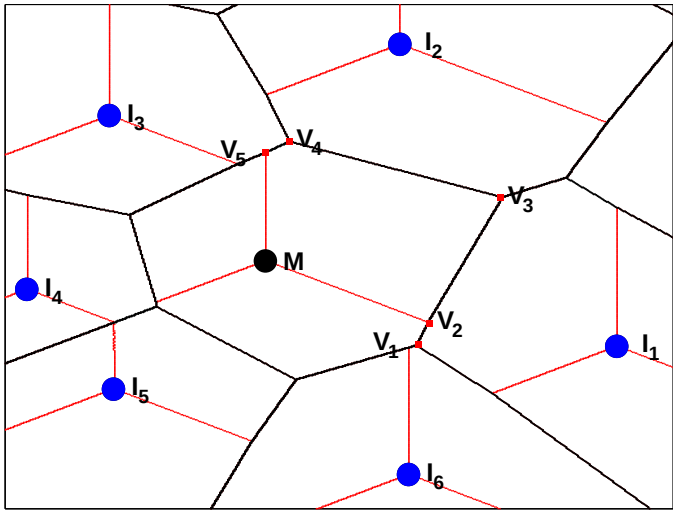


Figure 4.6: Vertices of sector $S_1$ of ref. BS $M$

Therefore as explained, for $S_1$, $\mathfrak{I}_1 = \{I_1, I_2\}$, for $S_2$, $\mathfrak{I}_2 = \{I_3, I_4\}$ and for $S_3$, $\mathfrak{I}_3 = \{I_5, I_6\}$. Line 1 of the algorithm creates two arrays which will be used to hold candidate coordinates for vertices at the coverage boundaries of each sector. The arrays $X_{swap,1}$ and $X_{swap,2}$ are $3 \times 1$ arrays since there are three sectors $(S_i)$ in $M$. Line 2 is a **for** statement that runs the algorithm for each sector $S_c, c = 1, 2, 3$ (i.e the algorithm runs three times). Lines $3 - 7$ selects $I_f$, the BS in the last index for the next clockwise sector in $M$ of $S_c$. For example, Fig. 4.6 shows that the sectors in $M$ are arranged in clockwise order $(S_1, S_2, S_3)$. Therefore, the portion of code in Lines $3 - 7$ specify that for $S_1$, $S_2$ and $S_3$, $I_f$ will be the last elements of $\mathfrak{I}_{1+1}, \mathfrak{I}_{2+1}$ and $\mathfrak{I}_{3-2}$ respectively. As the last element of the neighbour list of the next clockwise sector of $S_c$ is just before the first element of the neighbour list of $S_c$, $I_f$ is included to compute the candidate for the first vertex of the coverage area of $S_c$. For $S_1$, $I_f$ is $I_6$ as shown in the figure.

In Line 8, $X_R^c$ is created as the output array of vertices for $S_c$. Line 9 specifies $I_g$ as the BS at the first index in $\mathfrak{I}_c$, the list of neighbouring BSs of sector $S_c$. A sub-algorithm **JOINPoint** is called to return the first candidate vertex of the coverage of $S_c$. **JOINPoint** is presented in **Algorithm 2** as an algorithm that takes the coordinate locations of three BSs and returns the coordinates of the point where the coverage lines from of the three BSs meet. **JOINPoint** calls another sub-algorithm **INTERSECT** described in **Algorithm 3**. **INTERSECT** is an algorithm that computes the location of the point of intersection of two lines. **INTERSECT** takes as input the coordinate location of a point on each line and the slope of each line.

**Algorithm 2** JOINPoint$(X_m, X_1, X_2)$

**Input:** Points $X_m$, $X_1, X_2$, for BS $M$, $I_1$, $I_2$ respectively
**Output:** $X_q$ Point where coverage lines of 3 BS meet
1: $X_{m,1} = \frac{x_m+x_1}{2} + j\frac{y_m+y_1}{2}$, $X_{m,2} = \frac{x_m+x_2}{2} + j\frac{y_m+y_2}{2}$
2: $Z_{m,1} = \frac{y_m-y_1}{x_m-x_1}$, $Z_{m,2} = \frac{y_m-y_2}{x_m-x_2}$
3: $X_{q,1}$ =**INTERSECT**$(X_{m,1}, -(Z_{m,1})^{-1}, X_{m,2}, -(Z_{m,2})^{-1})$

Therefore Line 9 stores in the first index of $X_R^c$, the vertex of the point of intersection of the coverage lines of $M$ (the reference BS with coordinate $X_m$), $I_g$ (the first BS in $\mathcal{I}_c$ with coordinate $X_g$) and $I_f$ (the last BS in the set of interferers of the most clockwise sector in $M$ of $S_c$).

**Algorithm 3** INTERSECT$(X_a, Z_a, X_b, Z_b)$

**Input:** Points $X_a(x_a + jy_a)$, $X_b(x_b + jy_b)$, with slopes $Z_a$, $Z_b$ respectively
**Output:** $X_p(x_p + jy_p)$, Point of intersection
1: control $= 1$
2: **Case 1**: $Z_a = 0 \wedge (Z_b \neq (0 \vee \pm\infty))$
3: $X_p = \frac{y_a-(y_b-Z_bx_b)}{Z_b} + jy_a$
4: **Case 2**: $(Z_a \neq (0 \vee \pm\infty)) \wedge Z_b = 0$
5: $X_p = \frac{y_b-(y_a-Z_ax_a)}{Z_a} + jy_b$
6: **Case 3**: $Z_a = \pm\infty \wedge (Z_b \neq (0 \vee \pm\infty))$
7: $X_p = x_a + j(Z_bx_a + (y_b - Z_bx_b))$
8: **Case 4**: $(Z_a \neq (0 \vee \pm\infty)) \wedge Z_b = \pm\infty$
9: $X_p = x_b + j(Z_ax_b + (y_a - Z_ax_a))$
10: **Case 5**: $Z_a = \pm\infty \vee Z_b = 0$
11: $X_p = x_a + jy_b$
12: **Case 6**: $Z_a = 0 \vee Z_b = \pm\infty$
13: $X_p = x_b + jy_a$
14: **Case 7**: $(Z_a = \pm\infty \wedge Z_b = \pm\infty) \vee (Z_a = 0 \wedge Z_b = 0)$
15: control $= -1$
16: **Case 8**: **Default**
17: $x_p = \frac{y_b-y_a+Z_ax_a-Z_bx_b}{Z_a-Z_b} + j((\frac{y_b-y_a+Z_ax_a-Z_bx_b}{Z_a-Z_b})Z_a + (y_a - Z_ax_a))$

In lines 10 to 12 of **Algorithm 1**, more candidate vertices are computed and stored in the array $X_R^c$. $\mathcal{I}_c$ the set of interferers is looped through and repeated calls are made to **JOINPoint** to compute the point of intersection (vertex) formed from $M$, and successive adjacent BS $(I_g, I_h)$ in $\mathcal{I}_c$. Lines $13-18$ select the last candidate vertex of $X_R^c$ by considering the point of intersection of $M$, the last BS in the set $\mathcal{I}_c$ and the first BS in the list of interferers of the most anticlockwise sector in $M$ of $S_c$.

Finally, Lines $19-21$ define points formed on the most anticlockwise boundaries of $S_1, S_2, S_3$ as shown in Fig. 4.6. **INTERSECT** is called in line 23 to compute the point of intersection between the most clockwise boundary and the first element

of $\mathcal{I}_c$. **INTERSECT** is also called in line 30 to compute the point of intersection between the most anticlockwise boundary of $S_c$ and the last element in the set $\mathcal{I}_c$.

In summary, **Algorithm 1** gives as output 1) $X_R^1, X_R^2, X_R^3$, three arrays of candidate vertices for the coverage area formed from the three sectors of reference BS $M$. 2) $X_{swap,1}$ an array containing the points of intersections between the most anticlockwise boundaries of each sector in $M$ and the respective BS with the first index in the set of neighbours of the sectors. Similarly, $X_{swap,2}$, is an array containing the points of intersections between the most clockwise boundaries of each sector in $M$ and the respective BS with the last index in the set of neighbours of the sectors. In the next stage of GeoFRe, the elements of $X_R^1, X_R^2, X_R^3$ will be tested and candidate vertices that fail the test will be appropriately replaced by the elements of $X_{swap,1}, X_{swap,2}$.

### 4.8.2 Testing and selecting vertices

This sub-algorithm (**Algorithm 4**) works on the output of **Algorithm 1** and is the second stage of the implementation of GeoFRe. Specifically, the first and last elements in the output arrays $X_R^1, X_R^2$ and $X_R^3$ from **Algorithm 1** are tested. These elements refer to the proposed vertices which lie on the angular boundaries of the sector coverage lines. For each sector, these two tests are conducted to verify that the candidate vertices actually lie within the coverage of that sector. Lines $4, 6$ and $8$ list the test conditions for the three sectors of $X_m$ with index $1, 2$ and $3$ respectively. The Cartesian coordinate of each tested vertex is analysed with that of $X_m$ to determine its position. As Fig. 4.6 shows, the initial computations from **Algorithm 1** can result in some candidate vertices falling outside the coverage areas of their associated sectors e.g $V_1$. **Algorithm 4** highlights these cases and replaces those points with vertices from $X_{swap,1}, X_{swap,2}$ also obtained from **Algorithm 1**. Lines $10-12$ and $13-15$ use the control variable to test if a point passes the test and does the swap if it fails for the first and last boundary vertex respectively. Lines $16-18$ switch the test focus to the last vertex after the first vertex has been tested.

**Algorithm 4** Testing and selecting vertices

**Input:** $X_m, X_R^1, X_R^2, X_R^3, X_{swap,1}, X_{swap,2}$
**Output:** $X_R^1, X_R^2, X_R^3$

1: **for** $c = 1$ to $3$ **do**
2: $d = 1, X_t = X_R^c(d, 1)$
3: control $= -1$
4: **CASE** $c = 1 \wedge \{(x_t \geq x_m) \wedge [(y_t \geq y_m) \vee \arctan(\frac{x_t - x_m}{y_m - y_t}) \geq 60°]\}$
5: control $= 1$, **GO TO** 10
6: **CASE** $c = 2 \wedge \{(y_t \leq y_m) \wedge \{[(x_t < x_m) \wedge (\arctan(\frac{x_m - x_t}{y_m - y_t}) \leq 60°)] \vee [(x_t > x_m) \wedge (\arctan(\frac{x_t - x_m}{y_m - y_t}) \leq 60°)] \vee (x_t = x_m))\}\}$
7: control $= 1$, **GO TO** 10
8: **CASE** $c = 3 \wedge \{(x_t \leq x_m) \wedge [(y_t \geq y_m) \vee \arctan(\frac{x_m - x_t}{y_m - y_t}) \geq 60°]\}$
9: control $= 1$, **GO TO** 10
10: **if** control $= -1 \wedge d = 1$ **then**
11: $X_R^c(d, 1) = X_{swap,2}(c, 1)$
12: **end if**
13: **if** control $= -1 \wedge d = 2$ **then**
14: $X_R^c(end, 1) = X_{swap,1}(c, 1)$
15: **end if**
16: **if** $d = 1$ **then**
17: $d = 2, X_t = X_R^c(end, 1)$, **GO TO** 3
18: **end if**
19: **end for**

### 4.8.3 Area computation

**Algorithm 5** receives the verified vertices from the output of **Algorithm 4** and the value of the geometric coverage area of each sector in $X_m$ is computed. The irregular polygons defined by combining successive vertices of a sector with the Cartesian coordinate of $X_M$ are split into triangles. In lines $4 - 8$, the areas of the triangles are then computed using Heron's formula and added together to give the total area of coverage for each sector.

**Algorithm 5** Computing geometric coverage area of sectors of $X_m$

**Input:** $X_m, X_R^1, X_R^2, X_R^3$
**Output:** $A_1, A_2, A_3$

1: $A_1 = A_2 = A_3 = 0$
2: **for** $c = 1$ to $3$ **do**
3: **for** $d = 1$ to (**SIZE**$(X_R^c) - 1$) **do**
4: $f = \text{abs}(X_m - X_R^c(d, 1))$
5: $g = \text{abs}(X_m - X_R^c(d + 1, 1))$
6: $h = \text{abs}(X_R^c(d, 1) - X_R^c(d + 1, 1))$
7: $s = {}^{(f+g+h)}/_{2}$
8: $A_c = A_c + \sqrt{s(s - f)(s - g)(s - h)}$
9: **end for**
10: **end for**

### 4.8.4 Bandwidth Assignment

This is the final stage of execution of GeoFRe where bandwidth assignment is made for the center and edge regions of each sector. The bandwidths to the different regions are assigned proportional to the sector areas computed in **Algorithm 5** to maximize spectral efficiency. The input for **Algorithm 6** includes $X_m, X_R^1, X_R^2, X_R^3$ and $A_1, A_2, A_3$ from **Algorithm 5**.

**Algorithm 6** Bandwidth assignment

**Input:** $X_m(x_m + jy_m), X_R^1, X_R^2, X_R^3, A_1, A_2, A_3$
**Output:** $\psi_1, \psi_2, \psi_3$
1: **for** $s = 1$ to 3 **do**
2: $d = \min(|X_m - X_R^s(1)|, |X_m - X_R^s(end)|)$
3: Select interior boundary, $r_c \leq d$
4: $\psi_s = \max[0, ({}^{N_{prb}}/_3) - \text{floor}(\frac{(A_s - ({}^{120^\circ}/_{360^\circ})\pi r_c^2)N_{prb}}{A_s})]$
5: **end for**

Line 1 is a loop declaration to execute the algorithm three times for each sector of $M$. In line 2, $d$ is computed as the minimum between the distances of 1) $M$ and the most *anticlockwise* boundary for its sector with index $s$ and 2) $M$ and the most *clockwise* boundary for its sector with index $s$. Furthermore, the interior radius (threshold for center UEs) is selected in line 3 based on $d$. Finally, $\psi_s$ which is the unique edge frequency index allocation for sector with index $s$ is computed from the estimated area of the edge region of the sector and the total number of PRBs in the system. The number of edge PRBs is the floor (least integer) of the fraction of total PRBs based on the edge area to the total area. $\psi_s$ is the maximum between 0 and the difference of ${}^{N_{prb}}/_3$ and the total computed edge PRBs.

From $\psi_s$ obtained, equations for the interference probabilities ($\beta_{c,c}$, $\beta_{e,c}$) defined in Table. 4.2 are updated as:

$$\beta_{c,c} = \frac{\mathcal{F} - (2\mathcal{F}_{e,max} - \psi_s - \psi_j)}{\mathcal{F} - (\mathcal{F}_{e,max} - \psi_s)}, \tag{4.32}$$

$$\beta_{e,c} = \frac{\mathcal{F}_{e,max} - \psi_j}{\mathcal{F} - (\mathcal{F}_{e,max} - \psi_s)}, \tag{4.33}$$

where $\psi_s$, $\psi_j$ are the edge frequency allocations for a reference sector and one of its neighbouring BS sectors respectively.

$\beta_{c,c}$, $\beta_{e,c}$ are used to calculate the SFR SINR for center UEs, therefore, (4.21)

becomes:

$$SINR_{u,c}^{sfr} = \frac{\frac{P_{m,s}}{E_{m,i}(\mu_{m,s}-1)+N_{m,i}}\lambda^{-\alpha}}{\sum_{j\epsilon\mathcal{J}}\sum_{k\neq i}(\frac{\beta_{c,c}P_{m,s}+\mu_{m,s}\beta_{e,c}P_{m,s}}{E_{j,k}(\mu_{m,s}-1)+N_{j,k}})(\lambda^2+\gamma_k^2-2\lambda\gamma_k\cos(\omega_k-\theta))^{-\frac{\alpha}{2}}}, \tag{4.34}$$

which expands to

$$SINR_{u,c}^{sfr} = \frac{\frac{P_{m,s}}{E_{m,i}(\mu_{m,s}-1)+N_{m,i}}\lambda^{-\alpha}}{\sum_{j\epsilon\mathcal{J}}\sum_{k\neq i}(\frac{\frac{\mathcal{F}-(2\mathcal{F}_{e,max}-\psi_s-\psi_j)}{\mathcal{F}-(\mathcal{F}_{e,max}-\psi_s)}P_{m,s}+\mu_{m,s}\frac{\mathcal{F}_{e,max}-\psi_j}{\mathcal{F}-(\mathcal{F}_{e,max}-\psi_s)}P_{m,s}}{E_{j,k}(\mu_{m,s}-1)+N_{j,k}})(\lambda^2+\gamma_k^2-2\lambda\gamma_k\cos(\omega_k-\theta))^{-\frac{\alpha}{2}}}. \tag{4.35}$$

# 4.9 Results

## 4.9.1 Network scenarios

The network scenarios used to test GeoFRe algorithm are the same scenarios used in Chapter 3. The metric defined in (4.5) used to generate case studies for irregular BSs is used to define four network case studies. These include the hexagonal BS network and three irregular BSs, whose parameters are specified in Table. 4.3 and coverage plots shown in Fig. 4.7.

Table 4.3: Parameters for Network case studies

| | $d_{min}$ | $\delta_1$ | $\delta_2$ | $\delta_3$ | $\delta_{1,2}$ | $\delta_{2,3}$ | $\omega_1$ | **Remark** |
|---|---|---|---|---|---|---|---|---|
| **Case** 1 | $\sqrt{3}r$ | 0 | 0 | 0 | 0 | 0 | $0°$ | Hexagonal Layout |
| **Case** 2 | $\sqrt{3}r$ | 0 | 0 | 0 | 0 | 0 | $-20°$ | Irregular BS Layout-1 |
| **Case** 3 | $\sqrt{3}r$ | 0 | 0 | 0 | $0.27r$ | 0 | $-20°$ | Irregular BS Layout-2 |
| **Case** 4 | $\sqrt{3}r$ | 0 | $0.3r$ | $0.1r$ | $0.2r$ | 0 | $10°$ | Irregular BS Layout-3 |

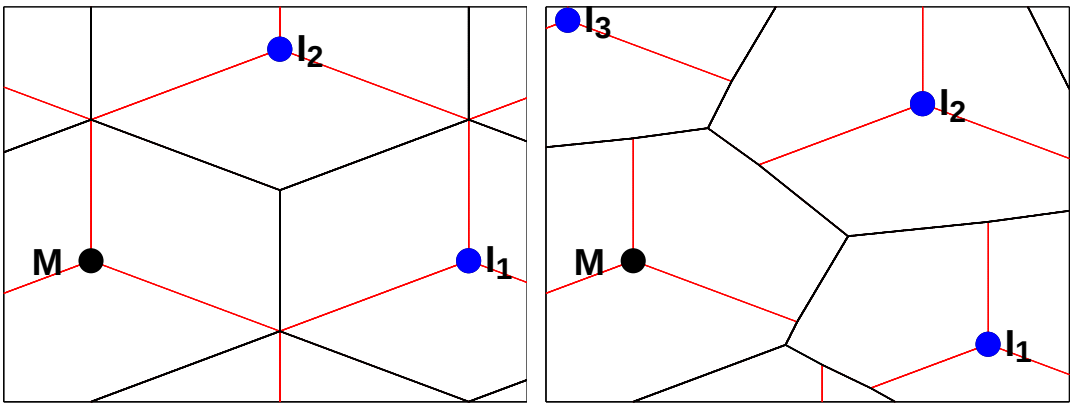


(a) Hexagonal Layout

(b) Irregular BS Layout-1

(c) Irregular BS Layout-2

(d) Irregular BS Layout-3

Figure 4.7: Network layout scenarios showing reference BS $M$ and interfering BSs $I$

### 4.9.2 Testing Area computation

Algorithm 5, which calculates the area of BS coverage areas including irregular networks is tested for its accuracy in computation. For each network scenario, pixels are generated in the coverage space and the area of the edge regions are calculated using Algorithm 5 and two circular model algorithms. The results are then compared with simulations as shown in Fig. 4.8. In all scenarios, the area computed from Algorithm 5 of the proposed GeoFRe algorithm generates the closest number of pixels to the simulation value.

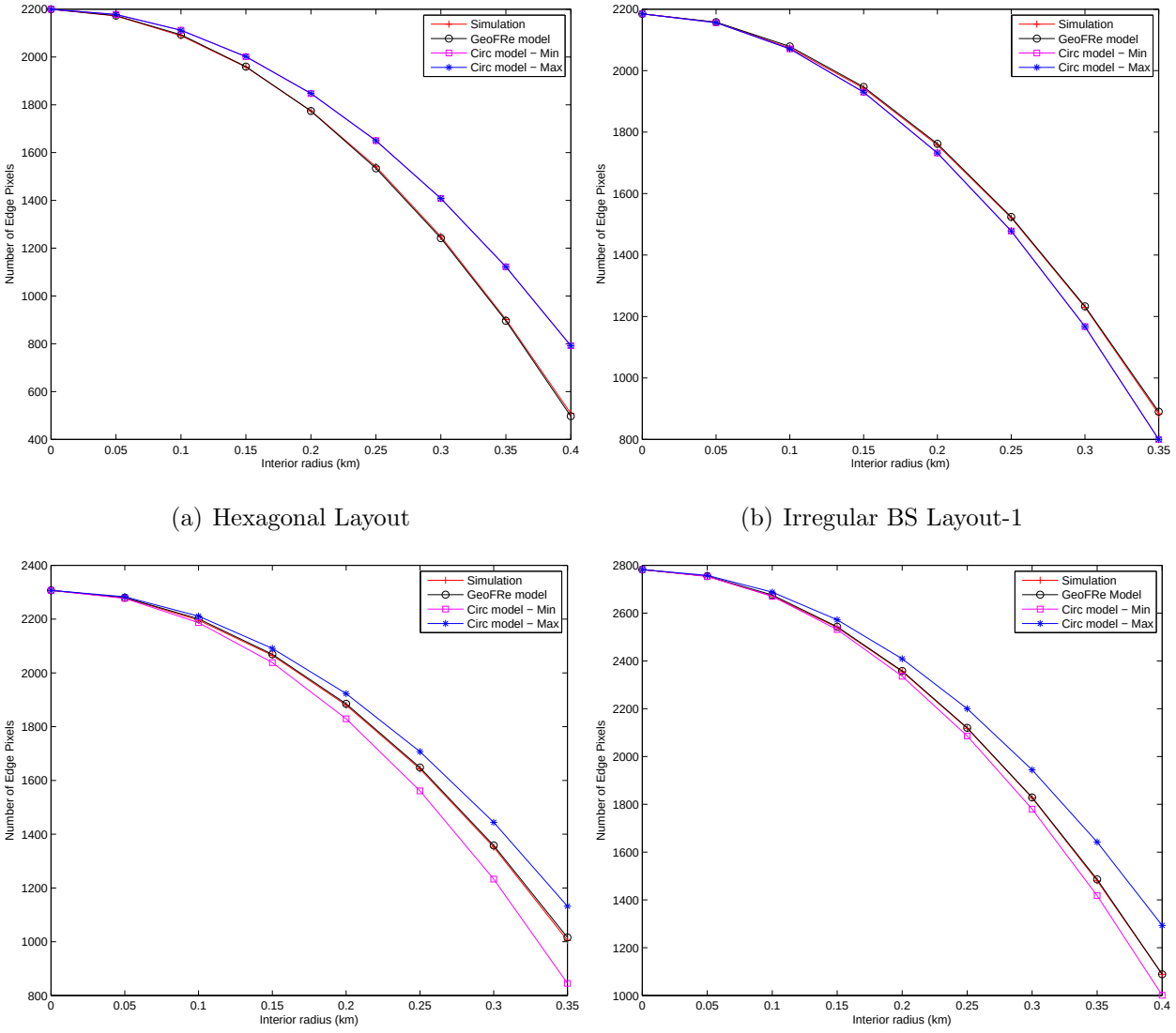


(a) Hexagonal Layout

(b) Irregular BS Layout-1

(c) Irregular BS Layout-2

(d) Irregular BS Layout-3

Figure 4.8: Testing Area of edge region using Algorithm 5

### 4.9.3 Testing Bandwidth from GeoFRe

Based on the parameter settings in Table. 4.4, the results shown in Fig. 4.9 are for the capacity and spectral efficiency for the four network scenarios over different values of $f_{e,i}$.

Table 4.4: Parameters and Results

| **Parameter** | **Case 1** | **Case 2** | **Case 3** | **Case 4** |
|---|---|---|---|---|
| **Center radius,** $r_c$ | $0.76r$ | $0.76r$ | $0.71r$ | $0.66r$ |
| **Power ratio,** $\mu_{m,s}$ | 4 | 4 | 4 | 4 |
| **Observed number of UEs,** $N_{m,i}$ | 49 | 46 | 49 | 58 |
| **Observed number of edge UEs,** $E_{m,i}$ | 14 | 11 | 17 | 33 |
| **GeoFRe Edge region bandwidth,** $f_{e,\psi}$ | $14 \times 180$kHz | $14 \times 180$kHz | $16 \times 180$kHz | $16 \times 180$kHz |

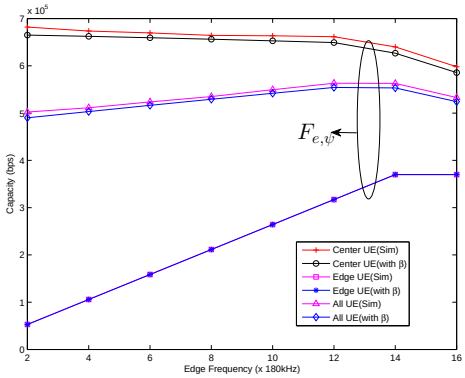


(a) Capacity (in bps) scenario 1

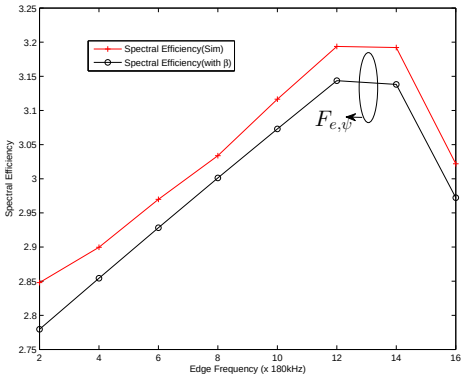


(b) Spectral Efficiency (in bps/Hz) scenario 1

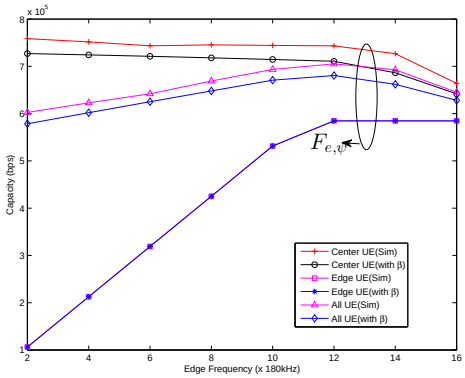


(c) Capacity (in bps) scenario 2

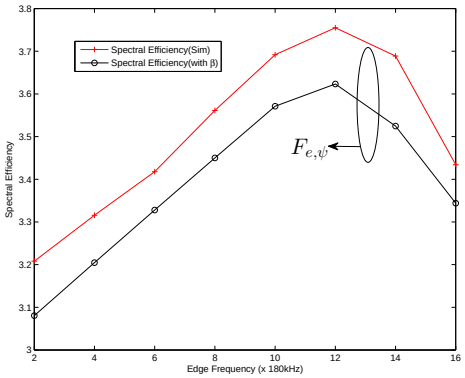


(d) Spectral efficiency (in bps/Hz) scenario 2

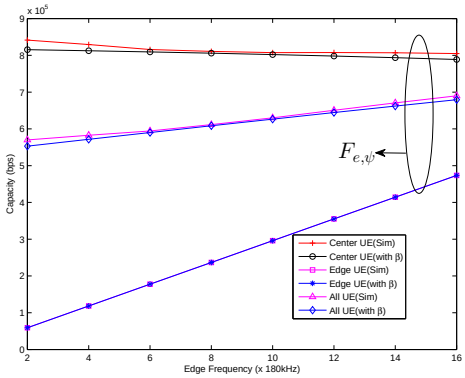


(e) Capacity (in bps) scenario 3

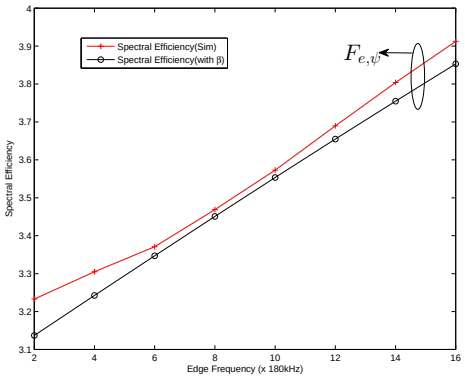


(f) Spectral Efficiency (in bps/Hz) scenario 3

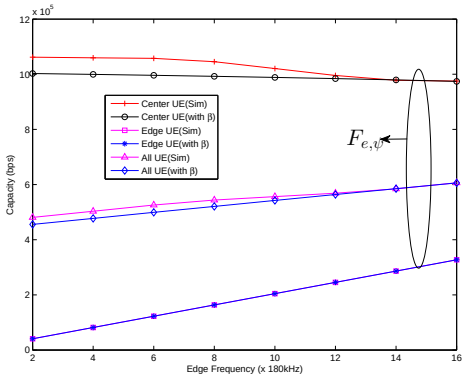


(g) Capacity (in bps) scenario 4

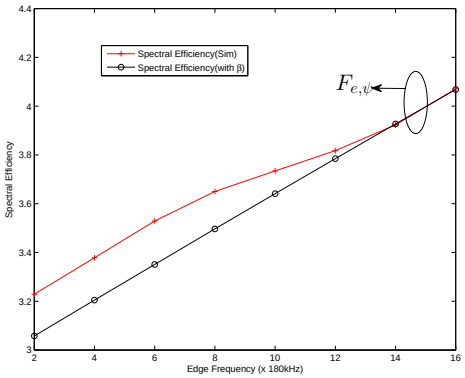


(h) Spectral efficiency (in bps/Hz) scenario 4



Figure 4.9: Results for GeoFRe algorithm

As noted from the results in Chapter 3, the SINR plots did not always follow the capacity plots, so since UE data rate is of utmost interest, only capacity is considered. As observed from the results, the value of edge bandwidth computed from GeoFRe corresponds with the maximum spectral efficiency and capacity measured for the different cases. This is consistent across center UEs, edge UEs and the combined average of all UEs in the reference BS.

## 4.10 Chapter summary

In this Chapter, an irregular BS network model was proposed for cellular networks. New equations were derived for the BS/UE positional relationships defining the distance between interfering BSs and a reference BS and between interfering BSs and UEs in a reference BS. Furthermore, new equations were also derived specifying FR parameters in partitioned FR schemes. An algorithm, GeoFRe was introduced which modifies partitioned FR schemes based on the geometry properties of the underlying macro BS network. Several analysis were carried out to verify the accuracy of the FR modified equations and the BS edge region estimation of the coverage areas. Finally, the bandwidth computed from GeoFRe was tested across several network scenarios specifying regular and irregular BS networks. The results show that GeoFRe offers selection of the edge bandwidth for optimal capacity and spectral efficiency in all cases considered.

# Chapter 5

# Optimal configuration for SFR in Irregular Cellular Networks

## 5.1 Introduction

The need to model and optimize cellular networks using realistic assumptions about BS and UE positioning is highlighted in [24]. This arises because real network deployments do not always follow regular grid BS patterns and uniform UE placements. In Chapters 3 and 4, a model for SFR that considers the irregular deployment of BSs was proposed and the exact amounts of ICI received by different UE classes were derived. In this Chapter, the irregular BS model earlier presented is simplified and an optimization algorithm proposed for efficient FR implementation. The SFR scheme is selected because its flexibility allows easy adjustment of BS parameters to achieve the desired optimization goal. The goal in this case is to select the power configuration at a macro BS that guarantees an acceptable performance of edge UEs, compared to center UEs, based on a fairness standard. The conflicts between these two UEs classes is highlighted in [34]; i.e the improved performance of cell center UEs occurs at a cost to edge UEs and vice versa.

Unlike in the previous Chapters where analysis and simulations were carried out by computing the average performance of all UEs in defined regions of a reference BS sector, the concept of a "virtual UE" is used here. The performance of UEs in a region (center or edge) within a macro BS sector is approximated by computing performance of only the virtual UE. The virtual UE, also called Center of Gravity (CoG) UE in a region is obtained by finding the central position (location) of UEs in

that region and then assuming a UE is placed at that point. The simplified nature of the optimization algorithm provides an easy means for SFR to be enhanced in irregular macro networks. Specifically, a technique is proposed for the power ratio selection based on a defined measure of fairness.

## 5.2 System Model

### 5.2.1 Location Parameters

Consider a neighbourhood of tri-sector macro BSs comprising; a reference BS, $M$ and $\mathfrak{I}(\{I_1, I_2\})$, a set of two interfering macro BSs as shown in Fig. 5.1. Analysis is carried for the performance of UEs within sector $S_1$ of $M$.

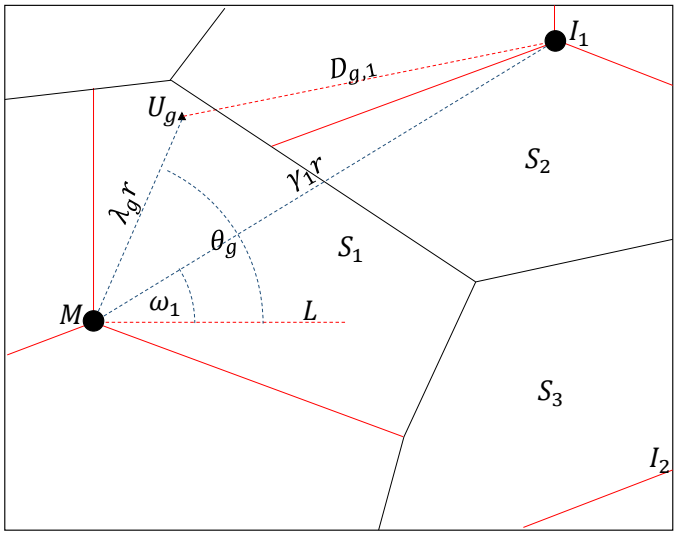


Figure 5.1: Layout of Irregular Macro BS networks

Similar to in [27], the performance of UEs within a region of $M$ is approximated by assuming, $U_g$ a virtual UE located at the CoG. $U_g$ is also the central UE position in that particular region of $M$. $r$ is the hexagonal BS coverage radius, $\lambda_g r$ is the distance between $U_g$ and $M$ while $\gamma_j r$ is the distance between an interfering BS, $I_j$ and $M$. Based on the description in Sections. 3.5 and 4.2 in Chapters 3 and 4 respectively, $\theta_g, \omega_j$ are the angles formed between Line $L$ and $U_g, I_j$ respectively. Therefore the distance, $D_{g,j}$, between $U_g$ and $I_j$ will be $D_{g,j} = r\sqrt{\lambda_g^2 + \gamma_j^2 - 2\lambda_g\gamma_j(\cos(\omega_j - \theta_g))}$.

### 5.2.2 Power parameters

Figs. 5.1 and 5.2 reveal that sector indexes for close sectors of neighbouring macro BSs will always be different. Sector $S_1$ of macro BS $M$ is bordered by neighbouring sectors $S_2$ and $S_3$. In Fig. 5.2, the SFR power and bandwidth allocations for sectors $S_1$, $S_2$ and $S_3$ for $M$, $I_1$ and $I_2$ are shown. Assuming $S_y$ is used to represent any of these sectors, then $\mathcal{F}_{e,y}$, $\mathcal{F}_{c,y}$ are the bandwidth allocations to the edge and center regions of $S_y$ respectively. Similarly, $P_{e,y}$, $P_{c,y}$ respectively define the power allocation to the edge and center regions of $S_y$. The power transmitted to each individual edge and center UEs is $p^e_{x,y} = \frac{P_{e,y}}{E_{x,y}}$, $p^c_{x,y} = \frac{P_{c,y}}{C_{x,y}}$ where $E_{x,y}$, $C_{x,y}$ are the total number of edge and center UEs respectively in $S_y$, $x = m$ for $M$ the reference BS, $x = 1, 2$ for $I_1$, $I_2$ respectively. Let $\mu_{x,y} = \frac{p^e_{x,y}}{p^c_{x,y}}$ be defined as the power ratio. The power budget, $P_{m,s}$ at any $S_y$ is given as $P_{m,s} = E_{x,y}P_{e,y} + C_{x,y}P_{c,y}$. Since $N_{x,y}$, the total number of UEs in $S_y$ is $E_{x,y} + C_{x,y} = N_{x,y}$, therefore $p^e_{x,y} = \frac{\mu_{x,y}P_{m,s}}{E_{x,y}(\mu_{x,y}-1)+N_{x,y}}$ and $p^c_{x,y} = \frac{P_{m,s}}{E_{x,y}(\mu_{x,y}-1)+N_{x,y}}$.

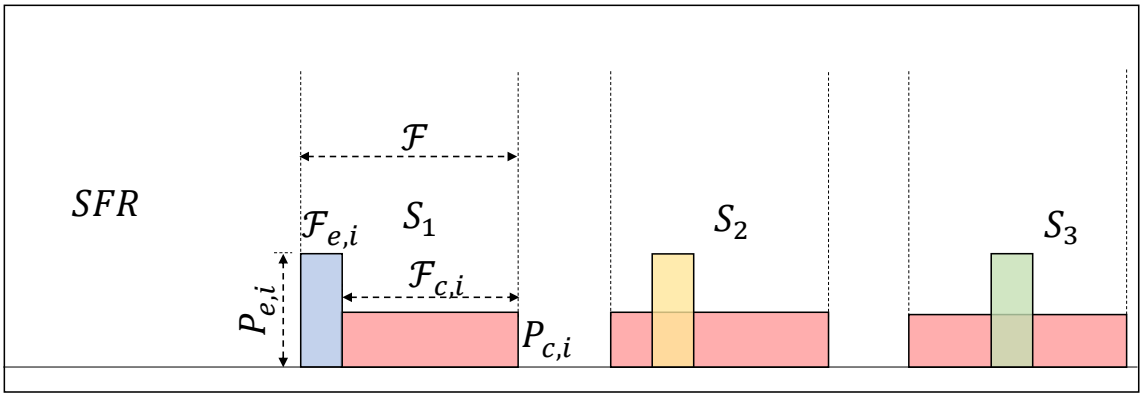


Figure 5.2: SFR Power and Bandwidth allocation for 3 Macro BSs

### 5.2.3 Interference parameters

Recall from Fig. 5.2 that $\mathcal{F}_{e,y}$ and $\mathcal{F}$ are the total frequency allocations to the edge region of any sector $S_y$ and the total available frequency in $S_y$, respectively. It can also be observed that the assigned frequencies in neighbouring BS sectors overlap across the different BS regions, therefore probabilities of interference due to these overlaps arise. The probability that transmission from the edge region of any interfering BS sector, (from $I_1$ or $I_2$) will interfere with the $U_g$ in the center region of sector $S_y$ of $M$ is $\beta_{e,c} = \frac{\mathcal{F}_{e,y}}{\mathcal{F}-\mathcal{F}_{e,y}}$ while the probability of interference from the center

region transmission to the $U_g$ in the center region is $\beta_{c,c} = \frac{\mathcal{F}-2\mathcal{F}_{e,y}}{\mathcal{F}-\mathcal{F}_{e,y}}$. The probability of interference from the edge and center regions of $I_1$ or $I_2$ to the $U_g$ in the edge region of $M$ are 0 and 1, respectively.

### 5.2.4 Performance parameters

Within reference BS $M$, let the $U_g$ in the center and edge regions of its sector $S_i$ be $U_{c,g}$ and $U_{e,g}$ respectively. The SINR of $U_{c,g}$ is given as:

$$SINR^i_{c,g} = \frac{p^c_{m,i} h(\lambda_{c,g} r)^{-\alpha}}{\sigma^2 + \sum_{j=1}^{2} [(\beta_{e,c} p^e_{j,j+1} + \beta_{c,c} p^c_{j,j+1}) h(D_{i,j})^{-\alpha}]}, \tag{5.1}$$

where $p^c_{m,i}$, $\lambda_{c,g} r$ are the center transmit power and distance from $M$ to $U_{c,g}$ respectively, h is the fading component, $\alpha$ is the path loss exponent and $\sigma^2$ is the noise component (which is negligible), $p^e_{j,j+1}$, $p^c_{j,j+1}$ represent the edge and center transmit power from the interfering BSs to $M$ (from Fig. 5.1 sector $S_2$ of $I_1$ is closest to $S_1$ of $M$ and sector $S_3$ of $I_2$ is closest to $S_1$ of $M$ hence $(j, j+1) = (1, 2)$, $(2, 3)$ for $I_1$, $I_2$ respectively), $D_{i,j}$ is the distance between $U_{c,g}$ and any interfering BS, $I_j$.

The SINR of $U_{e,g}$ can also computed as:

$$SINR^i_{e,g} = \frac{p^e_{m,i} h(\lambda_{e,g} r)^{-\alpha}}{\sigma^2 + \sum_{j=1}^{2} p^c_{j,j+1} h(D_{i,j})^{-\alpha}}, \tag{5.2}$$

with similar definitions to (5.1).

The capacity for $U_{c,g}$ is:

$$Cap^i_{c,g} = \mathcal{F}_{prb}[\log_2(1 + SINR^i_{c,g})], \tag{5.3}$$

where $\mathcal{F}_{prb}$ is the bandwidth allocation per UE from $M$, assumed to be the same for all UEs on the condition that $M$ is fully loaded. Similarly, the capacity for $U_{e,g}$ is:

$$Cap^i_{e,g} = \mathcal{F}_{prb}[\log_2(1 + SINR^i_{e,g})], \tag{5.4}$$

(5.1) and (5.2) can be expanded upon using the parameters specified earlier and assuming $E_{x,j}$ and $\mu_{x,j}$ have the same values in all BS, (5.3) and (5.4) can be refor-

mulated as:

$$Cap^{i}_{c,g} = \mathcal{F}_{prb}[\log_2(1 + \frac{(\lambda_{c,g}r)^{-\alpha}(\mathcal{F} - \mathcal{F}_{e,i})}{(\mu_{m,i}\mathcal{F}_{e,i} + \mathcal{F} - 2\mathcal{F}_{e,i})\sum_{j=1}^{2} D^{-\alpha}_{c,j}})], \tag{5.5}$$

$$Cap^{i}_{e,g} = \mathcal{F}_{prb}[\log_2(1 + \frac{\mu_{m,i}(\lambda_{e,g}r)^{-\alpha}}{\sum_{j=1}^{2} D^{-\alpha}_{e,j}})], \tag{5.6}$$

where $D_{c,j}$ and $D_{e,j}$ represent the distance between an interfering BS, $I_j$ and $U_{c,g}$, $U_{e,g}$ respectively. $\sigma^2$ is considered negligible because the interference component far exceeds that of noise.

## 5.3 Optimization problem

An optimization problem with a goal to providing an acceptable capacity for edge UEs based on the BS transmit power is formulated. The task is to find a value of $\mu_{m,i}$ that guarantees fairness to a certain degree in different UE performance. Recall that the edge UEs have been identified as the class of UEs more exposed to ICI from neighbouring BSs. The goal is to devise a means by which the power parameters of a macro BS can be selected with an assumed guarantee of the power transmitted to the edge UE. An increasing value of $\mu_{m,i}$ causes the SINR and capacity of $U_{e,g}$ to increase while that of $U_{c,g}$ decreases. As observed in Chapter 3, in certain macro BS placements, there is a scenario where $Cap^{i}_{c,g} = Cap^{i}_{e,g}$, obtained by finding where $|Cap^{i}_{c,g} - Cap^{i}_{e,g}| = 0$.

The optimization problem is given as:

$$minimize\ f(\mu_{m,i}) = [Cap^{i}_{c,g} - \psi Cap^{i}_{e,g}]^2 s.t\ \mu_{m,i} > 1. \tag{5.7}$$

$\psi$ is the parameter added to control and guarantee a minimum performance measure for edge UEs. $f(\mu_{m,i})$ is a continuous differentiable single-variable function whose differential is given as:

$$\frac{d_f}{d_{\mu_{m,i}}} = -2 \times (A_1(A_2 - A_3)) \times (B_1 + B2) \tag{5.8}$$

where $A_1 = \frac{\mathcal{F}_{prb}}{\ln 2}$,

$$A_2 = \ln(1 - \frac{(\lambda_{c,g} r)^{-\alpha}(\mathcal{F}_{e,i} - \mathcal{F})}{(\mathcal{F} - 2\mathcal{F}_{e,i} + \mathcal{F}_{e,i}\mu_{m,i}) \sum_{j=1}^{2} D_{c,j}}),$$

$$A_3 = \psi \ln(\frac{(\lambda_{e,g} r)^{-\alpha} \mu_{m,i}}{\sum_{j=1}^{2} D_{e,j}} + 1),$$

$$B_1 = \frac{\mathcal{F}_{prb}(\lambda_{e,g} r)^{-\alpha} \psi}{((\lambda_{e,g} r)^{-\alpha} \mu_{m,i} + \sum_{j=1}^{2} D_{e,j}) \ln 2} \text{ and}$$

$$B_2 = \frac{\mathcal{F}_{prb}(\lambda_{c,g} r)^{-\alpha} \mathcal{F}_{e,i}(\mathcal{F}_{e,i} - \mathcal{F})}{(\frac{(\lambda_{c,g} r)^{-\alpha}(\mathcal{F}_{e,i} - \mathcal{F})}{\mathcal{F} - 2\mathcal{F}_{e,i} + \mathcal{F}_{e,i}\mu_{m,i}} - \sum_{j=1}^{2} D_{c,j})(\mathcal{F} - 2\mathcal{F}_{e,i} + \mathcal{F}_{e,i}\mu_{m,i})^2 \ln 2}$$

Setting (5.8) to 0 and solving numerically gives the solution to (5.7).

## 5.4 Results and Analysis

The following assumptions were made for the system: $P_{m,s} = 43$dBm, $r = 0.5$Km, $h = 1, \alpha = 3, \lambda_{c,g} = 0.45, \lambda_{e,g} = 0.9, \gamma_1 = \gamma_2 = \sqrt{3}$ (where $\gamma_x$ is the distance between $I_x$ and $M$), $\theta_{c,g} = \theta_{e,g} = 30^o$ (where $\theta$ represents the angle between a UE and line $L$), $\omega_1 = 50^o, \omega_2 = -5^o$ (where $\omega_x$ represents the angle between an interfering BS $I_x$ and line $L$), $E_{m,i} = 8, N_{m,i} = 48$, $\mathcal{F} = 10$MHz and $\mathcal{F}_{prb} = 180$kHz. Simulations were carried out using MATLAB software.

The impact of $\mu_{m,i}$ on the performance difference between center and $U_{e,g}$ in an irregular homogeneous network is first investigated. Fig. 5.3 shows the plot of $|Cap^i_{c,g} - Cap^i_{e,g}|$ against $\mu_{m,i}$ over different selections of $\mathcal{F}_{e,i}$.

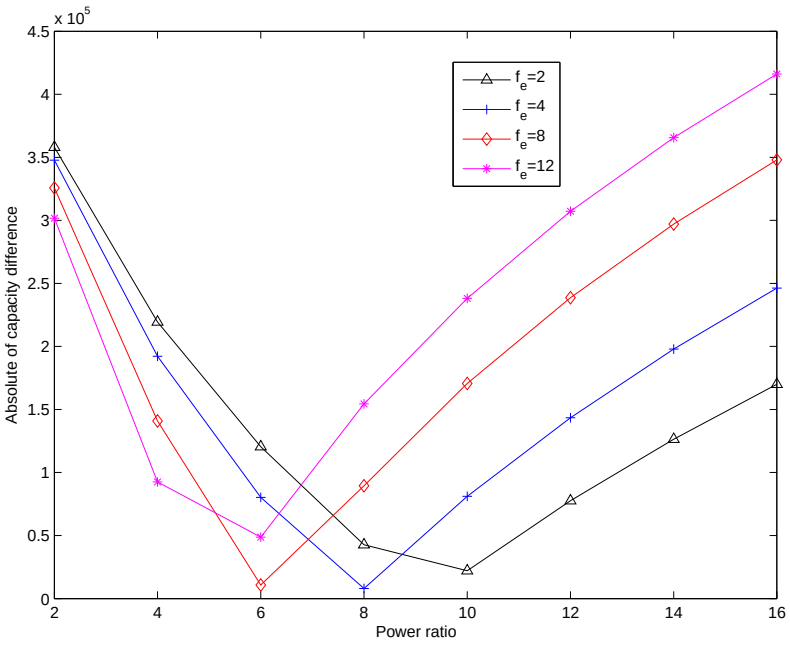


Figure 5.3: Comparison of capacity (in bps) differences for $CoG$ UE

The plots show that the absolute of the difference initially reduces with increasing $\mu_{m,i}$, then approaches a minimum value, and then it starts rising. This can be explained from (5.5)-(5.7) which show that $Cap^i_{c,g} > Cap^i_{e,g}$ for lower values of $\mu_{m,i}$ and $Cap^i_{c,g} < Cap^i_{e,g}$ for higher values of $\mu_{m,i}$. For any $\mathcal{F}_{e,i}$, there is a value of $\mu_{m,i}$ that minimizes the absolute difference i.e where $Cap^i_{c,g} = Cap^i_{e,g}$. As expected, lower values of $\mathcal{F}_{e,i}$ would require higher values of $\mu_{m,i}$ for the performance of $U_{e,g}$ to approach that of $U_{c,g}$. This preliminary analysis shows the significant impact of $\mu_{m,i}$ on the performance of center and edge UEs. It also implies that the solution of (5.7) will provide better fairness in the system and improve the performance of the edge UE.

To verify the proposed optimization framework, a cellular network using the parameters specified was modelled in MATLAB. The SINR and capacities of all the center and edge UEs were computed over different $\mathcal{F}_{e,i}$ and $\mu_{m,i}$. The values of $\mu_{m,i}$ used were $4, 6.19(\mu_{opt})$ and 12 where $\mu_{opt}$ is the power ratio obtained from solving (5.7). $\psi$ was selected as 1, which is the state that guarantees the highest fairness in performance between center and edge UE. This is the condition when the difference between the performance of $Cap^i_{c,g}$ and $Cap^i_{e,g}$ is minimal. Fig. 5.4 shows the plot of the absolute value of the difference of the average capacities of the center and edge UE.

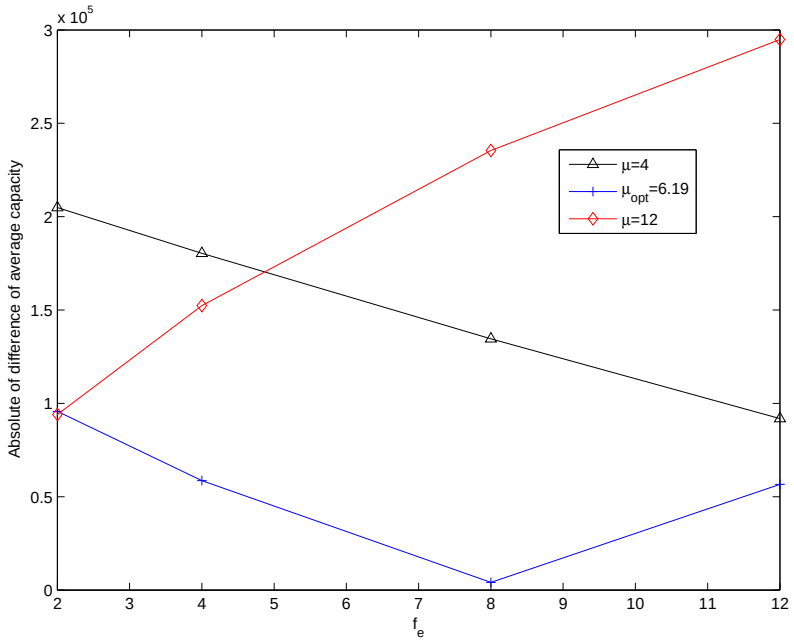


Figure 5.4: Capacity (in bps) differences with optimal $\mu_{m,i}$

As observed, $\mu_{opt}$ gave the least difference for all cases of $\mathcal{F}_{e,i}$. This proves the capability of the proposed framework in aiding the control of UE performance by specifying how much fairness (based on transmit power) should be allowed between different classes of UE.

## 5.5 Chapter Summary

In this chapter, an optimization framework for the transmit power parameter in SFR based cellular networks has been presnted. The concept of the CoG UE was adopted to approximate the overall UE performance. Closed-form expressions were derived for the performance of UE at the center and edge regions of the macro BS. An optimization framework that captures a fairness based system was presented. Results showed a guarantee for edge UE capacity enhancement through a greater control over the BS transmit power.

# Chapter 6

# Frequency Reuse model for Heterogeneous Cellular Networks

## 6.1 Introduction

The FR model for irregular networks presented in Chapter four is extended in this Chapter to the case of HetNets. A new system model for irregular HetNets is proposed that captures the location parameters of the macro BS network and the small BS network. The model also captures unique frequency allocation methods in multi-tier network scenarios. Equations are derived to measure UE performance and analysis is carried out over defined network scenarios. SFR which is the most flexible FR technique with more options to vary BS parameters is selected as the FR scheme.

## 6.2 Definition of entities

Consider a HetNet with two tiers of BS networks comprising $\mathcal{M}$ the set of indexes for the available macro BSs and $\Omega$ the set of indexes for the small (pico) BSs in the network. A reference macro BS $M$ is shown in Fig. 6.1, which has a close interfering macro BS $I$ and a pico BS $Q$ within the coverage of its sector $S_1$. While the macro BSs deploy tri-sector antennas dividing their coverage regions into three sectors, the pico BSs utilize single omnidirectional antennas.

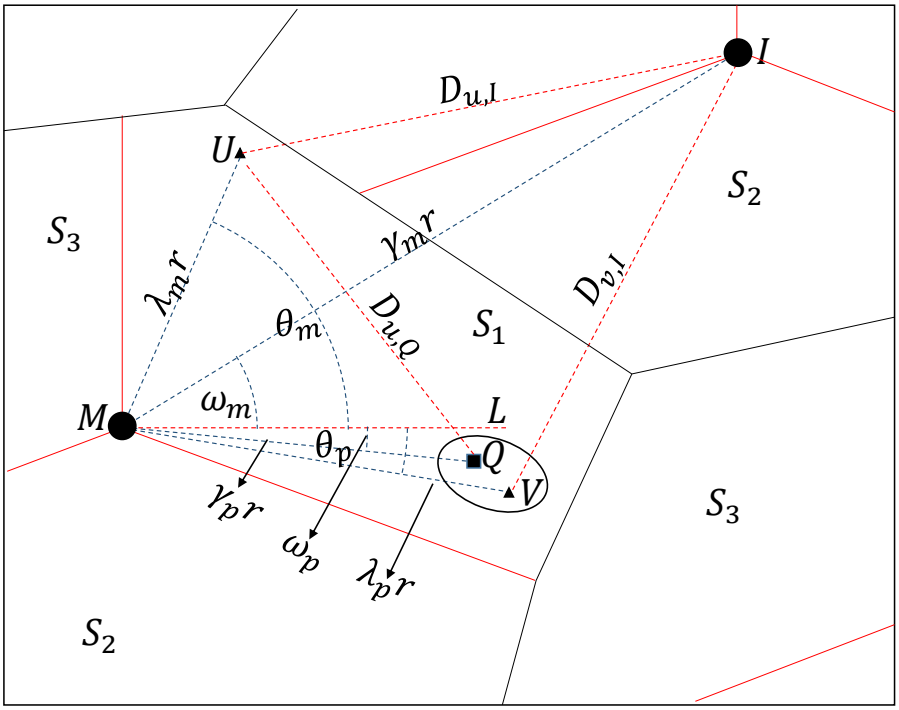


Figure 6.1: Positional layout of HetNet entities

The pico BSs transmit at smaller power levels (2dB budget) than the macro BS (43dB budget). Therefore, their coverage regions are smaller portions within the larger macro coverage region. The total bandwidth in the system, $\mathcal{F}$ is reused and allocated at each BS tier according to modified SFR algorithms. SFR is selected because of the flexibility it can provide when adjusting BS power and FR parameters to alter UE performance according to desired criteria.

The UEs in the system can be classified based on the BS they are connected to and their location thus:

- Macro UE
  - Macro center UE: UE connected to a macro BS and located within the macro BS interior (center) region.
  - Macro edge UE: UE connected to a macro BS and located within the macro BS exterior (edge) region.
- Pico UE

- Pico center UE: UE connected to a pico BS which is positioned within the macro BS interior region.
- Pico edge UE: UE connected to a pico BS which is positioned within the macro BS edge region.

## 6.3 HetNet Location model

The positional model adopted for FR implementation in HetNets is similar to that used in Chapter four. A reference BS, $M$ is identified and the proximity of both UEs within the region of $M$ and neighbouring BSs to $M$ are defined according to the Cartesian coordinate system with the aid of the horizontal line $L$ from $M$ as shown in Fig. 6.1. $I$ is an interfering macro BS, $Q$ is a pico BS, $U$ is a macro UE and $V$ is a pico UE. $\lambda_m r, \lambda_p r$ are the distances between $M$ and $U$, and between $M$ and $V$ respectively. Similarly, $\gamma_m r, \gamma_p r$ are the distances between $M$ and $I$, and between $M$ and $Q$ respectively. The model also defines the angles formed with respect to Line $L$, similar to the definition in Chapter four. $\theta_m, \theta_p$ are the angular displacements of $U$ and $V$ respectively from $L$ while $\omega_m, \omega_p$ are associated with $I$ and $Q$ respectively. The distance between $U$ and $I$ is given by:

$$D_{u,I} = r\sqrt{\lambda_m^2 + \gamma_m^2 - 2\lambda_m\gamma_m(\cos(\omega_m - \theta_m))}, \tag{6.1}$$

where $r$ is the standard coverage radius for all macro BS using regular placements. Similarly, the distance between $U$ and $Q$ is given by:

$$D_{u,Q} = r\sqrt{\lambda_p^2 + \gamma_m^2 - 2\lambda_p\gamma_m(\cos(\omega_m - \theta_p))}, \tag{6.2}$$

and the distance between $V$ and $I$ is:

$$D_{v,I} = r\sqrt{\lambda_m^2 + \gamma_p^2 - 2\lambda_m\gamma_p(\cos(\omega_p - \theta_m))}. \tag{6.3}$$

The sector, $S_i (i = 1, 2 \text{ or } 3)$ of $M$ within which a UE (macro or edge) is located is determined by measuring $\theta_m$ using line $L$ as Fig. 6.1 shows. The sector association

definition is according to the following rule:

$$\begin{cases} S_1 \rightarrow (-30^\circ < \theta \leq 90^\circ) \\ S_2 \rightarrow (90^\circ < \theta \leq 180^\circ) \vee (-180^\circ \leq \theta \leq -150^\circ) \\ S_3 \rightarrow (-150^\circ < \theta \leq -30^\circ) \end{cases} \tag{6.4}$$

The final location consideration concerns the proximity of macro BSs. The limit to the distance is controlled by setting a value for $d_{min}$, the minimum distance between any two macro BS in the system. The same equation defined in Chapter Four (Fig. 4.2 and (4.5)) is also adopted thus:

$$\omega_{i+1} = \omega_i - \cos^{-1}[\frac{(d_{min} + \delta_i)^2 + (d_{min} + \delta_{i+1})^2 - (d_{min} + \delta_{i,i+1})^2}{2(d_{min} + \delta_i)(d_{min} + \delta_{i+1})}], \tag{6.5}$$

where $d_{min}$ is the minimum distance between macro BSs in the network and for any interfering BS $I_Z$, $d_z = d_{min} + \delta_z$. In addition, $((d_{min} + \delta_i) - (d_{min} + \delta_{i+1}))^2 \leq (d_{min} + \delta_{i,i+1})^2$ by the principles of geometry.

## 6.4 FR model

### 6.4.1 Single tier case

Fig. 6.2 shows the Power versus Bandwidth description for SFR implementation in the three sectors of a macro BS $M$. At each sector, the maximum bandwidth size that can be allocated to the edge region is $\mathcal{F}_{e,max} = \mathcal{F}/3$ while the actual edge bandwidth allocated is given as $\mathcal{F}_{e,i} = \mathcal{F}_{e,max} - \psi_i$ where $i$ is the sector index. Unlike static SFR implementations, $\psi_i$ and $\mathcal{F}_{e,i}$ are selected differently for each sector.

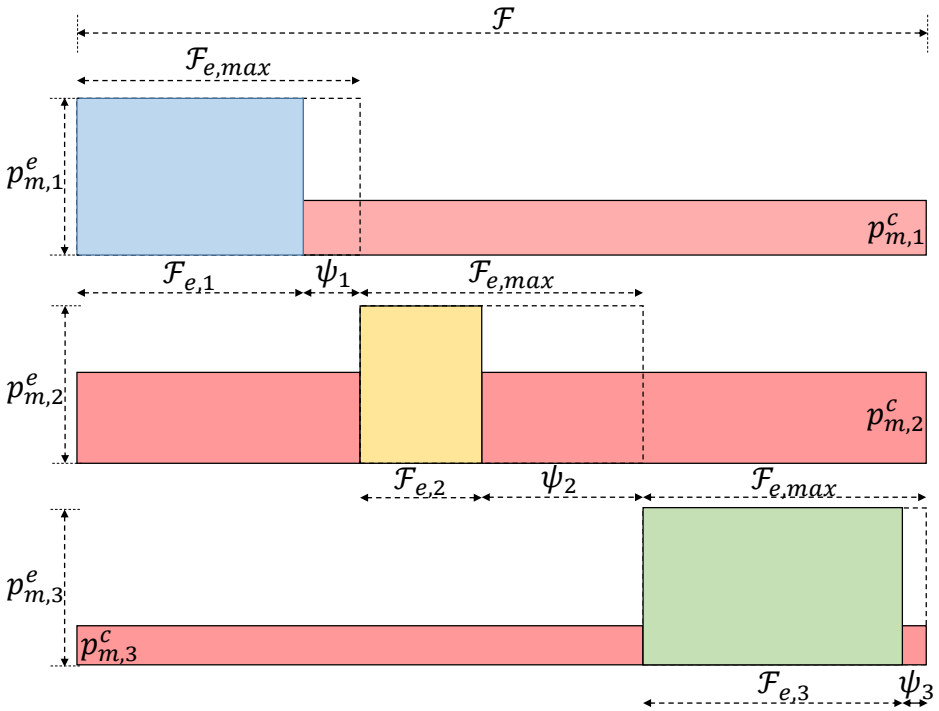


Figure 6.2: SFR: Power vs Bandwidth allocation for three sectors of $M$

Similar to previous derivations in the preceding chapter, $p^e_{m,i}$ the power transmitted from $M$ to an edge UE is given as:

$$p^e_{m,i} = \frac{\mu_{m,s} P_{m,s}}{E_{m,i}(\mu_{m,s} - 1) + N_{m,i}}. \tag{6.6}$$

where $\mu_{m,s}$ is the ratio of the transmit power towards an edge UE, to the transmit power towards a center UE, $P_{m,s}$ is the total power budget, $E_{m,i}$ the number of edge UE and $N_{m,i}$ the total number of UE in the sector under investigation.

The transmit power to a center UE, $p^c_{m,i}$ is given as:

$$p^c_{m,i} = \frac{P_{m,s}}{E_{m,i}(\mu_{m,s} - 1) + N_{m,i}}. \tag{6.7}$$

Fig. 6.2 can also be considered as the SFR bandwidth assignment for three sectors from three neighbouring BS. Therefore the bandwidth overlaps and probability of interference can be computed with the updated definition of $\mathcal{F}_{e,i}$. Considering two sectors (with indexes $x$ and $y$) from different macro BS, $\beta_{c,c}$, the probability that the center region of $S_y$ will cause interference to macro center UEs connected to $S_x$ and $\beta_{e,c}$, the probability that the edge transmissions from $S_y$ will cause interference

to macro center UEs connected to $S_x$ are:

$$\beta_{c,c} = \frac{\mathcal{F} - (2\mathcal{F}_{e,max} - \psi_x - \psi_y)}{\mathcal{F} - (\mathcal{F}_{e,max} - \psi_x)} \tag{6.8}$$

$$\beta_{e,c} = \frac{\mathcal{F}_{e,max} - \psi_y}{\mathcal{F} - (\mathcal{F}_{e,max} - \psi_x)} \tag{6.9}$$

### 6.4.2 HetNet FR model: Variant-1

The SFR algorithm is extended to accommodate the additional pico BS tier in the HetNet. The macro BS bandwidth assignment remains the same as in the single tier case shown in Fig. 6.2. For the pico BS, two variants are investigated as shown in Figs. 6.3 and 6.4 which show just a single sector (index 1) of $M$. In the first variant, all pico BS (located at center and edge of $S_1$ in $M$) utilize $\mathcal{F}$, the entire bandwidth available.

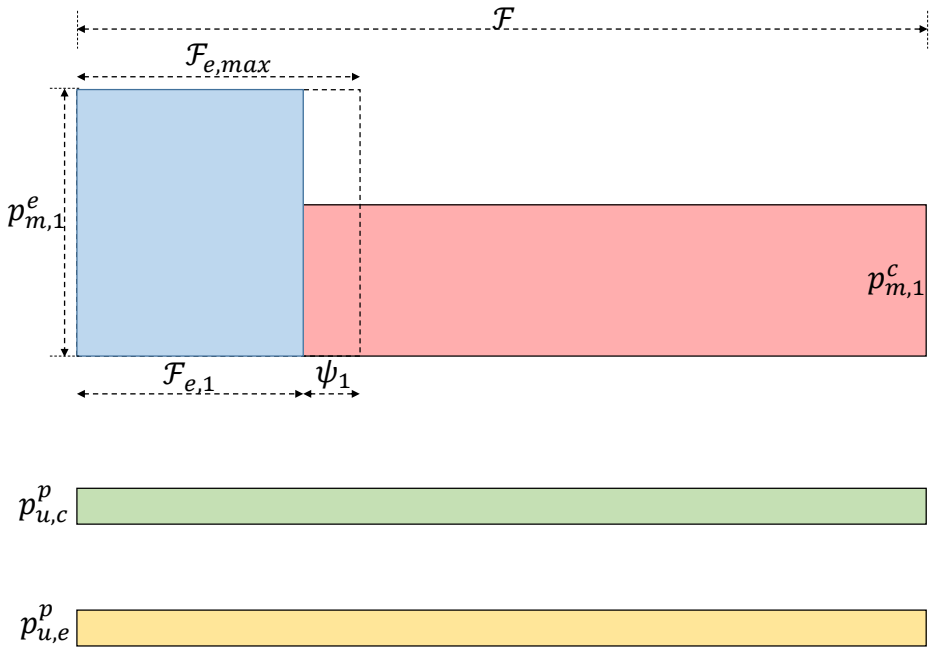


Figure 6.3: SFR HetNet Variant-1: Pico BS use full bandwidth

### 6.4.3 HetNet FR model: Variant-2

In the second variant of the algorithm, interference reduction is prioritized and the pico BS are restricted to allocate only bandwidth used in the center region of $S_1$.

By avoiding transmissions with the same frequencies as the high power macro edge region, bandwidth availability is sacrificed for SINR enhancement.

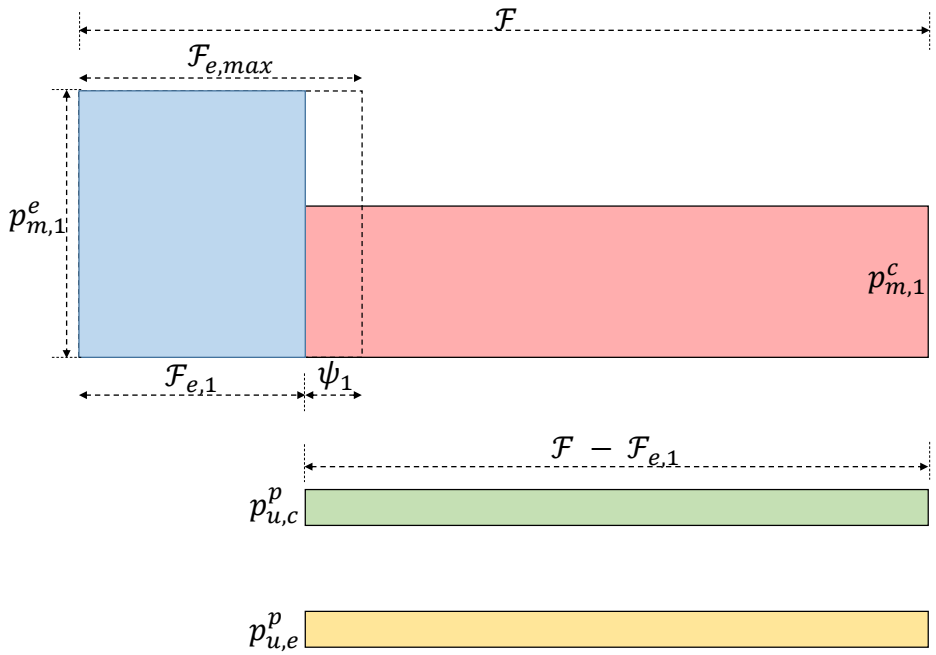


Figure 6.4: SFR HetNet Variant-2: Pico BS use macro center bandwidth

## 6.5 Signal-to-interference-plus-noise ratio equations

### 6.5.1 SFR HetNet Variant-1

**Macro center UE**: The SINR for a macro center UE connected to sector $S_i$ in reference BS $M$ considers interference from both macro and pico BS and is given as:

$$SINR^{sfr}_{u,c} = \frac{p^c_{m,i} h_{m,i} G_{m,i}}{\sigma^2 + \sum_{j \epsilon \mathcal{I}_m} \sum_{k \neq i} (\beta_{c,c} p^c_{j,k} + \beta_{e,c} p^e_{j,k}) h_{j,k} G_{j,k} + \sum_{l \epsilon \mathcal{I}_p} p^p_{u,l} h_{u,l} G_{u,l}}, \tag{6.10}$$

where $p^c_{u,x}, p^e_{u,x}$ represent respectively the transmit power from the center region and the edge region of a sector $S_x$ of a macro BS, while $p^p_{u,x}$ is the transmit power from a pico BS, $Q_x$. $h_{u,x}$ and $G_{u,x}$ are the fading component and path loss respectively associated with the UE and a macro sector defined by $S_x$ or a pico BS defined by $Q_x$. $\sigma^2$ is the noise component, $\mathcal{I}_m$ is the set of nearby interfering macro BS and $\mathcal{I}_p$ is the set of nearby interfering pico BS. $\sigma^2$ is considered negligible compared to the interference components and by substituting the power components and interference

probabilities, (6.10) becomes:

$SINR^{sfr}_{u,c} =$

$$\frac{\frac{P_{m,s}}{E_{m,i}(\mu_{m,s}-1)+N_{m,i}}\lambda_m^{-\alpha}}{\sum_{j\epsilon\mathcal{J}_m}\sum_{k\neq i}\frac{P_{m,s}[\mathcal{F}-2\mathcal{F}_{e,max}+\psi_i+\psi_k+\mu_{m,s}(\mathcal{F}_{e,max}-\psi_k)](\lambda_m^2+\gamma_{m,k}^2-2\lambda_m\gamma_{m,k}\cos(\omega_{m,k}-\theta_m))^{-\frac{\alpha}{2}}}{[\mathcal{F}-(\mathcal{F}_{e,max}-\psi_i)][E_{j,k}(\mu_{m,s}-1)+N_{j,k}]}+\sum_{l\epsilon\mathcal{J}_p}\frac{P_p(\lambda_m^2+\gamma_{p,l}^2-2\lambda_m\gamma_{p,l}\cos(\omega_{p,l}-\theta_m))^{-\frac{\alpha}{2}}}{N_{u,l}}}, \tag{6.11}$$

where all parameters are as previously defined. In addition, $\lambda_m$ is the distance between the UE and the reference BS $M$, $\gamma_{x,y}$ is the distance between $M$ and a close BS (macro if $x = m$ and pico if $x = p$) whose sector, $S_y$ is a neighbour to $S_i$ in $M$, $\theta_m$ is the angle between the UE and line $L$ shown in Fig. 6.1, $\omega_{m,y}, \omega_{p,y}$ are the angles between $L$ and the macro or pico BS respectively, $\alpha$ is the path-loss exponent, $P_p$ it the pico power budget which is assumed the same for all pico BS and $N_{u,l}$ is the total number of UEs connected to pico BS $Q_l$.

The transmit power components in (6.11) depend on the number of UE connected in each macro BS sector or pico BS. To avoid excessive power transmissions to a single UE due to low values of either of $E_{m,i}, N_{m,i}$ or $N_{u,l}$, in the simulations, thresholds are defined for the maximum power that a BS transmits to a UE.

**Macro Edge UE**: The SINR for the edge UE is dependent on interference from the center transmissions of neighbouring macro BS and from any close pico BS:

$$SINR^{sfr}_{u,e} = \frac{p^e_{m,i}h_{m,i}G_{m,i}}{\sigma^2 + \sum_{j\epsilon\mathcal{J}_m}\sum_{k\neq i}p^c_{j,k}h_{j,k}G_{j,k} + \sum_{l\epsilon\mathcal{J}_p}p^p_{u,l}h_{u,l}G_{u,l}}, \tag{6.12}$$

and substituting the power components gives:

$$SINR^{sfr}_{u,e} = \frac{\frac{\mu_{m,s}P_{m,s}}{E_{m,i}(\mu_{m,s}-1)+N_{m,i}}\lambda_m^{-\alpha}}{\sum_{j\epsilon\mathcal{J}}\sum_{k\neq i}\frac{P_{m,s}(\lambda_m^2+\gamma_k^2-2\lambda_m\gamma_k\cos(\omega_k-\theta_m))^{-\frac{\alpha}{2}}}{E_{j,k}(\mu_{m,s}-1)+N_{j,k}} + \sum_{l\epsilon\mathcal{J}_p}\frac{P_p(\lambda_m^2+\gamma_{p,l}^2-2\lambda_m\gamma_{p,l}\cos(\omega_{p,l}-\theta_m))^{-\frac{\alpha}{2}}}{N_{u,l}}} \tag{6.13}$$

**Pico UE**: Fig. 6.3 shows that pico BS in both the center and edge regions of $S_i$ utilize the entire system bandwidth in Variant-1. Therefore the SINR equation for both center pico and edge pico BS have similar interference sources. The SINR for a UE connected to a pico BS, $Q_x$ within $S_i$ of $M$ using the SFR Variant-1 technique

is:

$$SINR_{u,p}^{sfr} = \frac{p_{u,x}^{p} h_{u,x} G_{u,x}}{\sigma^2 + (p_{m,i}^{c} + p_{m,i}^{e}) h_{m,i} G_{m,i} + \sum_{j \epsilon \mathcal{J}_m} \sum_{k \neq i} (p_{j,k}^{c} + p_{j,k}^{e}) h_{j,k} G_{j,k} + \sum_{l \epsilon \mathcal{J}_p} p_{u,l}^{p} h_{u,l} G_{u,l}}, \tag{6.14}$$

where the second term in the denominator is the combined center and edge interference from $S_i$, the third term is the combined interference from the neighbouring sectors of $S_i$ and the last term is the interference from any nearby pico BS.
Expanding 6.14 gives:

$$SINR_{u,p}^{sfr} = \frac{\frac{P_p}{N_{u,x}} (\lambda_p^2 + \gamma_{p,x}^2 - 2\lambda_p \gamma_{p,x} \cos(\omega_{p,x} - \theta_p))^{-\frac{\alpha}{2}}}{\frac{P_{m,s}(1+\mu_{m,s})\lambda_p^{-\alpha}}{E_{m,i}(\mu_{m,s}-1)+N_{m,i}} + \sum_{j \epsilon \mathcal{J}_m} \sum_{k \neq i} \frac{P_{m,s}(1+\mu_{m,s})(\lambda_p^2 + \gamma_{m,k}^2 - 2\lambda_p \gamma_{m,k} \cos(\omega_{m,k} - \theta_p))^{-\frac{\alpha}{2}}}{E_{j,k}(\mu_{m,s}-1)+N_{j,k}} + \sum_{l \epsilon \mathcal{J}_p} \frac{P_p (\lambda_p^2 + \gamma_{p,l}^2 - 2\lambda_p \gamma_{p,l} \cos(\omega_{p,l} - \theta_p))^{-\frac{\alpha}{2}}}{N_{u,l}}}, \tag{6.15}$$

where $\lambda_p$ is the distance between the UE and $M$ and $\theta_p$ is the angle extended by the UE from $L$ as Fig. 6.1 shows.

### 6.5.2 SFR HetNet Variant-2

**Macro center UE**: Fig. 6.4 shows that the macro center region utilizes the same bandwidth as both center and edge pico BS within the reference BS, similar to Fig. 6.3. Therefore the SINR for macro center UE in SFR HetNet variant-2 is the same as (6.11).

**Macro edge UE**: Fig. 6.4 shows that in Variant-2, pico BS exclude the macro edge bandwidth in their allocations. Therefore, the SINR for macro edge UE in SFR HetNet variant-2 is equivalent to (6.13) without the second interference component of the denominator and similar to the case in the single-tier network scenario.

**Pico UE**: Following the variant-2 description in Fig. 6.4, the edge component of $S_i$ is restricted from the bandwidth allocation to pico UEs. However, there will be both center and edge region interference from the neighbouring macro BS of $M$ similar to the interference received by macro center UE. Excluding the interference component towards pico UEs from the edge (first in the denominator) component of $S_i$ from (6.15) and considering the interference from neighbouring macro center region as in the case of the first interference component in (6.11), the SINR for any

pico UE under variant-2 is:

$$SINR_{u,p}^{sfr} = \frac{\frac{P_p}{N_{u,x}}(\lambda_p^2+\gamma_{p,x}^2-2\lambda_p\gamma_{p,x}\cos(\omega_{p,x}-\theta_p))^{-\frac{\alpha}{2}}}{\frac{P_{m,s}\lambda_p^{-\alpha}}{E_{m,i}(\mu_{m,s-1})+N_{m,i}}+\sum_{j\in J_m}\sum_{k\neq i}\frac{P_{m,s}[\mathcal{F}-2\mathcal{F}_{e,max}+\psi_i+\psi_k+\mu_{m,s}(\mathcal{F}_{e,max}-\psi_k)](\lambda_m^2+\gamma_{m,k}^2-2\lambda_m\gamma_{m,k}\cos(\omega_{m,k}-\theta_m))^{-\frac{\alpha}{2}}}{[\mathcal{F}-(\mathcal{F}_{e,max}-\psi_i)][E_{j,k}(\mu_{m,s-1})+N_{j,k}]}+\sum_{l\in J_p}\frac{P_p(\lambda_p^2+\gamma_{p,l}^2-2\lambda_p\gamma_{p,l}\cos(\omega_{p,l}-\theta_p))^{-\frac{\alpha}{2}}}{N_{u,l}}}, \tag{6.16}$$

# 6.6 Capacity equations

**Macro center UE**: Consistent with Figs. 6.3 and 6.4, the capacity for a macro center UE within sector $S_i$ in $M$ is:

$$Cap_{u,c}^{sfr} = \min[\mathcal{F}_{u,max}, \frac{\mathcal{F}-(\mathcal{F}_{e,max}-\psi_i)}{N_{m,i}-E_{m,i}}][\log_2(1+SINR_{u,c}^{sfr})], \tag{6.17}$$

where $\mathcal{F}_{u,max}$ is the maximum bandwidth that can be allocated to a single UE.

**Macro edge UE**: Similarly, the capacity for a macro edge UE is:

$$Cap_{u,e}^{sfr} = \min[\mathcal{F}_{u,max}, \frac{(\mathcal{F}_{e,max}-\psi_i)}{E_{m,i}}][\log_2(1+SINR_{u,e}^{sfr})]. \tag{6.18}$$

**Pico UE**: For the variant-1 where pico BS utilize $\mathcal{F}$ the entire bandwidth as shown in Fig. 6.3, the capacity for any pico UE connected to a pico BS with index $Q_x$ is:

$$Cap_{u,p}^{sfr} = \min[\mathcal{F}_{u,max}, \frac{\mathcal{F}}{N_{u,x}}][\log_2(1+SINR_{u,p}^{sfr})]. \tag{6.19}$$

For the variant-2 depicted in Fig. 6.4 where the total bandwidth used by each BS is $\mathcal{F}-\mathcal{F}_{e,i}$ where $\mathcal{F}_{e,i} = \mathcal{F}_{e,max}-\psi_i$, the pico UE capacity is:

$$Cap_{u,p}^{sfr} = \min[\mathcal{F}_{u,max}, \frac{(\mathcal{F}-(\mathcal{F}_{e,max}-\psi_i))}{N_{u,x}}][\log_2(1+SINR_{u,p}^{sfr})]. \tag{6.20}$$

# 6.7 Results and Analysis

## 6.7.1 Simulation Parameters

For the simulations, the concept of the virtual UE was used to approximate the performance of UEs in a BS region to the performance of the UE at the center of gravity. This is similar to the assumptions in [27] and [40]. The analysis is carried out on a hexagonal macro BS layout with a pico BS additional BS tier. The

parameters used for analysis and simulations are listed in Table. 6.1

Table 6.1: Parameters for SFR HetNet Analysis

| **Parameter** | **Value** |
|---|---|
| $r$ | 0.5km |
| $P_{m,s}$ | 43dB |
| $P_p$ | 2dB |
| $\alpha$ | 3 |
| $\mathcal{F}_{e,max}$ | $16 \times 180$kHz |
| $E_{m,i} = E_{j,k}$ | 8 |
| $N_{m,i} = N_{j,k} = N_{u,l}$ | 48 |
| $\lambda_m$ **for macro center UE** | 0.45 |
| $\lambda_m$ **for macro edge UE** | 0.85 |
| $\theta_m$ **(macro center and edge UE)** | $30^\circ$ |
| $\gamma_{m,1} = \gamma_{m,2}$ **for** $\mathcal{I}$ | $\sqrt{3}r$ |
| $\omega_{m,1}, \omega_{m,2}$ **for** $\mathcal{I}$ | $0^\circ, 60^\circ$ |
| $\gamma_{p,i}, i = 1, 2, 3, 4$ **for** $\mathcal{Q}$ | $0.2r, 0.2r, r, r$ |
| $\omega_{p,i}, i = 1, 2, 3, 4$ **for** $\mathcal{Q}$ | $0^\circ, 60^\circ, 0^\circ, 60^\circ$ |
| $\lambda_p$ | $\gamma_{p,i} - 0.01$ |

### 6.7.2 Effect of power ratio on SINR and Capacity

In addition to the parameters listed in Table. 6.1, the analysis on the effect of the power ratio is carried out for $1 \leq \mu_{m,s} \leq 5$ where $\psi_i = \psi_k = 8 \times 180$kHz. Fig. 6.5 shows the result for SINR and Capacity when the two SFR variants are used.

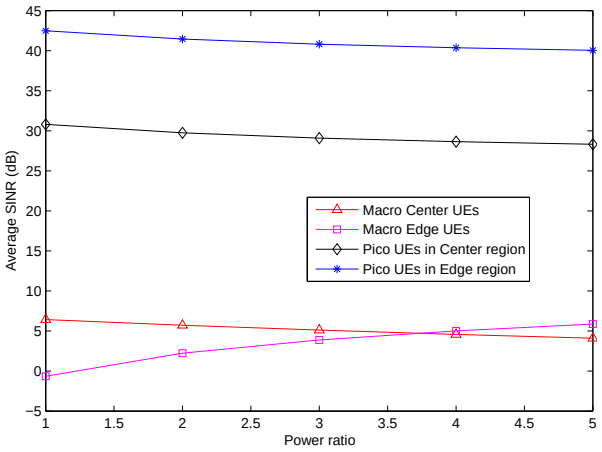


(a) SINR for SFR Variant-1 for HetNets

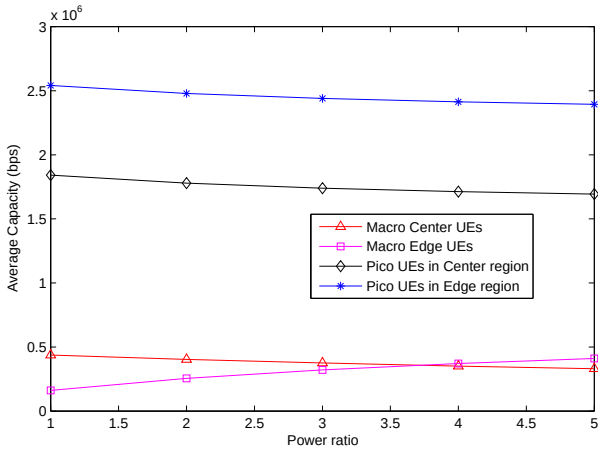


(b) Capacity (in bps) for SFR Variant-1 for HetNets

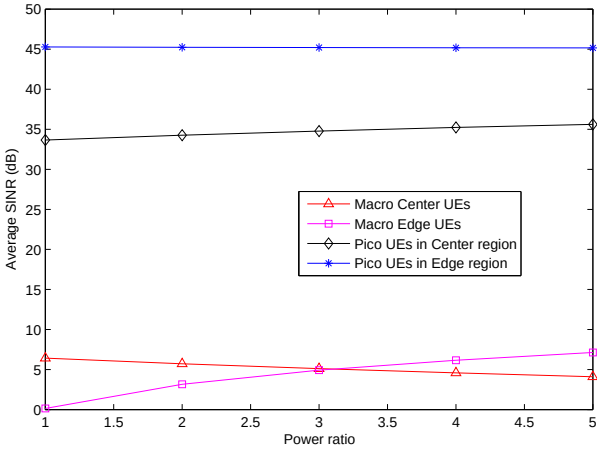


(c) SINR for SFR Variant-2 for HetNets

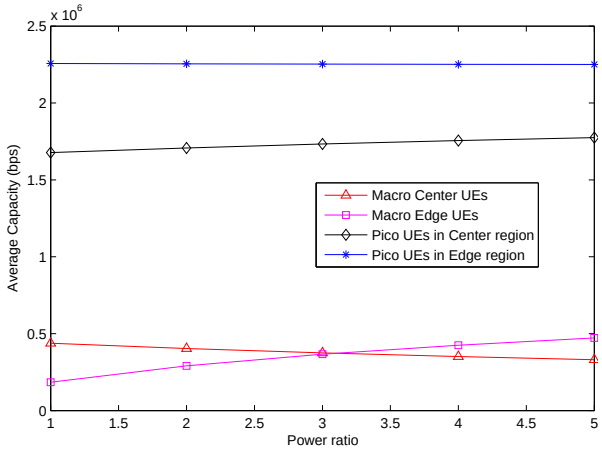


(d) Capacity (in bps) for SFR Variant-2 for HetNets

Figure 6.5: SINR and Capacity when $\mu_{m,s}$ is varied

The SINR and Capacity plots show a similar pattern for all values of $\mu_{m,s}$ and this is due to the values chosen for $\psi_i, \psi_k, E_{m,i}, E_{j,k}$ and $N_{u,l}$. Since the bandwidth is sufficient for the UEs available in each BS, the Capacity matches the SINR. Pico edge UEs experience the best SINR and Capacity performance because as they are farther away from the underlying macro BS, they receive the weakest interference. Pico center UEs experience higher interference but their performance is still better than both Macro center and edge UEs. This highlights the benefits of extending coverage and capacity in cellular networks via HetNets. The changing value of $\mu_{m,s}$ has minimal effect on pico UEs, but macro edge performance increases and macro center performance decreases with increasing $\mu_{m,s}$. Consequently, there is a meeting point for macro center and edge performance (approximately 3.75dB in Variant-1 and 3dB in Variant-2). The next investigation is to study and compare the performance of Macro UEs and Pico UEs across both variants.

Figs. 6.6 and 6.7 show a close relationship for macro UEs. It is observed that the performance for macro center UEs stays the same irrespective of the Variant used for both SINR and Capacity. In Variant-2, the edge SINR and Capacity outperforms Variant-1.

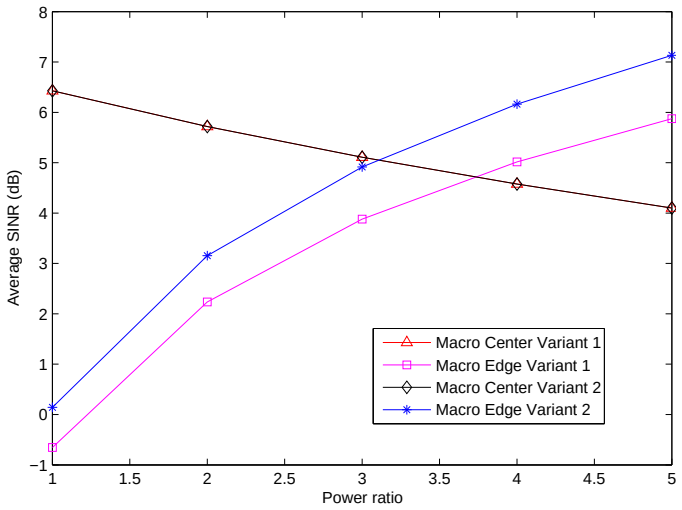


Figure 6.6: SINR for Macro UEs when $\mu_{m,s}$ is varied

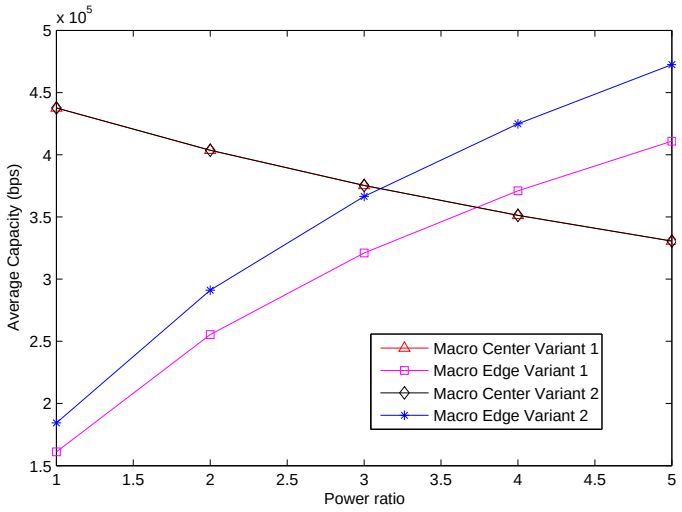


Figure 6.7: Capacity (in bps) for Macro UEs when $\mu_{m,s}$ is varied

Figs. 6.8 and 6.9 for the pico UEs case shows that the performance for Pico UEs is excellent and even though Pico edge Variant-2 outperforms Variant-1 in SINR, the reverse is the case for Capacity.

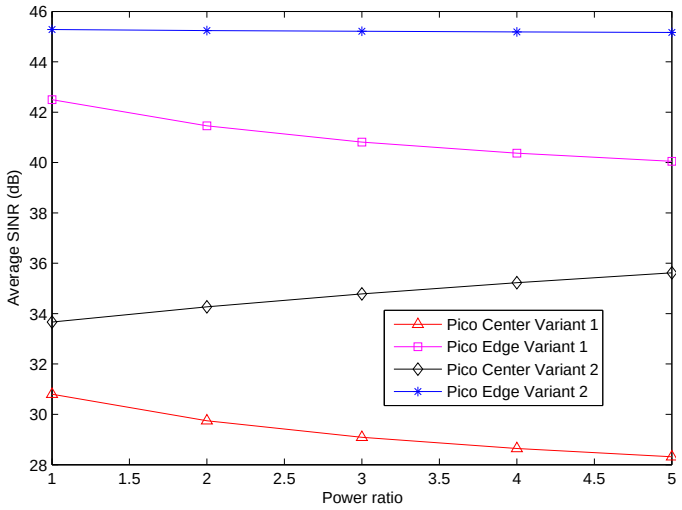


Figure 6.8: SINR for Pico UEs when $\mu_{m,s}$ is varied

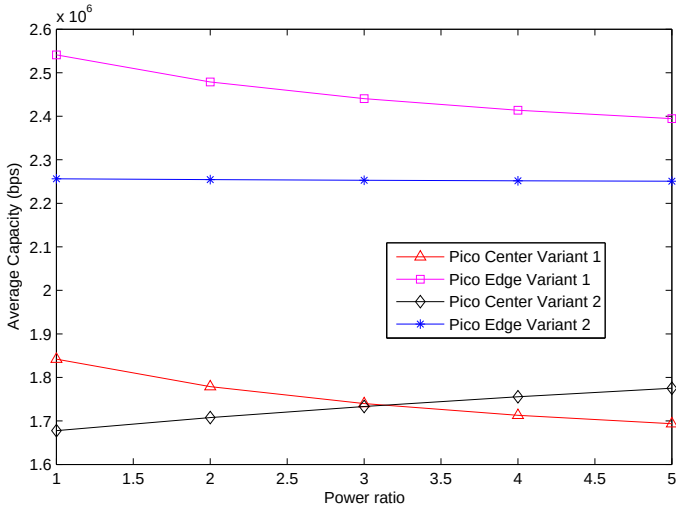


Figure 6.9: Capacity (in bps) for Pico UEs when $\mu_{m,s}$ is varied

### 6.7.3 Effect of edge Frequency on Capacity

In addition to the parameters listed in Table. 6.1, the analysis on the effect of the power ratio is carried out for $\psi_i \leq 8 \times 180\text{kHz} \leq 16 \times 180\text{kHz}$ where $\mu_{m,s} = 1.7\text{kHz}$. Fig. 6.10 shows a similar scenario of the Pico UEs outperforming the Macro UEs in both SINR and Capacity.

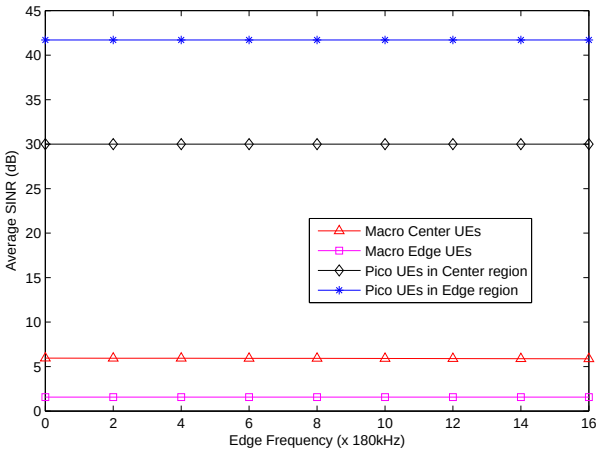


(a) SINR for SFR Variant-1 for HetNets

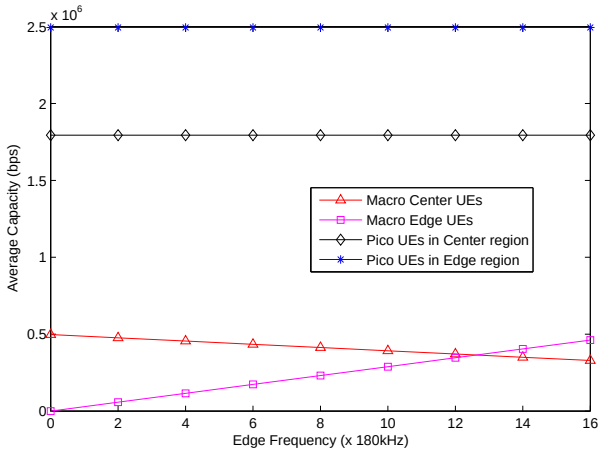


(b) Capacity (in bps) SFR Variant-1 for HetNets

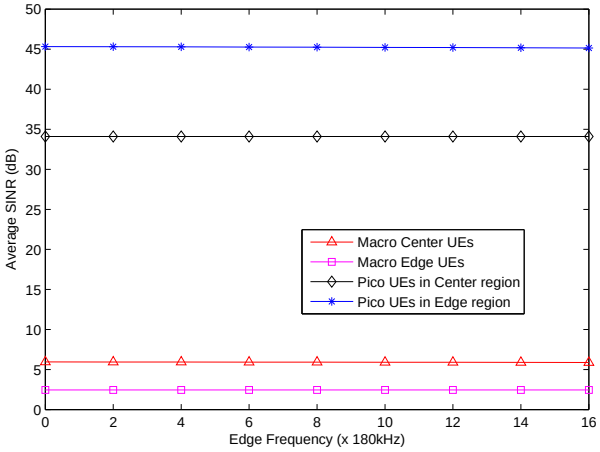


(c) SINR for SFR Variant-2 for HetNets

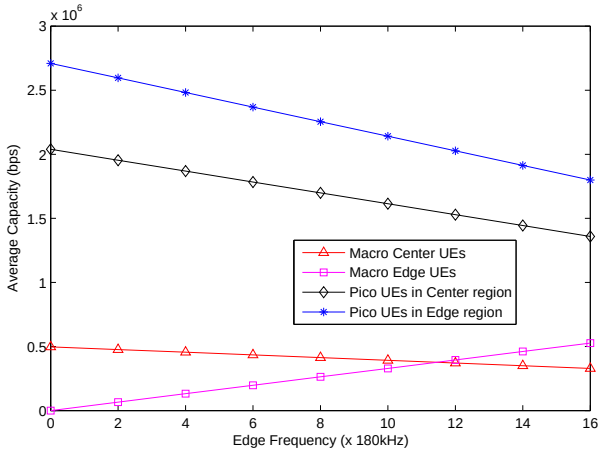


(d) Capacity (in bps) SFR Variant-2 for HetNets

Figure 6.10: SINR and Capacity when edge frequency is varied

This suggests that an increased density of the pico BS tier will result in an increase in the overall network SINR and capacity, however to the detriment of macro UEs due to the likely increase in interference. Unlike the case where $\mu_{m,s}$ was altered, the SINR values stay relatively constant all through and are not exactly matched with the Capacity performance. Just as the increase in $\mu_{m,s}$ results in a better performance in capacity for Macro edge UEs, and poorer performance for macro center UEs, this is also the case for increasing the edge frequency (by reducing $\psi_i$). Due to the constant performance observed in SINR, the comparison of different UE groups will be conducted only on the capacity.

Fig. 6.11 shows the performance of the capacity for macro UEs when the edge frequency is varied through $\psi_i$.

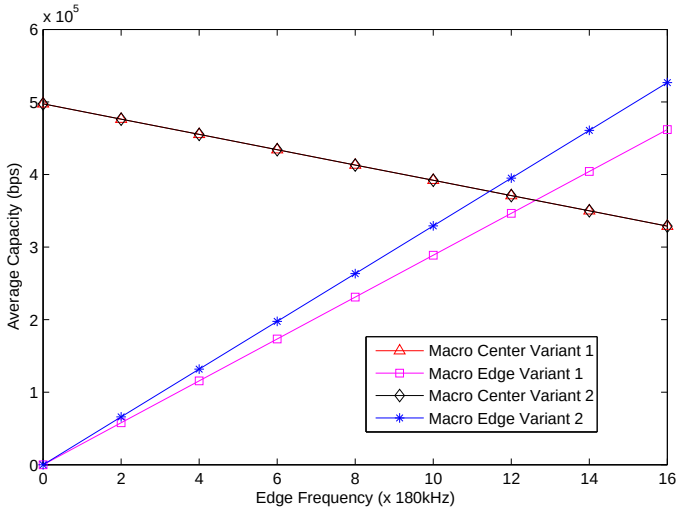


Figure 6.11: Capacity (in bps) macro UEs when $\psi_i$ is varied

The macro center UEs experience the same performance irrespective of the variant adopted. However, macro edge UEs under Variant-2 have a better performance than in Variant-1. These results highlight the need for intelligent selection of BS parameters based on the prevailing network conditions for better UE performance.

Finally, in Fig. 6.12, the performance for pico UEs shows that under Variant-1, the capacity stays constant with the pico edge UEs outperforming the center UEs. However in Variant-2, the performance is more sensitive to the edge frequency and changes drastically.

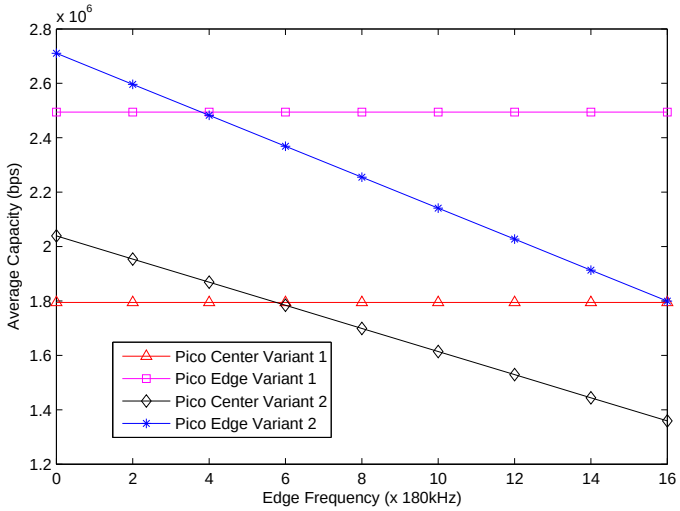


Figure 6.12: Capacity (in bps) for pico UEs when $\psi_i$ is varied

### 6.7.4 Chapter summary

In this Chapter, HetNets were analysed based on a positional model for macro and pico BS tiers. This defined the relationship between the BS entities based on their locations using a reference BS sector as reference. In addition, a resource allocation model based on SFR was developed for HetNets. Equations defining the performance of different classes of UEs were then defined. Furthermore, analysis was carried out by varying the power ratio and edge frequency parameters for the reference sector and investigating the UE performance.

# Chapter 7

# Conclusion and Further research

Frequency reuse is a vital technology for the provision of improved user performance in cellular networks. As the network evolves into 5G and the data demand continues to increase exponentially, it is crucial that existing techniques be improved upon. These include modelling of cellular networks which has to be accurate representation of real scenarios and optimization techniques for user performance. In this thesis, investigation and analysis has been carried out on frequency reuse application in cellular networks with specific reference to geometry of the network. Heterogeneous cellular networks were also considered and included in the analysis. In this Chapter, a brief summary of the thesis is outlined and then suggestions are made for future research in the study area.

## 7.1 Conclusion

Chapter Two contains the relevant theory behind interference in long term evolution networks, frequency reuse in cellular networks, heterogeneous cellular networks and the modelling and design approaches. A review of recent research works on frequency reuse is then provided with classification based on popular approaches like multiobjective optimization, center of gravity user concept, selection of minimum data rate requirement and range expansion for mobile user association.

In Chapter Three, extensive analysis is provided for user performance when the different frequency reuse algorithms are implemented in single-tier (homogeneous) cellular networks. The main frequency reuse algorithms (integer and partitioned) are first described based on their bandwidth and power allocation rules. Initial investigations to determine base station parameters for the analysis revealed the usefulness

of restricting investigations to specific base station regions. In addition, user performance was hugely dependent on location, hence, it was beneficial to group and analyse the users according to their positions. Therefore, more insightful analysis was obtained by considering defined user groups as opposed to average performance of all users in a base station. A model was proposed for irregular macro base stations that considered location between network entities and the maximum proximity between base stations. Based on this model, four network scenarios were developed composed of the hexagonal and three irregular macro base station placements. Results from the analysis which incorporated the irregular base station models showed the impact of base station center radius, power ratio and bandwidth allocation on user performance. It was observed that signal-to-interference-plus-noise ratio and capacity do not always follow the same performance patterns. Users at the boundary of base stations were more sensitive to changes in their classification (as either center or edge users). Therefore, the user classification is a key factor affecting performance, in addition to the power allocation and interference received per user. The effect of irregularity on user performance was also more significant with larger coverage regions.

Chapter Four contains analytical derivations for the location model between base stations and users, and frequency/power allocation model for the main frequency reuse algorithms; i.e reuse-1, reuse-3, fractional frequency reuse and soft frequency reuse. The location model builds on the irregular network model presented in Chapter Three. A reference base station is considered, and the parameters for its connected users and other neighbouring base stations are defined based on their relationships with the reference base station. Investigation into the resource parameters (frequency/power) in partitioned frequency reuse schemes (fractional frequency reuse and soft frequency reuse) revealed interference probabilities that arise. Based on this observation, the proposed frequency/power allocation model captured resource allocation rules accurately. New equations were then derived for user performance parameters. A modified frequency reuse algorithm called Geometric frequency reuse was developed for improving the static schemes. The algorithm consists of four sub-algorithms that determine the vertices and coverage areas of irregular base station regions. The area computed was used to guide intelligent bandwidth allocation based on user distribution. The accuracy of computed coverage areas for the network scenarios were tested and the algorithm was implemented

in the case of soft frequency reuse. Results show the proposed geometric frequency reuse algorithm guaranteed optimal selection of bandwidth for capacity and spectral efficiency.

In Chapter five, power configuration parameters for single-tier cellular networks deploying soft frequency reuse were optimized. The concept of a virtual user being used to approximate the performance of users in a base station region was considered. In addition a fairness metric was defined to specify a standard for expected minimal user performance. Based on these, an optimization framework was developed, built on the irregular location and resource allocation models earlier designed. The results showed significant improvement in the performance of vulnerable edge users when the optimized power ratio was used. Based on the framework, base station parameters can also be tuned by operators to attain any desired fairness level in center and edge user performance.

In Chapter Six, the irregular base station model and resource allocation model was extended to the case of heterogeneous cellular networks. New equations for user performance were derived for the macro base station users as well as the pico base station users at different locations. This was based on two variants of the soft frequency algorithm with varying limits on the bandwidth overlaps between base station tiers. Network scenarios were generated using the models and performance analysis was carried out on the macro and pico user performance under both variants of soft frequency reuse that were assumed. Results provide useful insights into the performance of heterogeneous cellular networks.

## 7.2 Further research

There are opportunities for enhancement of existing techniques in network modelling for cellular networks using irregular coverage patterns, interference management using frequency reuse and optimization of heterogeneous cellular networks. These include:

- Investigation into the minimum and maximum coverage areas obtainable in irregular macro base station networks. This will enhance resource allocation and network planning
- Full deployment of geometry-based frequency reuse in heterogeneous cellular

networks to improve performance of users across all base station tiers.

- Investigation into the impact of various scheduling techniques on user performance when geometry-based frequency reuse is deployed in cellular networks.
- Applying game theory and multiobjective optimization concepts with geometry based frequency-reuse techniques

# References


[1] C. Cox, *An introduction to LTE: LTE, LTE-advanced, SAE and 4G mobile communications*. John Wiley & Sons, 2012.

[2] N. Panwar, S. Sharma, and A. K. Singh, "A survey on 5g: The next generation of mobile communication," *Physical Communication*, vol. 18, pp. 64–84, 2016.

[3] M. Agiwal, A. Roy, and N. Saxena, "Next generation 5g wireless networks: A comprehensive survey," *IEEE Communications Surveys Tutorials*, vol. 18, no. 3, pp. 1617–1655, thirdquarter 2016.

[4] N. Al-Falahy and O. Y. Alani, "Technologies for 5g networks: Challenges and opportunities," *IT Professional*, vol. 19, no. 1, pp. 12–20, Jan 2017.

[5] (2017, Feb. 7) Cisco visual networking index: Global mobile data traffic forecast update, 20162021 white paper. Cisco. [Online]. Available: http://www.cisco.com/c/en/us/solutions/collateral/service-provider/visual-networking-index-vni/mobile-white-paper-c11-520862.html

[6] R. N. Mitra and D. P. Agrawal, "5g mobile technology: A survey," *ICT Express*, vol. 1, no. 3, pp. 132–137, 2015.

[7] I. F. Akyildiz, S. Nie, S.-C. Lin, and M. Chandrasekaran, "5g roadmap: 10 key enabling technologies," *Computer Networks*, vol. 106, pp. 17–48, 2016.

[8] A. Gupta and R. K. Jha, "A survey of 5g network: Architecture and emerging technologies," *IEEE Access*, vol. 3, pp. 1206–1232, 2015.

[9] M. Dohler, R. W. Heath, A. Lozano, C. B. Papadias, and R. A. Valenzuela, "Is the phy layer dead?" *IEEE Communications Magazine*, vol. 49, no. 4, pp. 159–165, April 2011.

[10] D. Liu, L. Wang, Y. Chen, M. Elkashlan, K. K. Wong, R. Schober, and L. Hanzo, "User association in 5g networks: A survey and an outlook," *IEEE Communications Surveys Tutorials*, vol. 18, no. 2, pp. 1018–1044, Secondquarter 2016.

[11] A. S. Hamza, S. S. Khalifa, H. S. Hamza, and K. Elsayed, "A survey on inter-cell interference coordination techniques in ofdma-based cellular networks," *IEEE Communications Surveys Tutorials*, vol. 15, no. 4, pp. 1642–1670, Fourth 2013.

[12] S. Schwarz, J. C. Ikuno, M. imko, M. Taranetz, Q. Wang, and M. Rupp, "Pushing the limits of lte: A survey on research enhancing the standard," *IEEE Access*, vol. 1, pp. 51–62, 2013.

[13] I. F. Akyildiz, D. M. Gutierrez-Estevez, R. Balakrishnan, and E. Chavarria-Reyes, "Lte-advanced and the evolution to beyond 4g (b4g) systems," *Physical Communication*, vol. 10, pp. 31–60, 2014.

[14] J. G. Andrews, S. Buzzi, W. Choi, S. V. Hanly, A. Lozano, A. C. K. Soong, and J. C. Zhang, "What will 5g be?" *IEEE Journal on Selected Areas in Communications*, vol. 32, no. 6, pp. 1065–1082, June 2014.

[15] F. Boccardi, R. W. Heath, A. Lozano, T. L. Marzetta, and P. Popovski, "Five disruptive technology directions for 5g," *IEEE Communications Magazine*, vol. 52, no. 2, pp. 74–80, February 2014.

[16] J. G. Andrews, "Seven ways that hetnets are a cellular paradigm shift," *IEEE Communications Magazine*, vol. 51, no. 3, pp. 136–144, March 2013.

[17] I. F. Akyildiz, D. M. Gutierrez-Estevez, and E. C. Reyes, "The evolution to 4g cellular systems: Lte-advanced," *Physical communication*, vol. 3, no. 4, pp. 217–244, 2010.

[18] A. Adejo and S. Boussakta, "Performance analysis of frequency reuse techniques under varying cellular network scenarios," in *2016 IEEE Wireless Communications and Networking Conference*, April 2016, pp. 1–6.

[19] A. Adejo, S. Boussakta, and J. Neasham, "Interference modelling for soft frequency reuse in irregular heterogeneous cellular networks," in *2017 Ninth Inter-*

*national Conference on Ubiquitous and Future Networks (ICUFN)*, July 2017, pp. 381–386.

[20] A. Adejo, J. Hussein, and S. Boussakta, "Optimal transmit power configuration for soft frequency reuse in irregular cellular networks," in *2017 Ninth International Conference on Ubiquitous and Future Networks (ICUFN)*, July 2017, pp. 711–713.

[21] A. Ghosh, N. Mangalvedhe, R. Ratasuk, B. Mondal, M. Cudak, E. Visotsky, T. A. Thomas, J. G. Andrews, P. Xia, H. S. Jo, H. S. Dhillon, and T. D. Novlan, "Heterogeneous cellular networks: From theory to practice," *IEEE Communications Magazine*, vol. 50, no. 6, pp. 54–64, June 2012.

[22] H. S. Dhillon, R. K. Ganti, and J. G. Andrews, "Modeling non-uniform ue distributions in downlink cellular networks," *IEEE Wireless Communications Letters*, vol. 2, no. 3, pp. 339–342, June 2013.

[23] N. Saquib, E. Hossain, and D. I. Kim, "Fractional frequency reuse for interference management in lte-advanced hetnets," *IEEE Wireless Communications*, vol. 20, no. 2, pp. 113–122, April 2013.

[24] D. G. G, M. Garcia-Lozano, S. R. Boque, and D. S. Lee, "Optimization of soft frequency reuse for irregular lte macrocellular networks," *IEEE Transactions on Wireless Communications*, vol. 12, no. 5, pp. 2410–2423, May 2013.

[25] W. Guo, S. Wang, X. Chu, J. Zhang, J. Chen, and H. Song, "Automated small-cell deployment for heterogeneous cellular networks," *IEEE Communications Magazine*, vol. 51, no. 5, pp. 46–53, May 2013.

[26] S. Deb, P. Monogioudis, J. Miernik, and J. P. Seymour, "Algorithms for enhanced inter-cell interference coordination (eicic) in lte hetnets," *IEEE/ACM Transactions on Networking*, vol. 22, no. 1, pp. 137–150, Feb 2014.

[27] O. G. Aliu, M. Mehta, M. A. Imran, A. Karandikar, and B. Evans, "A new cellular-automata-based fractional frequency reuse scheme," *IEEE Transactions on Vehicular Technology*, vol. 64, no. 4, pp. 1535–1547, April 2015.

[28] T. Novlan, J. G. Andrews, I. Sohn, R. K. Ganti, and A. Ghosh, "Comparison of fractional frequency reuse approaches in the ofdma cellular downlink," in *2010*

*IEEE Global Telecommunications Conference GLOBECOM 2010*, Dec 2010, pp. 1–5.

[29] (2005) 3gpp r1-050507, soft frequency reuse scheme for utran lte. Huawei. [Online]. Available: http://www.3gpp.org/ftp/tsgran/WG1RL1/TSGR141/Docs/R1-050507.zip

[30] X. Yang, "A multilevel soft frequency reuse technique for wireless communication systems," *IEEE Communications Letters*, vol. 18, no. 11, pp. 1983–1986, Nov 2014.

[31] A. Damnjanovic, J. Montojo, Y. Wei, T. Ji, T. Luo, M. Vajapeyam, T. Yoo, O. Song, and D. Malladi, "A survey on 3gpp heterogeneous networks," *IEEE Wireless Communications*, vol. 18, no. 3, pp. 10–21, June 2011.

[32] D. Lopez-Perez, I. Guvenc, G. de la Roche, M. Kountouris, T. Q. S. Quek, and J. Zhang, "Enhanced intercell interference coordination challenges in heterogeneous networks," *IEEE Wireless Communications*, vol. 18, no. 3, pp. 22–30, June 2011.

[33] M. Assaad, "Optimal fractional frequency reuse (ffr) in multicellular ofdma system," in *2008 IEEE 68th Vehicular Technology Conference*, Sept 2008, pp. 1–5.

[34] Y. Yu, E. Dutkiewicz, X. Huang, M. Mueck, and G. Fang, "Performance analysis of soft frequency reuse for inter-cell interference coordination in lte networks," in *2010 10th International Symposium on Communications and Information Technologies*, Oct 2010, pp. 504–509.

[35] H. S. Dhillon, R. K. Ganti, F. Baccelli, and J. G. Andrews, "Modeling and analysis of k-tier downlink heterogeneous cellular networks," *IEEE Journal on Selected Areas in Communications*, vol. 30, no. 3, pp. 550–560, April 2012.

[36] M. Haenggi, J. G. Andrews, F. Baccelli, O. Dousse, and M. Franceschetti, "Stochastic geometry and random graphs for the analysis and design of wireless networks," *IEEE Journal on Selected Areas in Communications*, vol. 27, no. 7, pp. 1029–1046, September 2009.

[37] Q. C. Li, R. Q. Hu, Y. Xu, and Y. Qian, "Optimal fractional frequency reuse and power control in the heterogeneous wireless networks," *IEEE Transactions on Wireless Communications*, vol. 12, no. 6, pp. 2658–2668, June 2013.

[38] D. Chen, T. Jiang, and Z. Zhang, "Frequency partitioning methods to mitigate cross-tier interference in two-tier femtocell networks," *IEEE Transactions on Vehicular Technology*, vol. 64, no. 5, pp. 1793–1805, May 2015.

[39] G. Huang and J. Li, "Interference mitigation for femtocell networks via adaptive frequency reuse," *IEEE Transactions on Vehicular Technology*, vol. 65, no. 4, pp. 2413–2423, April 2016.

[40] M. Qian, W. Hardjawana, Y. Li, B. Vucetic, X. Yang, and J. Shi, "Adaptive soft frequency reuse scheme for wireless cellular networks," *IEEE Transactions on Vehicular Technology*, vol. 64, no. 1, pp. 118–131, Jan 2015.

[41] A. Y. Al-Zahrani and F. R. Yu, "An energy-efficient resource allocation and interference management scheme in green heterogeneous networks using game theory," *IEEE Transactions on Vehicular Technology*, vol. 65, no. 7, pp. 5384–5396, July 2016.

[42] M. Masoudi, H. Zaefarani, A. Mohammadi, and C. Cavdar, "Energy and spectrum efficient resource allocation in two-tier networks: A multiobjective approach," in *2017 IEEE Wireless Communications and Networking Conference (WCNC)*, March 2017, pp. 1–6.

[43] G. Giambene, V. A. Le, T. Bourgeau, and H. Chaouchi, "Iterative multi-level soft frequency reuse with load balancing for heterogeneous lte-a systems," *IEEE Transactions on Wireless Communications*, vol. 16, no. 2, pp. 924–938, Feb 2017.

[44] B. Xie, Z. Zhang, R. Hu, G. Wu, and A. Papathanassiou, "Joint spectral efficiency and energy efficiency in ffr based wireless heterogeneous networks," *IEEE Transactions on Vehicular Technology*, vol. PP, no. 99, pp. 1–1, 2017.

[45] G. Giambene and T. A. Yahiya, "Lte planning for soft frequency reuse," in *2013 IFIP Wireless Days (WD)*, Nov 2013, pp. 1–7.

[46] M. A. AboulHassan, M. Yassin, S. Lahoud, M. Ibrahim, D. Mezher, B. Cousin, and E. A. Sourour, "Classification and comparative analysis of inter-cell interference coordination techniques in lte networks," in *2015 7th International Conference on New Technologies, Mobility and Security (NTMS)*, July 2015, pp. 1–6.

[47] B. M. Hambebo, M. M. Carvalho, and F. M. Ham, "Performance evaluation of static frequency reuse techniques for ofdma cellular networks," in *Proceedings of the 11th IEEE International Conference on Networking, Sensing and Control*, April 2014, pp. 355–360.

[48] A. Gk and M. Koca, "Performance evaluation of frequency planning and scheduling schemes in ofdma networks," in *2014 IEEE International Black Sea Conference on Communications and Networking (BlackSeaCom)*, May 2014, pp. 149–153.

[49] J. G. Andrews, S. Singh, Q. Ye, X. Lin, and H. S. Dhillon, "An overview of load balancing in hetnets: old myths and open problems," *IEEE Wireless Communications*, vol. 21, no. 2, pp. 18–25, April 2014.

[50] Q. Ye, B. Rong, Y. Chen, M. Al-Shalash, C. Caramanis, and J. G. Andrews, "User association for load balancing in heterogeneous cellular networks," *IEEE Transactions on Wireless Communications*, vol. 12, no. 6, pp. 2706–2716, June 2013.

[51] S. Singh and J. G. Andrews, "Joint resource partitioning and offloading in heterogeneous cellular networks," *IEEE Transactions on Wireless Communications*, vol. 13, no. 2, pp. 888–901, February 2014.

[52] S. H. Ali and V. C. M. Leung, "Dynamic frequency allocation in fractional frequency reused ofdma networks," *IEEE Transactions on Wireless Communications*, vol. 8, no. 8, pp. 4286–4295, August 2009.

[53] A. Mahmud and K. A. Hamdi, "A unified framework for the analysis of fractional frequency reuse techniques," *IEEE Transactions on Communications*, vol. 62, no. 10, pp. 3692–3705, Oct 2014.

[54] R. Y. Chang, Z. Tao, J. Zhang, and C. C. Kuo, "A graph approach to dynamic fractional frequency reuse (ffr) in multi-cell ofdma networks," in *2009 IEEE International Conference on Communications*, June 2009, pp. 1–6.

[55] (2011) 3gpp technical report tr 36.942 v10.2.0, radio frequency (rf) system scenarios. ETSI. [Online]. Available: http://www.etsi.org/deliver/etsi_tr/136900_136999/136942/10.02.00_60/tr_136942v100200p.pdf

[56] J. Riihijärvi, P. Mähönen, and M. Petrova, "What will interference be like in 5g hetnets?" *Physical Communication*, vol. 18, pp. 85–94, 2016.

[57] L. Sanguinetti, A. L. Moustakas, and M. Debbah, "Interference management in 5g reverse tdd hetnets with wireless backhaul: A large system analysis," *IEEE Journal on Selected Areas in Communications*, vol. 33, no. 6, pp. 1187–1200, June 2015.

[58] D. Ramasamy, R. Ganti, and U. Madhow, "On the capacity of picocellular networks," in *2013 IEEE International Symposium on Information Theory*, July 2013, pp. 241–245.

[59] J. Ling and D. Chizhik, "Capacity scaling of indoor pico-cellular networks via reuse," *IEEE Communications Letters*, vol. 16, no. 2, pp. 231–233, February 2012.

[60] H. S. Dhillon, R. K. Ganti, and J. G. Andrews, "Load-aware heterogeneous cellular networks: Modeling and sir distribution," in *2012 IEEE Global Communications Conference (GLOBECOM)*, Dec 2012, pp. 4314–4319.

[61] ——, "Load-aware modeling and analysis of heterogeneous cellular networks," *IEEE Transactions on Wireless Communications*, vol. 12, no. 4, pp. 1666–1677, April 2013.

[62] H. S. Jo, Y. J. Sang, P. Xia, and J. G. Andrews, "Heterogeneous cellular networks with flexible cell association: A comprehensive downlink sinr analysis," *IEEE Transactions on Wireless Communications*, vol. 11, no. 10, pp. 3484–3495, October 2012.

[63] W. Guo, S. Wang, T. O'Farrell, and S. Fletcher, "Energy consumption of 4g cellular networks: A london case study," in *2013 IEEE 77th Vehicular Technology Conference (VTC Spring)*, June 2013, pp. 1–5.

[64] F. Kaup, F. Michelinakis, N. Bui, J. Widmer, K. Wac, and D. Hausheer, "Assessing the implications of cellular network performance on mobile content access," *IEEE Transactions on Network and Service Management*, vol. 13, no. 2, pp. 168–180, June 2016.

[65] L. Chen and D. Yuan, "Generalized frequency reuse schemes for ofdma networks: Optimization and comparison," in *2010 IEEE 71st Vehicular Technology Conference*, May 2010, pp. 1–5.

[66] S. Hashima, S. Elnoubi, M. Alghoniemy, H. Shalaby, O. Muta, and I. Mahmoud, "Analysis of frequency reuse cellular systems using worst case signal to interference ratio," in *Proceedings of the 12th International Conference on Telecommunications*, June 2013, pp. 185–190.

[67] A. Mahmud and K. Hamdi, "Uplink analysis for ffr and sfr in composite fading," in *2012 IEEE 23rd International Symposium on Personal, Indoor and Mobile Radio Communications - (PIMRC)*, Sept 2012, pp. 1285–1289.

[68] Y. Yang, L. Chen, P. Zhao, and W. Wang, "Adaptive power ratio updating algorithm in soft frequency reuse scheme," in *2013 IEEE 78th Vehicular Technology Conference (VTC Fall)*, Sept 2013, pp. 1–5.

[69] L. Chen and D. Yuan, "Soft frequency reuse in large networks with irregular cell pattern: How much gain to expect?" in *2009 IEEE 20th International Symposium on Personal, Indoor and Mobile Radio Communications*, Sept 2009, pp. 1467–1471.

[70] J. Garca-Morales, G. Femenias, and F. Riera-Palou, "Analysis and optimization of ffr-aided ofdma-based heterogeneous cellular networks," *IEEE Access*, vol. 4, pp. 5111–5127, 2016.

[71] V. Singh, M. Lentz, B. Bhattacharjee, R. J. La, and M. A. Shayman, "Dynamic frequency resource allocation in heterogeneous cellular networks," *IEEE Transactions on Mobile Computing*, vol. 15, no. 11, pp. 2735–2748, Nov 2016.